Government of Western Australia

Department of
**Mines and Petroleum**

REPORT
119

# CENOZOIC EVOLUTION OF THE NULLARBOR PLAIN PALEOKARST, SOUTHERN AUSTRALIA

by CR Miller

Queen's UNIVERSITY

Geological Survey of Western Australia

Government of Western Australia
Department of Mines and Petroleum

REPORT 119

# CENOZOIC EVOLUTION OF THE NULLARBOR PLAIN PALEOKARST, SOUTHERN AUSTRALIA

by
Cody R Miller

Perth 2012

Geological Survey of
Western Australia

**MINISTER FOR MINES AND PETROLEUM**
**Hon. Norman Moore MLC**

**DIRECTOR GENERAL, DEPARTMENT OF MINES AND PETROLEUM**
**Richard Sellers**

**EXECUTIVE DIRECTOR, GEOLOGICAL SURVEY OF WESTERN AUSTRALIA**
**Rick Rogerson**

**National Library of Australia Cataloguing-in-Publication entry**

Author: Miller, Cody R.

Title: Cenozoic evolution of the Nullarbor Plain paleokarst, southern Australia [electronic resource] / Cody R Miller.

ISBN: 9781741684728 (ebook : pdf)

Subjects: Sediments (Geology)--Australia, Southern--Nullarbor Plain.
Sedimentary rocks--Australia, Southern--Nullarbor Plain.
geology, Stratigraphic--Cenozoic

Other Authors/Contributors:
Geological Survey of Western Australia

Dewey Number: 551.7

**Notice to the reader**

This Report reproduces a Doctoral thesis researched, written and compiled by a student from the Department of Geological Sciences and Geological Engineering, Queens University, Kingston, Ontario, Canada. GSWA has provided field and logistic support for this project, but the scientific content and the drafting of figures has been the responsibility of the author and his supervisors. No editing has been undertaken by GSWA.

**REFERENCE**
**The recommended reference for this publication is:**
Miller, Cody R 2012, Cenozoic evolution of the Nullarbor Plain paleokarst, southern Australia: Geological Survey of Western Australia, Report 119, 185p.

**Published 2012 by Geological Survey of Western Australia**
This Report is published in digital format (PDF) and is available online at <http://www.dmp.wa.gov.au/GSWApublications>.

**Further details of geological publications and maps produced by the Geological Survey of Western Australia are available from:**

Information Centre
Department of Mines and Petroleum
100 Plain Street
EAST PERTH WESTERN AUSTRALIA 6004
Telephone: +61 8 9222 3459 Facsimile: +61 8 9222 3444
**http://www.dmp.wa.gov.au/GSWApublications**

**Cover image:** The Nullarbor Plain, near Eucla (photograph courtesy Noel James)

# CENOZOIC EVOLUTION OF THE NULLARBOR PLAIN PALEOKARST, SOUTHERN AUSTRALIA

Cody R. Miller

A thesis submitted to the Department of Geological Sciences and Geological Engineering

in conformity with the requirements for the degree of

Doctor of Philosophy

Queen's University

Kingston, Ontario, Canada

July, 2012

## ABSTRACT

The Nullarbor Plain in southern Australia is an uplifted succession of Cenozoic marine carbonates whose surface has been exposed for ~14 m.y. This succession of limestones, particularly in the surfical middle Miocene Nullarbor Limestone, hosts a complex and prolonged record of meteoric diagenesis. Alteration took place through 3 broad phases of diagenesis encompassing 8 stages that are interpreted to have taken place over a dramatic regional climate change. Phase 1 diagenesis occurred under a humid middle Miocene climate and involved mineralogical equilibration with meteoric fluids, calcite cementation, widespread microkarst, and regional lacustrine and palustrine sedimentation producing copious amounts of ooids. These ooids are interpreted to have formed via microbial secretions and sediment aggradation over multiple seasons of changing rainfall and soil hydration states. Cortical laminations are proposed to represent microbial mucus envelopes during wet seasons alternating with dehydration during dry seasons and precipitation of fibrous clay minerals and $CaCO_3$ that preserve the pre-existing microbial fabrics. Phase 2 alterations took place under a more temperate climate from the late Miocene to Pliocene with a later pronounced humid interlude. This phase encompassed ~8 m.y. and was dominated by karst process where deep cave dissolution occurred at depressed water tables related to globally low sea levels and later shallow caves developed during a Pliocene sea level highstand. Phase 3 has occurred since the late Pliocene and is indicative of the onset of modern semi-arid climatic conditions. This final phase involved the creation of subsoil hollows filled with blackened limestone lithoclasts, deep and shallow dolines, and indurated pedogenic calcrete that now forms much of the surface of the Nullarbor Plain. Blackened limestone clasts have been shown

to form at the B-C boundary in soil profiles where roots have their cellular structures calcified and during this process incorporate trapped organics that ultimately produce the distinctive black colouration. The importance of this comprehensive diagenetic record is its direct applicability to the understanding of ancient subaerial exposure surfaces.

## STATEMENT OF CO-AUTHORSHIP

The following is my own original work, although Noel P. James and T. Kurt Kyser offered intellectual and scientific guidance and are recognized as co-authors in the attached manuscripts. Yvonne Bone also contributed to the scientific contributions through both logistical support and scientific guidance.

## ACKNOWLEDGEMENTS

This portion of my thesis is probably the hardest to write because there have been so many people in my life that have contributed to this project and made my time here at Queen's enjoyable. Here is my best attempt at thanking everyone for his or her support.

First and foremost I would like to thank Dr. Noel James, who I consider not only a supervisor but also a colleague and dear friend. Noel your illimitable enthusiasm, knowledge, creativity, demeanor, and passion for science have sculpted me into the scientist I am today. We have shared many laughs, confusion, and success through the years and I am sure there will be many more for years to come. Noel and I both thank the helpful staff at the Geological Survey of Western Australia for field and financial support, especially Roger Hocking for his encouragement and planning. I would also like to thank Dr. Kurt Kyser for his innovative mind, enthusiasm, and patience with my foray into geochemistry. Staying with geochemistry, I also thank April Vuletich, Al Grant, Dr. Steve Beyer, Dr. Don Chipley, Dr. Yulia Uvarova, and Kerry Klassen for their help and assistance in the lab. Thank you as well to Dr. Yvonne Bone for her cheerful disposition and vast scientific knowledge. I thank Dr. Bob Dalrymple and Dr. Guy Narbonne for always asking the tough questions and teaching me about what it takes to be an academic and professional. Thank you to Dr. Brian Jones and his SEM lab (George Braybrook and Dee-Ann Rollings) for microbial advice and the SEM imagery that allowed for new interpretations. Also thank you to Dr. Paul Wright for many enlightened discussions about root mats and blackened limestone clasts. Last but certainly not least, Dr. Bill Martindale, I value the guidance you have given me regarding geology, academics, and career choices.

Graduate school wouldn't have been complete without the friendships I have made here over my years. Thank you to Geoffo Reith, Anthony Hommik, Kain Michaud, Duncan MacKay, Anna Crockford, and Matt Lato for their participation in "stress relieving" tactics such as ping-pong, coffee breaks, foosball, chats, and barley beverages. In particular, Bryce Jablonski you made the transition back to school extremely easy and have been a close friend. We have shared a lot of fun times here and I know that there will be many more ahead of us (with Marcia of course!). Kris Nelson and Kellie Haines, your friendship means a lot to Meg and I, we look forward to many more laughs and bowling competitions. Laura O'Connell you have been a great friend and somehow put up with me for 6 weeks in the middle of a desert. Finally, Meg Seibel, what can I say, as words do not express how much I care for and love you. Your love, unconditional support, and carbonate knowledge over the years have made this journey so much easier and I look forward to the many new adventures we will experience together!

Lastly I want to thank my parents, you have taught me the true values of life and your guidance has made me into the person I am today. Your unconditional love and support is more cherished than you know and I am so appreciative for all you have done for me! To my brothers, who have always been there for me, thank you for keeping me humble, your support, and being great role models.

## TABLE OF CONTENTS

## LIST OF TABLES

### Chapter 2



### Chapter 4

## LIST OF FIGURES

### Chapter 2



### Chapter 3

**Chapter 4**

*To my family, whose never-ending love and support made all of this possible.*

# CHAPTER 1

## GENERAL INTRODUCTION

Subaerial unconformities are of profound importance to carbonate sedimentology, stratigraphy, paleoclimatology, economic geology, and paleogeography (Esteban and Klappa 1983; James and Choquette 1990; Alonso Zarza 2006; Brasier 2011; Miller et al. 2012). Prolonged exposure of limestones and dolostones inevitably leads to meteoric diagenesis that forever modifies the preexisting carbonates. Such alteration can lead to significant loss of carbonate in both surface and subsurface environments, extensive porosity development or occlusion, calcareous paleosols, and the formation of unique carbonate grains (Bathurst 1975; Esteban and Klappa 1983; James and Choquette 1990; Flügel 2004). These changes are of major economic importance because some of the world's largest hydrocarbon reservoirs and base metal deposits are hosted within these features (Esteban and Klappa 1983). The recognition of meteoric alteration fabrics not only allows a detailed account of the processes operating at the exposure surface but their presence provides crucial information regarding past climates, hydrogeologic systems, and terrestrial vegetation.

Geomorphic aspects of recent karst systems are well documented (Bögli 1980; Esteban and Klappa 1983; Ford 1988; James and Choquette 1988; Frisia and Borsato 2010); however, much less is understood about the processes and products of multistage meteoric diagenesis at major unconformities under changing climate. To address this knowledge gap research was directed towards the Nullarbor Plain in southern Australia, the largest areal paleokarst on the planet. The surface of which has been exposed since the middle Miocene to an evolving climate and yet is understood in only a rudimentary way.

In order to achieve a better understanding of the Nullarbor Plain's diagenetic response to climate change specific questions needed to be answered, including; 1) what is the paragenetic history of this immense plain, 2) how have the processes and products changed relative to time, 3) how are such changes associated with climate and eustasy, and 4) are there particular aspects of this paleokarst system that can be used to refine past interpretations of prolonged unconformities in the geologic record.

The surface of the Plain is developed on the middle Miocene Nullarbor Limestone, a vast elevated subtropical carbonate platform (Dunkley and Wigley 1967; Lowry and Jennings 1974; Hocking 1990; Drexel and Preiss 1995; Miller et al. 2012; O'Connell et al. 2012). The Nullarbor Limestone and underlying Cenozoic marine carbonates have imprinted on them the record of complex and prolonged Neogene history of meteoric diagenesis. The main focus of this study was to address the direct effects of climate and sea level on the style and nature of meteoric diagenesis in the Nullarbor Plain in particular, and by inference low lying carbonate plains in general. Specifically, various alteration fabrics pertaining to specific paleoclimates were analyzed in order to i) illustrate how climate change can be recognized in modern subaerial exposure surfaces (Chapter 2), ii) document and interpret the *in situ* formation of palustrine ooids (Chapter 3), and iii) document the nature of blackened limestone lithoclasts and propose an interpretation on their genesis (Chapter 4).

The approach was to use multiple scales of investigation to unravel the paragenesis of the many commonly superimposed meteoric diagenetic fabrics. The techniques used for differentiation between individual fabrics and their interpreted formation ranged from digital elevation models for the entire Nullarbor Plain, outcrop observations, binocular microscopy, petrography, and scanning electron microscopy. Stable carbon and oxygen

isotope ratios, inductively coupled plasma mass spectrometry, and elemental analyses provided further insights into the origins of many of the diagenetic features. This thesis used an integrated approach combining all of the above investigative techniques and past research from the realms of not only geology but also biology to arrive at new interpretations of many subaerial alteration fabrics.

## THE NULLARBOR PLAIN

The carbonate rocks that form the Nullarbor Plain are a series of middle Cenozoic limestones that belong to the Eucla Group, a suite of sedimentary rocks that extend today offshore underneath the continental shelf. Three formations were deposited in cool to sub-tropical neritic paleoenvrionments that partially fill the shallow broad epicontinental Eucla Basin. The Eocene Wilson Bluff Limestone is a soft, poorly lithified, and bryozoan rich cool water carbonate. The overlying Oligocene to early Miocene Abrakurrie Limestone is also a bryozoan rich cool water carbonate; however, it is somewhat more lithified than the Wilson Bluff Limestone (Lowry 1970; James and Bone 1991). The early to middle Miocene Nullarbor Limestone forms much of the Nullarbor Plain surface and may be the most extensive Cenozoic carbonate platform described to date. These carbonates are fossiliferous grainstones to rudstones composed of both temperate and tropical skeletal components including coralline algae, large and small benthic foraminifera, gastropods, bivalves, scaphopods, infaunal echinoids, serpulid worm tubes, planktonic foraminifera, and both zooxanthellate and azooxanthellate corals (O'Connell et al. 2012). Most of the Nullarbor Limestone is structureless as prominent depositional bedding planes and sedimentary structures are absent. Today, the Nullarbor Limestone is well lithified by

means of extensive low-Mg calcite cement but with extensive mouldic porosity.

## NEOGENE CLIMATE HISTORY

Climatic history throughout the Neogene is relatively well constrained for much of southern Australia (Goede et al. 1990; White 1994; Benbow et al. 1995; Webb and James 2006). The Plain was initially exposed during the middle Miocene to a humid climate that supported cool temperate rainforests near the coast and expansive woodlands further inland (White 1994; Drexel and Preiss 1995; Alley et al. 1999; Johnson 2009). During the late Miocene the climate became increasingly dry; however, little climatic documentation exists for this period of time. This trend towards drier climate conditions was interrupted by a humid climate interlude at the beginning of the Pliocene (~ 5 Ma) that lasted ~ 2 m.y. Today the Nullarbor Plain is under the influence of a semi-arid to arid climate with a considerable annual temperature difference from 23º - 26º C in summer to 10º - 12º C in the winter (Goede et al. 1990). Annual rainfall ranges from 150 mm in the northern regions to 250 mm closer to the southern coast, whereas potential evaporation exceeds 2000 – 3000 mm supporting only sparse steppe foliage. The climate has been interpreted to have reached its present level of dryness ~ 1 Ma (Goede et al. 1990; Webb and James 2006).

## CLIMATE AND THE METEORIC DIAGENESIS OF CARBONATE SEDIMENT AND ROCKS

### *Overview*

The broad diversity of limestone fabrics resulting from meteoric diagenesis

is ultimately the result of several reactions, governed by intrinsic and extrinsic factors. Alteration taking place in the meteoric realm can either be mineral-controlled or water-controlled (Bathurst 1975; James and Choquette 1990). Mineral-controlled diagenesis can be seen taking place today along many warm coastlines where recently deposited marine sediments are introduced to meteoric fluids. High Mg-calcite particles are first to alter in these conditions as they neomorphose into stable low-Mg calcite, often keeping their original microstructure. Next aragonite allochems alter to low-Mg calcite, however, unlike Mg-calcite, the process involves complete aragonite dissolution and precipitation of calcite (Bathurst 1975; James and Choquette 1990). Mineral-controlled diagenesis occurred early in the Nullarbor Plain history as marine sediments rapidly equilibrated with meteoric fluids. Water-controlled diagenesis, as the name states, has processes driven by the availability of fresh water. The products of such alteration are wide ranging and include surface karst, subsurface karst, calcrete, and subsurface calcite precipitation in the form of speleothems. Water-controlled processes have governed the majority of diagenetic products seen within the Nullarbor Plain but with important and as yet unappreciated roles of soils and microbes. The type of water-controlled diagenesis that occurs at subaerial exposure surfaces is to a large degree dependent upon the climate. Relationships between climate and alteration features are well understood, particularly within humid and arid climates.

### *Humid Climates*

Surface and subsurface dissolution processes dominate carbonate lithologies that are exposed to humid climates. Humid climates are typified by varying ambient temperatures and intensive rainfall. This rainfall allows for groundwater movement and surface water drainage that together result in extensive dissolution (Esteban and Klappa 1983; Ford 1988;

Tucker 1990; Frisia and Borsato 2010). The products of such surface karst processes range from the micro- to macro-scale. The most impressive features develop in elevated warm tropical settings where tower karst dominants the landscape, whereas in low lying carbonate plains (like the Nullarbor Plain) surface karst plays a minor role in sculpting the surfical topography. Instead, subsurface dissolution leads to the formation of large and small cave systems that are ultimately controlled by meteoric water recharge and groundwater flow. This distinction in surfical karst can provide valuable information for paleogeographic reconstructions as it points to the subaerial exposure surface's past topography.

### *Temperate Climates*

Many temperate climates are characterized by two distinct seasons that have large variations in rainfall and only moderate temperature differences. Such conditions have a significant effect on terrestrial environments and influence the diagenesis occurring in near surface carbonates. Such changes are commonly associated with lacustrine and palustrine deposition where seasonal rainfall and temperature variations dramatically change lake levels and result in pedogenic alteration of the lacustrine deposits. Although the organic rich soils typically associated with temperate to semi arid climates are not continuously hydrated as in humid soils, they do nevertheless still have complex root systems associated with overlying vegetation. This seasonal change from periods of water saturation to periods of dryness creates chemical, physical, biological processes that produce unique grains and fabrics discussed in the following sections. Temperate climates have proportionate seasons of wet and dry conditions, whereas semi-arid climates have disproportionate seasons towards drier conditions.

### *Arid to Semi-Arid Climates*

Semi-arid climate systems are characterized by a lack of available meteoric water due to high evaporation and low rainfall. Evaporative processes result in near surface calcite precipitation. Calcareous soils, commonly termed calcrete or caliche, are prevalent under these climate conditions if there is a source of calcium carbonate (Tucker 1990; Wright 1994; Alonso-Zarza and Wright 2010a). Calcrete is the result of bicarbonate leaching in the upper sections of soil horizons and microcrystalline calcite precipitation below. Calcretes, because they are accretionary with distinctive, micritic, hard, nodular, and irregular laminated attributes, are the most widely recognized features associated with ancient subaerial exposure surfaces. The last decade has brought significant advances to the understanding of calcrete development, particularly the role of microbes.

## MAJOR RESULTS

### *Introduction*

A major outcome of this research is the realization that meteoric diagenesis of the Nullarbor Plain took place during three broad phases encompassing a total of eight smaller stages (Chapter 2). These effects were both destructive in terms of dissolution and constructive in the formation of various carbonates unique to such exposure. The unraveling of such alteration fabrics via cross-cutting relationships can be related to the dramatic climate change that occurred across this part of southern Australia during the last 14 m.y. This change from humid climate in the middle Miocene to a semi-arid one today has been worked out by careful analyses of the carbonate diagenetic fabrics. Such a complete record of meteoric alteration here can offer important insights into the effects

of climate, tectonics, sea level, topography, hydrogeology, and surface vegetation on the alteration of low lying carbonate plains throughout geologic time.

### *Neogene History of the Nullarbor Plain*

The ~ 14 m.y. history of the Nullarbor Plain has involved a wide variety of alteration events that have combined to create a complex and entwined paragenetic sequence related to climate change. Early diagenesis on the Plain involved mineral-controlled diagenesis involving the equilibration of metastable marine particles with newly introduced meteoric fluids. This is manifest as abundant mouldic porosity representing originally aragonitic skeletons. The calcium carbonate sourced from this reaction was shortly thereafter precipitated as sparry calcite cement, which gives the Nullarbor Limestone its distinctive crystalline nature. This was followed by extensive microkarst and lacustrine sedimentation. The muddy lacustrine sediments filtered into the underlying cavities where they were pedogenically overprinted in a palustrine environment, which resulted in the production of ooids that are discussed in the succeeding section. A prolonged period (~ 8 m.y.) of subsurface dissolution created expansive deep caves along the coast at approximately the same depth as the modern sea level and more regional shallow caves that host exquisite speleothems. These diagenetic features encompass the majority of the time since the Plain was initially exposed and are dominated by water-controlled processes indicative of humid to temperate climates.

The last series of diagenetic events to have affected the Plain record a rapid transition into increasingly arid conditions. This is apparent in the forms of shallow karst depressions that are filled with distinctive blackened limestone clasts, interpreted below. Shallow and deep dolines now dot the surface of the Plain with the former being filled with moderate red

coloured colluvium. Pedogenic calcrete is the final diagenetic product and is still actively forming today under a semi-arid to arid climate. An outgrowth of this geohistory analysis was the realization of the importance of palustrine soil ooids and ubiquitous blackened limestone clasts.

### *Palustrine Ooids*

Palustrine environments include wetlands, marshes, and other shallow fresh to brackish water settings where pedogenesis modifies subaqueous lacustrine deposits (Alonso Zarza et al. 1992; Platt and Wright 1992; Alonso-Zarza and Wright 2010b). Palustrine sediments and features are unique and complex largely because of the multitude of changing biological, chemical, and physical conditions inherent in their formation. Characteristics of palustrine deposits include micritic ooids, pisoids, peloids, laminated micrite, mottled fabrics, pseudo-microkarst, sediment and circumgranular cracking, root traces, charophytes, ostracods, and Mg-Si clay mineralization. Many of these features, specifically palustrine ooids and circumgranular cracking, are a record of temperate to semi-arid climates. The mechanisms that form such terrestrial coated grains have been long debated and previously required constant grain movement. Chapter 3 will describe a new mechanism for terrestrial ooid formation that does not require grain movement but instead invokes microbial activities.

### *Origin of Blackened Limestone Clasts*

Blackened limestone fragments are common constituents of many post-Carboniferous unconformities and are commonly used as a defining characteristic of subaerial exposure. They are reworked carbonate clasts with a distinctive light gray to

black colouration. Such clasts are sub-millimeter to decimeter in size with a morphology that is commonly angular, structureless, and fractured. They are dominantly poorly sorted and form calcareous breccias within surface karst depressions.

Blackened limestone clasts have puzzled carbonate researchers for decades and, as a consequence, their origins are not universally agreed upon with past interpretations including forest fires (Shinn and Lidz 1988), manganese/iron oxide staining (Lang and Tucci 1997), particulate organic substances (Strasser 1984), and microbial alterations (Folk et al. 1973). Increasing evidence suggests that organic carbon in some form is responsible for the black colouration; however, a viable mechanism for organic impregnation is still poorly understood, as is the climate under which this process occurs. The Nullarbor Plain with a diverse suite of blackened clasts from different ages and paleogeographic settings allows for a more detailed assessment of genesis than heretofore possible, which is discussed in Chapter 4.

## REFERENCES


ALLEY, N.F., CLARKE, J.D.A., MACPHAIL, M., and TRUSWELL, E.M., 1999, Sedimentary infillings and development of major Tertiary palaeodrainage systems of south-central Australia: Special Publication of the International Association of Sedimentologists, v. 27, p. 337-366.

ALONSO ZARZA, A.M., 2006, Paleoenvironmental record and applications of calcretes and palustrine carbonates: Special Paper - Geological Society of America, v. 416, p. 239.

ALONSO ZARZA, A.M., CALVO, J.P., and GARCIA DEL CURA, M.A., 1992, Palustrine

sedimentation and associated features--grainification and pseudo-microkarst--in the middle Miocene (Intermediate Unit) of the Madrid Basin, Spain: Sedimentary Geology, v. 76, p. 43-61.

ALONSO-ZARZA, A.M., and WRIGHT, V.P., 2010a, Calcretes, *in* Alonso-Zarza, A.M., and Tanner, L.H., eds., Carbonates in Continental Settings: Facies, Environments and Processes: Developments in Sedimentology: Oxford, Elsevier, p. 225-267.

ALONSO-ZARZA, A.M., and WRIGHT, V.P., 2010b, Palustrine Carbonates, *in* Alonso-Zarza, A.M., and Tanner, L.H., eds., Carbonates in Continental Settings: Facies, Environments and Processes: Developments in Sedimentology: Oxford, Elsevier, p. 103-131.

BATHURST, R.G.C., 1975, Carbonate sediments and their diagenesis, v. 12: Amsterdam, Elsevier Sci. Publ. Co., 658 p.

BENBOW, M.C., ALLEY, N.F., CALLEN, R.A., and GREENWOOD, D.R., 1995, Geological History and Paleoclimate, *in* Drexel, J.F., and Preiss, W.V., eds., The geology of South Australia; Volume 2, The Phanerozoic: Adelaide, Geological Survey of South Australia, p. 208-217.

BÖGLI, A., 1980, Karst hydrology and physical speleology: Berlin, Springer-Verlag, 284 p.

BRASIER, A.T., 2011, Searching for travertines, calcretes and speleothems in deep time: Processes, appearances, predictions and the impact of plants: Earth-Science Reviews, v. 104, p. 213-239.

DREXEL, J.F., and PREISS, W.V., 1995, The geology of South Australia; Volume 2, The Phanerozoic: Bulletin - Geological Survey of South Australia, v. 54, Geological Survey of South Australia, Adelaide, South Aust., Australia, 347 p.

DUNKLEY, J.R., and WIGLEY, T.M.L., 1967, Caves of the Nullarbor; a review of speleological

investigations in the Nullarbor plain, southern Australia, Speleol. Res. Counc.; (Sydney University, Speleological Society-Cave Exploration Group, South Australia), 61 p.

ESTEBAN, M., and KLAPPA, C.F., 1983, Subaerial exposure environment, *in* Scholle, P.A., Bebout, D.G., and Moore, C.H., eds., Carbonate Depositional Environments: Tulsa, American Association of Petroleum Geologists, p. 1-54.

FLÜGEL, E., 2004, Microfacies of carbonate rocks: analysis, interpretation and application: Berlin, Springer-Verlag, 976 p.

FOLK, R.L., ROBERTS, H.H., and MOORE, C.H., 1973, Black Phytokarst from Hell, Cayman Islands, British West Indies: Geological Society of America Bulletin, v. 84, p. 2351-2360.

FORD, D., 1988, Characteristics of dissolutional cave systems in carbonate rocks, *in* James, N.P., and Choquette, P.W., eds., Paleokarst: New York, Springer-Verlag, p. 25-57.

FRISIA, S., and BORSATO, A., 2010, Karst, *in* Alonso-Zarza, A.M., and Tanner, L.H., eds., Carbonates in Continental Settings: Facies, Environments and Processes: Developments in Sedimentology: Oxford, Elsevier, p. 269-318.

GOEDE, A., HARMON, R.S., ATKINSON, T.C., and ROWE, P.J., 1990, Pleistocene climatic change in southern Australia and its effect on speleothem deposition in some Nullarbor caves: Journal of Quaternary Science, v. 5, p. 29-38.

HOCKING, R.M., 1990, Eucla Basin: Geological Survey of Western Australia, v. Memoir 3, p. 548-561.

JAMES, N.P., and BONE, Y., 1991, Origin of a cool-water, Oligo-Miocene deep shelf limestone, Eucla Platform, southern Australia: Sedimentology, v. 38, p. 323-341.

JAMES, N.P., and CHOQUETTE, P.W., 1988, Paleokarst: New York, Springer-Verlag, 416 p.

JAMES, N.P., and CHOQUETTE, P.W., 1990, Limestones - The meteoric diagenetic environment, *in* McIlreath, I.A., and Morrow, D.W., eds., Diagenesis: Ottawa, Geological Association of Canada, p. 35-74.

JOHNSON, D., 2009, The geology of Australia, Cambridge University Press, 355 p.

LANG, R.A., and TUCCI, P., 1997, A preliminary study of the causes of the blackening of pebbles in the Cenomanian "breccia with black pebbles" of Camporosello (Lepini Mountains, Italy): Geologica Romana, v. 33, p. 89-97.

LOWRY, D.C., 1970, Geology of the Western Australian part of the Eucla Basin: Bulletin - Geological Survey of Western Australia, v. 122: Perth, Geological Survey of Western Australia, 199 p.

LOWRY, D.C., and JENNINGS, J.N., 1974, The Nullarbor karst Australia: Zeitschrift fuer Geomorphologie, v. 18, p. 35-81.

MILLER, C.R., JAMES, N.P., and BONE, Y., 2012, Prolonged carbonate diagenesis under and evolving late Cenozoic climate; Nullarbor Plain, southern Australia: Sedimentary Geology, v. 261-262, p. 33-49.

O'CONNELL, L.G., JAMES, N.P., and BONE, Y., 2012, The Miocene Nullarbor Limestone, southern Australia; deposition on a vast subtropical epeiric platform: Sedimentary Geology, v. 253-254, p. 1-16.

PLATT, N.H., and WRIGHT, V.P., 1992, Palustrine carbonates and the Florida Everglades; towards an exposure index for the fresh-water environment?: Journal of Sedimentary Petrology, v. 62, p. 1058-1071.

SHINN, E.A., and LIDZ, B.H., 1988, Blackened limestone pebbles; fire at subaerial unconformities, *in* James, N.P., and Choquette, P.W., eds., Paleokarst: New York, Springer-Verlag, p. 117-131.

STRASSER, A., 1984, Black-pebble occurrence and genesis in Holocene carbonate sediments (Florida Keys, Bahamas, and Tunisia): Journal of Sedimentary Petrology, v. 54, p. 1097-1109.

TUCKER, M., 1990, Diagenetic processes, products and environments, *in* Tucker, M.E., Wright, V.P., and Dickson, J.A.D., eds., Carbonate Sedimentology: Oxford, Blackwell Sci. Publ., p. 314-364.

WEBB, J.A., and JAMES, J.M., 2006, Karst evolution of the Nullarbor Plain, Australia, *in* Harmon, R.S., and Wicks, C.M., eds., Perspectives on Karst Geomorphology, Hydrology, and Geochemistry - A tribute volume to Derek C. Ford and William B. White: Boulder, Geological Society of America p. 65-78.

WHITE, M.E., 1994, After the greening: The browning of Australia: Kenthurst, Kangaroo Press Pty Ltd., 288 p.

WRIGHT, V.P., 1994, Paleosols in shallow marine carbonate sequences: Earth-Science Reviews, v. 35, p. 367-395.

# CHAPTER 2

# PROLONGED CARBONATE DIAGENESIS UNDER AN EVOLVING LATE CENOZOIC CLIMATE; NULLARBOR PLAIN, SOUTHERN AUSTRALIA

Cody R. Miller, Noel P. James and Yvonne Bone

## ABSTRACT

The Nullarbor Plain in southern Australia, the largest areal karst on the globe, is a ~ 240, 000 $km^2$ uplifted succession of Cenozoic marine carbonates whose surface has been exposed for 14 to 15 m.y. The middle Miocene Nullarbor Limestone forms the upper surface of the plain and hosts a complex and prolonged record of meteoric diagenesis. Such a complete record offers unique insights into the effects of climate, tectonics, sea level, topography, and hydrology on the style and placement of numerous diagenetic events in flat low lying carbonate plains. Alteration took place during three broad phases comprising eight stages that are interpreted to have formed against a background of dramatic climate change. Middle Miocene phase one diagenesis took place under a humid climate and resulted in rapid mineral equilibration, calcite cementation, extensive karst development, and finally widespread lacustrine and palustrine sedimentation. Resultant palustrine sediments, especially terrestrial ooids, are now preserved at the surface and in underlying karst cavities. Latest middle Miocene to middle Pliocene phase two diagenesis occurred during a prolonged period (~ 8 m.y.) of temperate climate and resulted in initial deep cave dissolution during low sea levels and later shallow cave development in the

course of a high sea level. Onset of a somewhat more arid climate in the latest Pliocene led to the development of the modern desolate landscape of the Plain. This final phase of diagenesis involved creation of solution pits filled with black limestone pebbles, open and closed dolines with associated colluvium fill, and pervasive pedogenic calcrete. The Nullarbor Plain demonstrates that low lying carbonate plains can have low surfical erosion rates, precisely record relative sea level positions, be able to have extensive caves with extended periods of arrested calcite precipitation, and finally host extensive terrestrial ooid deposits. The importance of this comprehensive paragenetic record is its applicability to not only recognize unconformities in the rock record but to better appreciate the climate in which they formed.

## INTRODUCTION

Subaerial unconformities are of profound importance in carbonate sedimentology and stratigraphy (Esteban and Klappa 1983; James and Choquette 1990; Tucker 1990; Wright 1994; Clari et al. 1995; Hillgaertner 1998; Sattler et al. 2005; Alonso Zarza 2006; Brasier 2011). They are typically sites of intense meteoric diagenesis or dolomitization that forever alters the fabrics of associated carbonate rocks. Prolonged exposure can lead to loss of carbonate, extensive porosity development, calcrete paleosols, and surface and subsurface karst (Esteban and Klappa 1983; James and Choquette 1990; Alonso-Zarza and Wright 2010a; Frisia and Borsato 2010). Such unconformities are of major economic significance because the related karst can host significant hydrocarbon reservoirs and base metal deposits (Brown 1970; Carlisle 1983; Esteban and Wilson 1993). The unconformity itself, because it is a terrestrial feature, also contains subtle but critical information about

past climate and hydrogeologic systems (Esteban and Klappa 1983; James and Choquette 1990; Budd et al. 1995; Alonso-Zarza 2003).

The history of most large unconformities is deciphered by careful analysis of paragenetic features that are then interpreted by comparison with other similar breaks in the geological record. There are, however, relatively few detailed studies of extant subaerial surfaces that have developed via known climate change over prolonged periods of time. This paper is the record of one such surface, the Nullarbor Plain, the largest aerial karst in the modern world (Fig. 2.1). The specific aims of this paper are; 1) to document the depositional and diagenetic changes that took place during 14 my of subaerial exposure, and 2) to discuss the importance of various features when interpreting similar systems in the geological record.

## THE NULLARBOR PLAIN

The Nullarbor Plain is a vast ~ 240,000 km$^2$ planar karst surface that covers almost 1/3 of southern Australia (Fig. 2.1). It faces the Southern Ocean as a series of formidable 50-90 m high sea cliffs and passes imperceptibly northward and landward into the arid heart of the continent. Much of the Plain is a broad undulating surface of low rocky ridges separated by large shallow clay filled depressions, locally known as dongas. The region is sparsely vegetated by shrubby steppe foliage with coastal regions and the Roe Plain, a low marginal coastal plateau lying just above sea level, supporting small eucalypts and acacias (Dunkley and Wigley 1967; Lowry and Jennings 1974). The climate is semi-arid to arid with a marked annual temperature difference from 23° – 26° C in summer to 10° – 12° C in winter (Goede et al. 1990). Annual rainfall ranges from 150 – 250 mm but potential

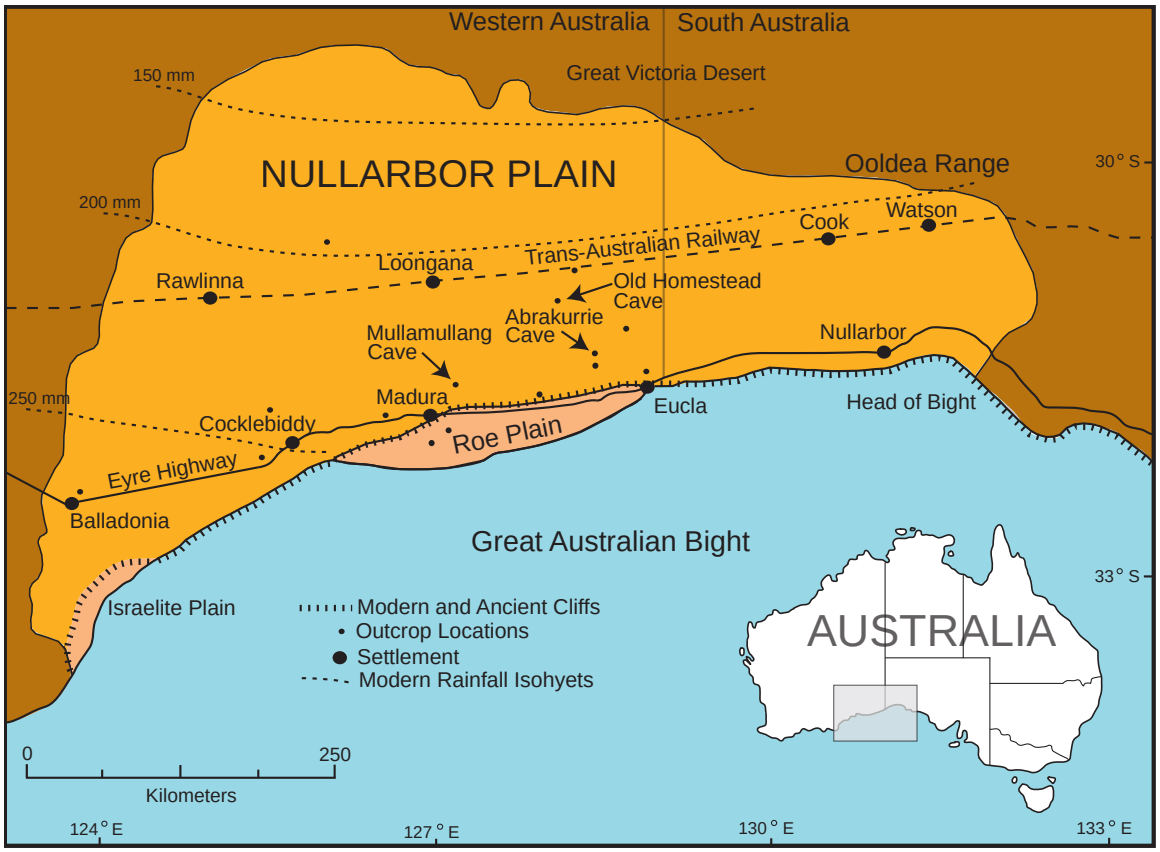


**Figure 2.1.** Nullarbor and Roe Plain location map showing sample sites, modern rainfall isohyets, and important geographic features.

evaporation exceeds 2000 – 3000 mm (Australian Water Resources Council 1976).

Carbonate rocks underlying the Plain are a series of Cenozoic limestones that were deposited in cool to sub-tropical ocean neritic paleoenvironments. They are part of the Eucla Group (Fig. 2.2A), a suite of sedimentary rocks that extends southward beneath the modern continental shelf. The shallow broad epicontinental depression that contains these rocks, the Eucla Basin, is filled by three formations.

The Eocene Wilson Bluff Limestone (maximum thickness 300 m) is a soft, poorly lithified, muddy to chalky bryozoan-rich cool-water carbonate. The overlying Abrakurrie Limestone (maximum thickness 100 m) is a grainy Oligocene – early Miocene neritic, bryozoan-rich, cool-water carbonate that is somewhat better lithified than the Wilson Bluff and contains numerous hardgrounds (Lowry 1970; Hocking 1990; James and Bone 1991). The middle Miocene Nullarbor Limestone (maximum thickness 45 m) that forms the top of the Eucla Group and the surface of the Nullarbor Plain is, by contrast, a hard abundantly fossiliferous sub-tropical deposit (Lowry 1970; O'Connell et al. 2012). The grainstone to rudstone lithology is laterally extensive, extremely fossiliferous, and dominated by numerous large and small benthic foraminifers, corals (zooxanthellate and azooxanthellate), coralline algae (encrusting and articulated), gastropods, bivalves, and echinoids (Lowry 1970; Hocking 1990; O'Connell et al. 2012).

Deposition of the Eucla Group was abruptly terminated by late middle Miocene tectonic uplift of the whole southern margin of the continent that accompanied initial subduction of northern Australia beneath Indonesia (Hocking 1990; Dickinson et al. 2002; Sandiford 2007; Hou et al. 2008). Such uplift was amplified by coeval Antarctic glaciation that resulted in a major eustatic sea-level fall. Thus, most of the Nullarbor Plain is a ~14 m.y. old exposure surface (Fig. 2.2B). The only exception is the Roe Plain (Fig. 2.1). This

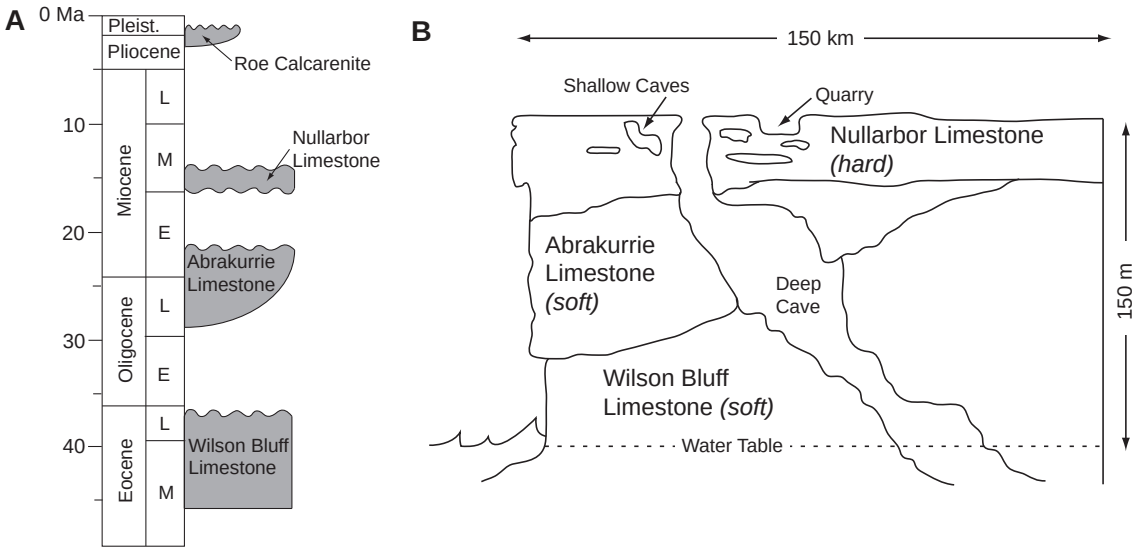


**Figure 2.2.** A) Stratigraphic column of the central Eucla Basin since the middle Eocene. B) Diagrammatic cross-section showing the lithologic units and major caves underlying the Nullarbor Plain surface (modified from James and Bone, 1991).

narrow plain is a younger late Pliocene erosion surface that is cut into older Cenozoic carbonates in the central part of the Great Australian Bight (Lowry 1970; James et al. 2006). Since uplift, meteoric diagenesis, as a result of this study, is now recognized as having taken place during 3 discrete phases over a known climate change event (Table 2.1).

## METHODOLOGY

This is largely a field study with a total of 21 locations examined across the Nullarbor Plain. Outcrops are restricted to dolines, railway embankments, road cuttings, and quarries (Fig. 2.2B). Such exposures are not numerous and are typically separated by considerable distances; the modern sea cliffs are overhanging and largely inaccessible. Emphasis was placed on carefully documenting cross-cutting relationships in the upper 20 m of the Nullarbor Limestone.

Hand samples of all lithologies and diagenetic phases were collected from 16 of the sites (Fig. 2.1). Polished thin sections were prepared from these samples and analyzed with standard transmission light microscopy. Colours of the different diagenetic fabrics are expressed in terminology defined by the Munsell colour chart. Bulk mineralogy was determined using x-ray diffraction (Hardy and Tucker 1988). Samples were subsequently selected for oxygen and carbon stable isotope analyses using techniques outlined by Kyser (1987). Oxygen and carbon isotope data are reported relative to the Pee Dee Belemnite (PDB) reference standard.

**Table 2.1**
Nullarbor Plain Diagenetic Phases

| Phase | Age | Description | Interpretation | Climate |
|---|---|---|---|---|
| **Phase 3 – Arid Paleosols** | | | | |
| Stage 8<br>Accretionary<br>Pedogenic Calcrete | Pleistocene to Recent | - accretionary pedogenic calcrete forms the modern surface of the Nullarbor Plain<br>- basal laminar calcrete grading up into calcrete pisoids and blocky fabric, abundant quartz | - pedogenic calcrete formation signifies the first dominant arid climate conditions<br>- laminar fabrics and calcrete pisoids have microbial features | Arid |
| Stage 7<br>Dolines & Colluvium | Pleistocene | - deep (largest) and shallow (smallest) dolines<br>- collapse breecia at base of dolines<br>- infill of red colluvium with abundant biologic and evaporative fabrics in shallow dolines | - created by roof collapse of deep and shallow caves<br>- infill of shallow dolines is episodic<br>- isotope values illustrate an organic influence and open meteoric conditions | Semi-Arid to Arid |
| Stage 6<br>Subsoil Hollows | late Pliocene | - shallow paleokarst depressions, consistent size and shape<br>- infilled with breecia composed of blackened clasts, parent clasts, gastropods, and first appearance of quartz | - hollows are formed under trees through stem flow drainage processes<br>- represent the last large trees on the Nullarbor Plain<br>- first appearance of aeolian quartz grains signify a loss of surface vegetation | Semi-Arid |
| **Phase 2 – Caves** | | | | |
| Stage 5<br>Shallow Caves &<br>Precipitates | Pliocene | - widespread shallow cave dissolution<br>- located wholly in the Nullarbor Limestone<br>- occur in isolated clusters of chambers cm - m scale with common connecting passages to surface | - shallow caves formed at a high water table during a humid climate interlude in the Pliocene<br>- calcite speleothems precipitated with later Pleistocene salt precipitation | Humid |
| Stage 4<br>Deep Caves | middle Miocene to Pliocene | - localized to 60 km zone along the present day coast<br>- long linear passages with domal cross-sections<br>- abundant tafoni structures on cave walls<br>- distinct lack of calcite decoration | - early dissolution of deep caves initiated along fractures<br>- isolated to coast because of rainfall amount<br>- dissolution at fluctuating deep water table then phreatic dissolution during the Pliocene humid interlude | Humid to Temperate |
| **Phase 1 – Microkarst and Sedimentation** | | | | |
| Stage 3<br>Post-Karst<br>Sedimentation | middle Miocene | - infill of cavities with ooids, parent clasts, dense micrite with charophytes and ostracods | - formation of large scale lacustrine systems across Nullarbor Plain, later overprinted by palustrine processes<br>- palustrine alteration produces copious amounts of ooids that now fill the underlying microkarst cavities | Humid to Temperate |
| Stage 2<br>Microkarst | middle Miocene | - extensive (10 - 75 %) dissolution of Nullarbor Lst.<br>- fabric selective dissolution, cm to deci-meter scale cavities with smaller interconnecting conduits | - meteoric waters diffuse through barren limestone surface<br>- dissolution at fluctuating water table<br>- deposition of lacustrine sediments on surface and into underlying microkarst with later palustrine modification | Humid to Temperate |
| Stage 1<br>Fabric Specific<br>Diagenesis | middle Miocene | - deposition on a shallow temperate water carbonate platform<br>- subaerial aragonite allochem dissolution<br>- intergranular sparry meteoric calcite precipitation | - uplift and exposure of middle Miocene sea floor<br>- sparry calcite precipitation from $CaCO_3$ rich fluids derived from aragonite dissolution<br>- lithification of Nullarbor Limestone | Humid |

## THE NULLARBOR UNCONFORMITY

General aspects of the Nullarbor karst system have been previously documented by King (1950), Jennings (1963), Dunkley and Wigley (1967), Goede et al. (1990), Turney et al. (2001), and Webb and James (2006). This research builds on these studies but focuses on carbonate diagenesis and paragenesis. Meteoric diagenesis, as a result of this study, can now be recognized as having taken place during 3 discrete phases composed of eight different stages (Fig. 2.3).

## PHASE 1 – MIDDLE MIOCENE MICROKARST AND SEDIMENTATION

Phase 1 was the most widespread phase of diagenesis in Nullarbor Plain history. Such diagenesis and associated sedimentation occurred in three stages: 1) lithification of the Nullarbor Limestone, 2) dissolution and microkarst, and 3) surfical and internal sedimentation.

### *Stage 1 – Fabric specific diagenesis*

**Description.—**The Nullarbor Limestone today is a fossiliferous grainstone to rudstone that has been extensively cemented by diagenetic low-Mg calcite spar, except at Cook quarry (Fig. 2.1) (O'Connell et al. 2012). Gastropods, infaunal bivalves, and corals that form aragonitic skeletons in modern marine realms, are common as moulds throughout the Nullarbor Limestone. Mouldic components form approximately 0 – 40 % of the Nullarbor Limestone with calcitic fossils ranging from 60 – 100 % (O'Connell et al. 2012).

**Interpretation.—**The well lithified nature of the limestone is interpreted to have resulted

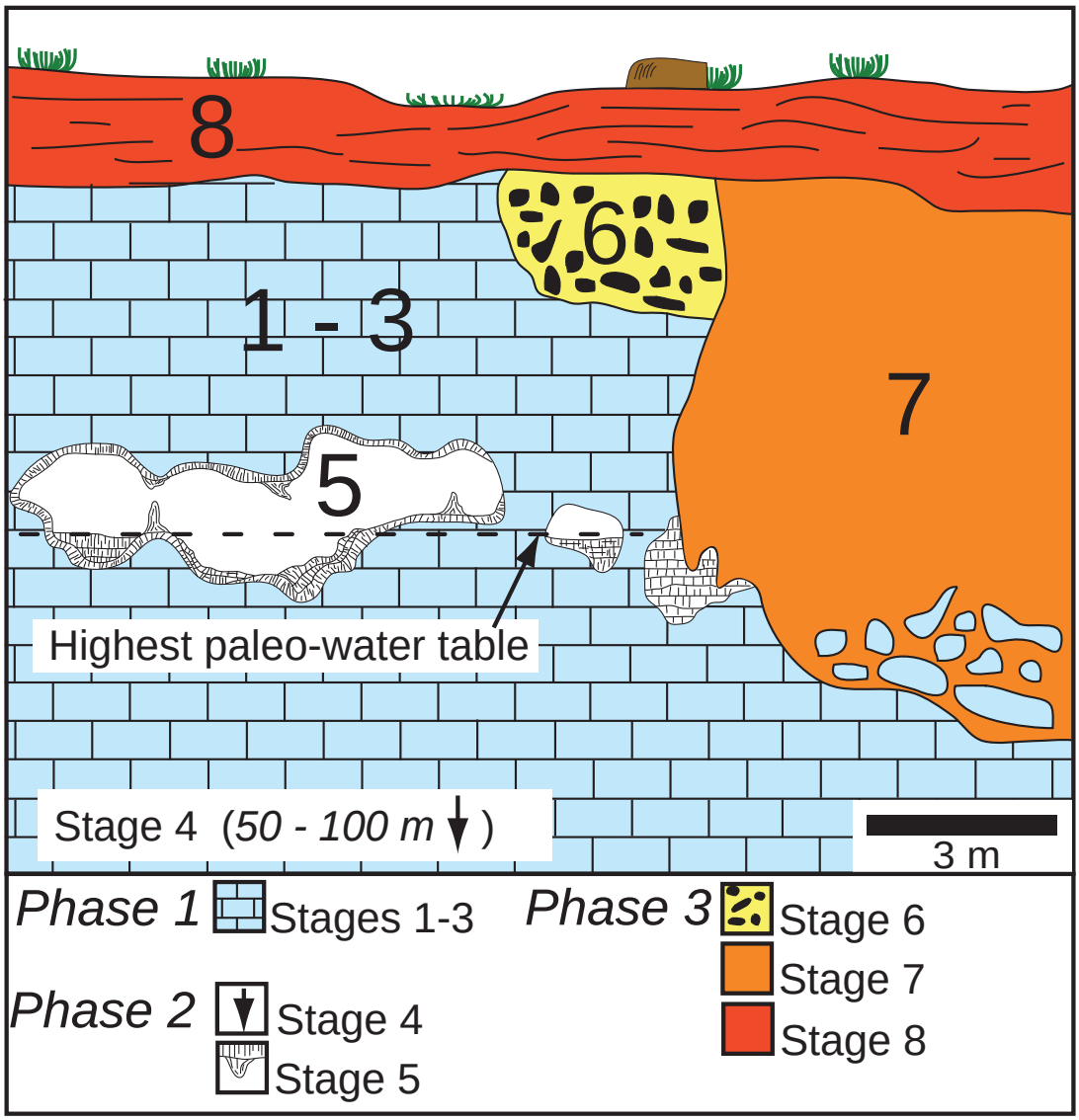


**Figure 2.3.** Diagrammatic cross section of the uppermost 20 meters of the Nullarbor Limestone showing the nature and cross-cutting relationships of the eight phases of diagenesis preserved on the surface and in the shallow subsurface of the Nullarbor Plain. Stage 1 – Fabric selective diagenesis; Stage 2 – Microkarst; Stage 3 – Post karst sedimentation; Stage 4 – Deep caves (located in underlying formations); Stage 5 – Shallow caves and precipitates; Stage 6 – Subsoil Hollows; Stage 7 – Dolines & Colluvium; Stage 8 – Accretionary pedogenic calcrete.

from early calcite cementation wherein the carbonate was derived from dissolution of the numerous aragonite biofragments, a common process in young limestones exposed in the meteoric environment (Bathurst 1975; James and Choquette 1990). The only Nullarbor Limestone to remain friable and contain little cement is at Cook Quarry (Fig. 2.1) where the original sediment lacked aragonite bioclasts. All calcitic allochems were changed to diagenetic low-mg calcite during early meteoric diagenesis.

*Stage 2 – Microkarst*

**Description.—**Microkarst is defined herein as cavities that range in size from 2 to 30 cm. Such cavities are restricted to the upper 25 m of the Nullarbor Limestone wherein the complex network is interconnected by small 0.1 – 2.0 cm diameter conduits (Fig. 2.4A). It is estimated that approximately 25 % of the Nullarbor Limestone is represented by microkarst cavities with local variations ranging between 10 and 75 %.

Dissolution preferentially left most diagenetically stable biofragments unaffected and instead was focused in fine grained lithologies. Cavities have digitate margins, smooth floors, and rare vertical stoping features. They are typically vuggy with wide vertical and lateral heterogeneity, although locally they occur as crudely stratified microkarst horizons.

Cook Quarry (Fig. 2.1) is the only location where microkarst is not present and is also the only locality with friable limestone. The quarry walls are instead chalky bioclastic grainstone that is cross-cut by 10 – 15 m wide vertical conduits that are filled with pisoids and Nullarbor Limestone clasts.

**Interpretation.—**Nullarbor microkarst developed under a sub-humid to temperate climate during the middle Miocene in southern Australia (White 1994; Alley et al. 1999; Johnson 2009). Initial microkarst is interpreted to have been open to the surface and developed

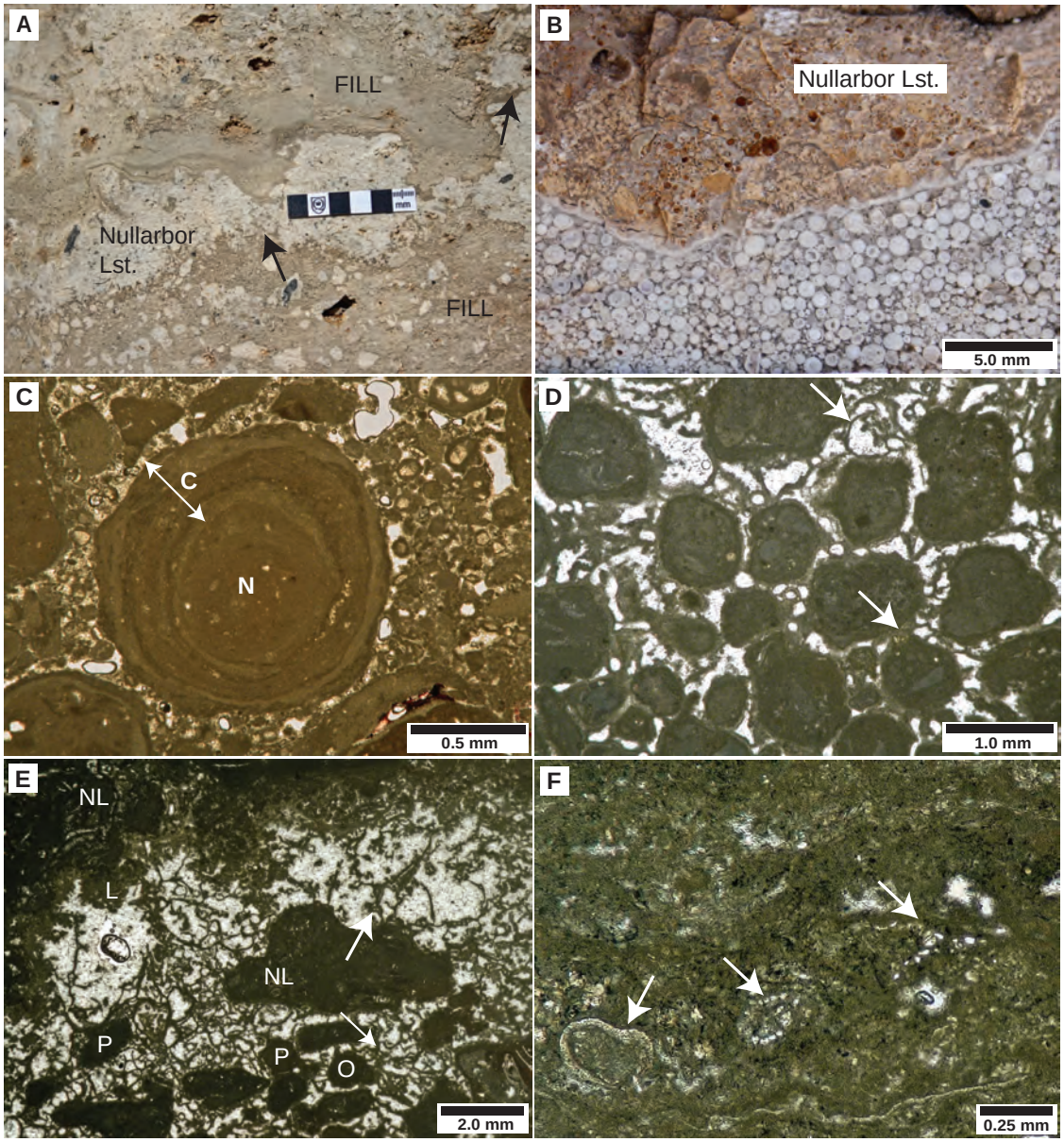


**Figure 2.4.** Phase 1. A) Microkarst cavity in outcrop showing irregular boundaries at Watson Quarry. Arrows point to small connecting conduits. B) Microkarst cavity fill composed entirely of ooids at Eucla Quarry. (C) Photomicrograph in plane polarized light (PPL) of individual ooid, showing dense micrite nucleus (N) and multigenerational laminated cortex (C). D) Photomicrograph (PPL) of ooids with micritic filaments bridging and binding grains (arrows). The micrite filaments show branching and curved morphology; Eucla Quarry. E) Photomicrograph (PPL) of microkarst cavity at Rawlinna Quarry showing a gradual transition from Nullarbor Limestone (NL) to a dendritic and clotted micrite lining (L), then to ooids (O) and peloids (P) being bound and supported by filamentous fabrics (arrows). Sparry calcite cement completely fills the pore spaces. F) Photomicrograph (PPL) showing dense micrite, micrite laminations and scattered poorly preserved charophyte fragments (arrows) in a microkarst cavity at Rawlinna Quarry.

shortly after the lithification of the Nullarbor Limestone. Lack of speleothems that would be expected from soil $pCO_2$ degassing in cavities connected to the surface, implies that dissolution occurred beneath a barren or partially soil covered limestone surface (Ford 1988; James and Choquette 1988; White 1988; Frisia and Borsato 2010). The flat and featureless surface paleokarst is similar to low lying and flat karst plains elsewhere where surface karsting is replaced by extensive subsurface dissolution (Ford 1988; Worthington et al. 2000; Webb and James 2006). Vertical stoping, digitate roofs, and lack of phreatic features imply mostly vadose zone corrosion in rapidly shifting water table levels (Ford 1988; James and Choquette 1988). The low porosity and permeability is thought to have inhibited diffusive vadose groundwater movement and focused fluid flow along specific dissolution pathways. This is evident at Cook quarry where the friable grainstone lithologies show no evidence of microkarst dissolution.

### *Stage 3 – Post-Karst Sedimentation*

#### *Description*

Post-karst sediments occur in the microkarst cavities described above and are only found on the surface of the Nullarbor Limestone at Cook quarry (Fig. 2.1). These unstratified sediments are composed of 1) small allochems, 2) filamentous and alveolar micrite, and 3) biomicrite and laminations.

**Allochems.—**These grains are found in microkarst cavities across the Nullarbor Plain, and are preserved as an ~ 1 m thick section on the surface of the Nullarbor Limestone at Cook quarry. The particles comprise, in order of abundance, sand – size ooids, peloids, coated grains, Nullarbor Limestone fragments (0.5 – 30.0 mm in size), and small (<5 mm) black carbonate clasts.

Post-karst sediments range from only ooids (common), to only peloids (rare) or both (exceptionally rare). The peloids are either single large grains (0.5 to 5 mm) or they form an ooid nucleus. Such particles are dense structureless micrite and somewhat less spherical than ooids. These grains, when an ooid nucleus, rarely contain small unidentifiable bioclasts and charophyte fragments. Peloids, other than those in an ooid nucleus, typically contain the most bioclastic fragments.

Ooids are well-rounded and sand-size (0.5 – 2.2 mm) with a large peloidal nucleus and a thin (25 – 100 μm) laminated micrite cortex (Fig. 2.4B – C). They are poorly sorted although inverse grading occurs locally in isolated cavities. Clotted micrite and dark organic material is present but minor in the nucleus and cortex.

**Filamentous and Alveolar Micrite.—**Microkarst cavities are locally lined by micrite with a dendritic fabric and clotted texture. Such linings grade laterally into branching micritic filaments, alveolar fabrics, and particles, examples of which are also seen in the surface deposits at Cook quarry (Fig. 2.4D). Anastomosing micrite filaments (25 – 50 μm thick) create a complex intergranular network in ooid-filled cavities (Fig. 2.4D – E). They connect and bridge between ooids and each other creating a web-like network. Some filamentous structures have a curved morphology that branches and protrudes into interparticle voids (Fig. 2.4E). Ooids are locally bound together by these fabrics and there are few grain-to-grain contacts. Alveolar fabrics are associated with more dense micrite fills wherein small tubules filled with calcite cement are common. Clear sparry calcite cement fills open spaces inside and between the alveolar and filamentous fabrics.

**Laminated Micrite.—**These sediments together with sparry calcite cement are not present at Cook quarry but the floors of microkarst cavities and comprise moderate brown laminated and clotted micrite and microspar. Laminations are composed of millimeter

to sub-millimeter thick layers and are bounded by minor amounts of botryoidal calcite cement. Vermiform fabric (Armenteros and Daley 1998) with small voids filled with sparry calcite cement is locally associated with laminated fills. The vermiform fabric comprises thin (50 – 75 μm) micrite networks, with double micritic linings (10 μm thick) and circular voids. Rare circular charophyte fragments < 100 μm in size (Fig. 2.4F), whole charophyte gyrogonite forms (Freeman et al. 1982; Platt 1989; Alonso Zarza et al. 1992; Climent-Domènech et al. 2009; Alonso-Zarza and Wright 2010b; Renaut 2010) and ostracods in these micritic fills are fragmented, and poorly preserved.

*Interpretation*

**Ooids & Peloids.—**Complete absence of marine bioclasts and the presence of fresh to brackish water biofragments implies that these coated particles are not marine in origin; instead are terrestrial. Non-marine ooids can form in many different lacustrine, palustrine, and calcrete environments (Siesser 1973; Popp and Wilkinson 1983; Alonso-Zarza and Wright 2010b). Nullarbor Plain ooids' close association with charophytes and ostracods suggests that they are lacustrine or palustrine. Lacustrine ooids precipitated out of fresh or brackish water typically have radial aragonite composition resulting in widespread grain dissolution fabrics (Halley 1977; Milroy and Wright 2002; Gierlowski-Kordesch 2010; Renaut and Gierlowski-Kordesch 2010). They can also be micritic like those from the Nullarbor, however, such ooids would be bedded and well sorted. This aspect is not present on the Nullarbor Plain. Ooids formed in palustrine environments are again micritic, but host only trace fabrics and bioclastic remnants of the former lacustrine sediments, lack sedimentary structures, are poorly sorted, and have a thin laminated micrite cortex (Alonso Zarza et al. 1992; Platt and Wright 1992; Armenteros and Daley 1998; Freytet and Verrecchia

2002; Alonso-Zarza and Wright 2010b).

The oolites herein are most similar in appearance and composition to those described from palustrine settings (Alonso Zarza et al. 1992; Armenteros and Daley 1998; Freytet and Verrecchia 2002; Alonso-Zarza 2003; Alonso-Zarza and Wright 2010b; Armenteros 2010) and are interpreted as such. Their formation is poorly understood overall, but it appears that they are not precipitated out of water, but are formed via sediment binding and grainification caused by pedogenic process and microbes (Alonso Zarza et al. 1992; Armenteros and Daley 1998; Miller and James in press).

**Filamentous and Alveolar Micrite.—**The terms alveolar and vermiform fabric have traditionally been used to described preserved remains of roots and associated cellular structures (Klappa 1978; Klappa 1979; Wright 1988; Armenteros and Daley 1998). The fabrics documented in structureless micrite fill here are interpreted to have a similar origin. Filamentous fabrics bind the ooids and are also organic (Hillgärter et al. 2001). Various microorganisms are capable of producing these structures, but cyanobacteria and fungi have been shown to form calcified epi – and chasmolithic filaments under vadose conditions (Wright 1986; Hillgärter et al. 2001). Filaments that are straight and regular in thickness could represent chasmolithic networks of *Bacinella irregularis* (Hillgärter et al. 2001). Microkarst cavity linings are also thought to be the result of high organics and the presence of microbes in a vadose setting (cf. Hillgärter et al. 2001), producing the clotted, branching and radiating fabrics that record the transition into micrite filaments.

**Depositional History.—**Microkarst cavity sediment has a uniform character across the Nullarbor Plain and is similar to the surfical sediments at Cook quarry, indicating similarity of origin. The extensive micrite sediment with rare and poorly preserved ostracods and charophytes is interpreted to represent original lacustrine deposits (Esteban and Klappa

1983; Alonso Zarza et al. 1992; Wright et al. 1997; Milroy and Wright 2002). Lacustrine sediments were deposited on the surface of the plain in their original depositional environment and also in the underlying microkarst cavity networks that were open to the surface.

Lacustrine sediments were then altered through pedogenesis in a palustrine setting where the original depositional nature of the lacustrine sediment was lost. Palustrine environments develop when lacustrine systems desiccate and are replaced by soils whose formative processes altered the lake sediments (Fig. 2.5) (Armenteros and Daley 1998; Alonso-Zarza and Wright 2010b; Renaut and Gierlowski-Kordesch 2010). Absence of distinctive original lacustrine fabrics and the abundance of palustrine ooids, peloids, fossil fragmentation, and intensity of pedogenic modification seen in Nullarbor microkarst cavities and on the surface at Cook quarry when compared to examples elsewhere indicate that the components are relatively mature and would have developed over an extended period of time (Alonso Zarza et al. 1992; Armenteros and Daley 1998). The formation of peloids, ooids, and filamentous micrite associated with palustrine modification not only took place inside the cavities but on the surface as well, in similar soil conditions.

The interpreted lacustrine and palustrine sediments are not preserved as surfical deposits, except at Cook quarry where a thin (~1 m) section exists on top of the Nullarbor Limestone. These grains are the only record of such a lake or system of lakes that are otherwise preserved in the microkarst cavities; most of lake floor sediment has since been removed by surfical erosion and subsequent diagenesis.

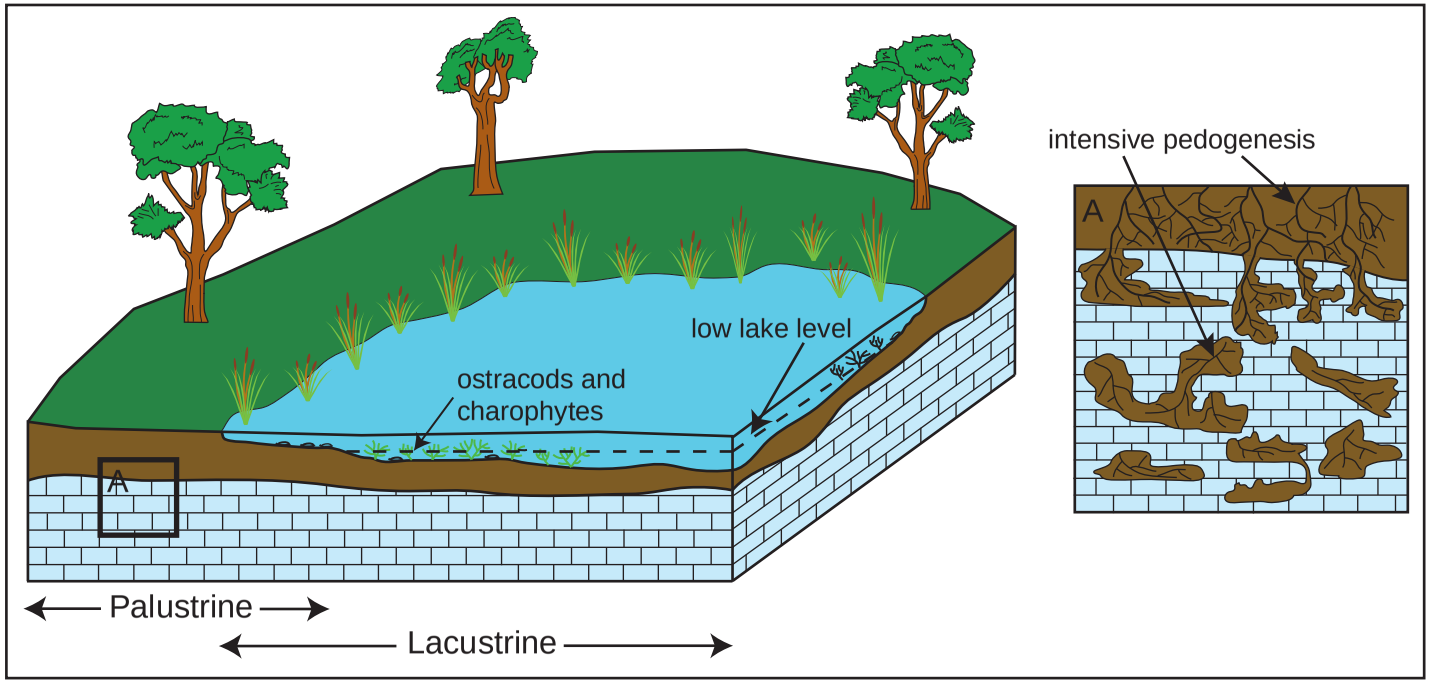


**Figure 2.5.** Paleogeographic reconstruction of phase 1 that illustrates the transition between lacustrine deposition and palustrine alteration. Lacustrine sediments are pedogenically altered when they are exposed to palustrine environments. This occurs in both the extensive microkarst cavities and on the surface.

## PHASE 2 – LATE MIOCENE TO PLIOCENE CAVES

The Nullarbor Plain is renowned for hosting one of the largest cave systems in the world. Cave formation involved extensive dissolution of enclosing lithologies including phase 1 alteration fabrics described above. The caves are categorized and defined in terms of their depths as 'deep' or 'shallow' (Jennings 1963; Dunkley and Wigley 1967; Lowry and Jennings 1974; Webb and James 2006).

### *Stage 4 – Deep caves*

**Description.—**Deep caves are the largest paleokarst features, extending 50 – 150 m below the surface and host extensive passages (e.g. >30 km of surveyed passages in Old Homestead Cave) (Webb and James, 2006). These large features cross-cut regional stratigraphy and are best developed in the soft Wilson Bluff Limestone. The caves are localized to a 60 km wide zone that parallels the coastline. Cave passages orientated NNW/SSE and E/W are simple, can be large (~ 10 m high and 20 m wide), and consist of long straight halls linked by rounded bends (Fig. 2.6A). They have rounded and smoothly arching walls with abundant tafoni structure (Jennings, 1963). The passages and chambers have flat or domal roofs that are typically a more resistant lithology, such as the overlying Abrakurrie Limestone (Fig. 2.6A). They are relatively horizontal and have steep drop offs into lower passages, giving a stepped morphology. Few deep caves have any calcite decoration on their walls; instead they are locally adorned with gypsum and halite crusts (Caldwell et al. 1982; Goede et al. 1990).

**Interpretation.—**Deep cave development in the Nullarbor Plain was localized to and parallels the highest modern isohyets that are near the coast (Fig. 2.1). Trend of higher

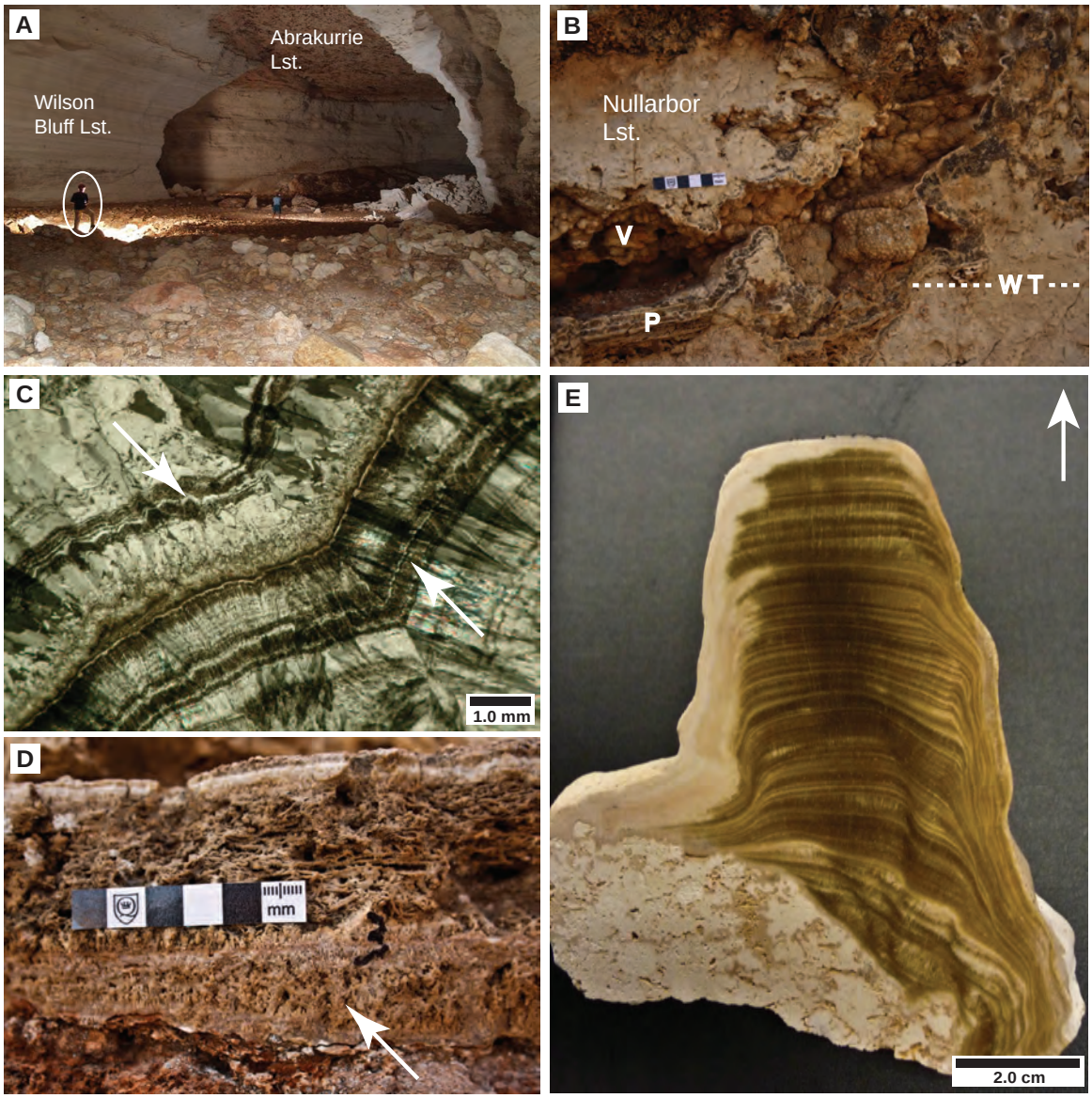


**Figure 2.6.** Phase 2. A) Photograph of Abrakurrie Cave, Western Australia, showing a large passage sculpted into the Wilson Bluff Limestone with Abrakurrie Limestone forming the roof. Person is circled for scale. (Image courtesy S.J. Milner and C.E.G.S.A.) B) Shallow cave chamber (stage 5) showing vadose (V) and phreatic (P) phases of calcite precipitation, representing the position of a paleo-water table (WT). Located at Watson Quarry. C) Photomicrograph in cross-polarized light (XPL) of multigenerational radial fibrous calcite cements in phreatic cement. Arrows point to the inclusion rich zones along the boundaries between different crystal growth segments; Watson Quarry. D) Branching networks of low-Mg calcite tufa cements (arrow) with overlying layers of thin plates of calcite cements creating zones of extensive porosity; Watson Quarry. E) A stalagmite formed in a shallow cave approximately 12 meters below the ground surface. Dark and light brown colours denote the different periods of growth in the speleothem; Rawlinna Quarry.

rainfall towards the coast would have been similar during this phase of cave development. This could explain why deep caves are more abundant closer to the coastline as more precipitation occurred along this zone.

Dissolution of deep caves in the Nullarbor Plain is interpreted to have begun at a deep fluctuating water table in older, less resistant carbonate lithologies, such as the Wilson Bluff Limestone, after phase 1 alteration. Cave passage and entrance orientations coincide with major joint sets on the Nullarbor Plain (Jennings 1963; White 2002; Sandiford et al. 2009). Such relationships can be further linked to surface undulations interpreted to be structural lineations that are related to underlying faults (Hou et al. 2008; Sandiford et al. 2009). This is particularly apparent in digital elevation models (DEM) as numerous lineations align across the Nullarbor Plain (Fig. 2.7A). Mullamullang Cave and its underground passage orientations coincide precisely with overlying surface topography, further supporting this interpretation (Fig. 2.7B). Cave entrances at Abrakurrie Cave, Chowilla Doline, Winbirra Cave, and numerous other dolines along the same trend show a similar relationship where the entrance dolines follow the exact orientation of the main cave passage in Abrakurrie Cave (Fig. 2.7C). Tafoni structures on deep cave walls point to later periods of turbulent phreatic water flow in the cave passages, leading to rapid dissolution of the surrounding limestone and enlargement of the cave passages (Jennings 1963; Goede et al. 1990; White 2002). The planar morphology of cave passages and tafoni structures indicates that two periods of dissolution occurred in deep caves, the first at a deep water table and the second under phreatic conditions.

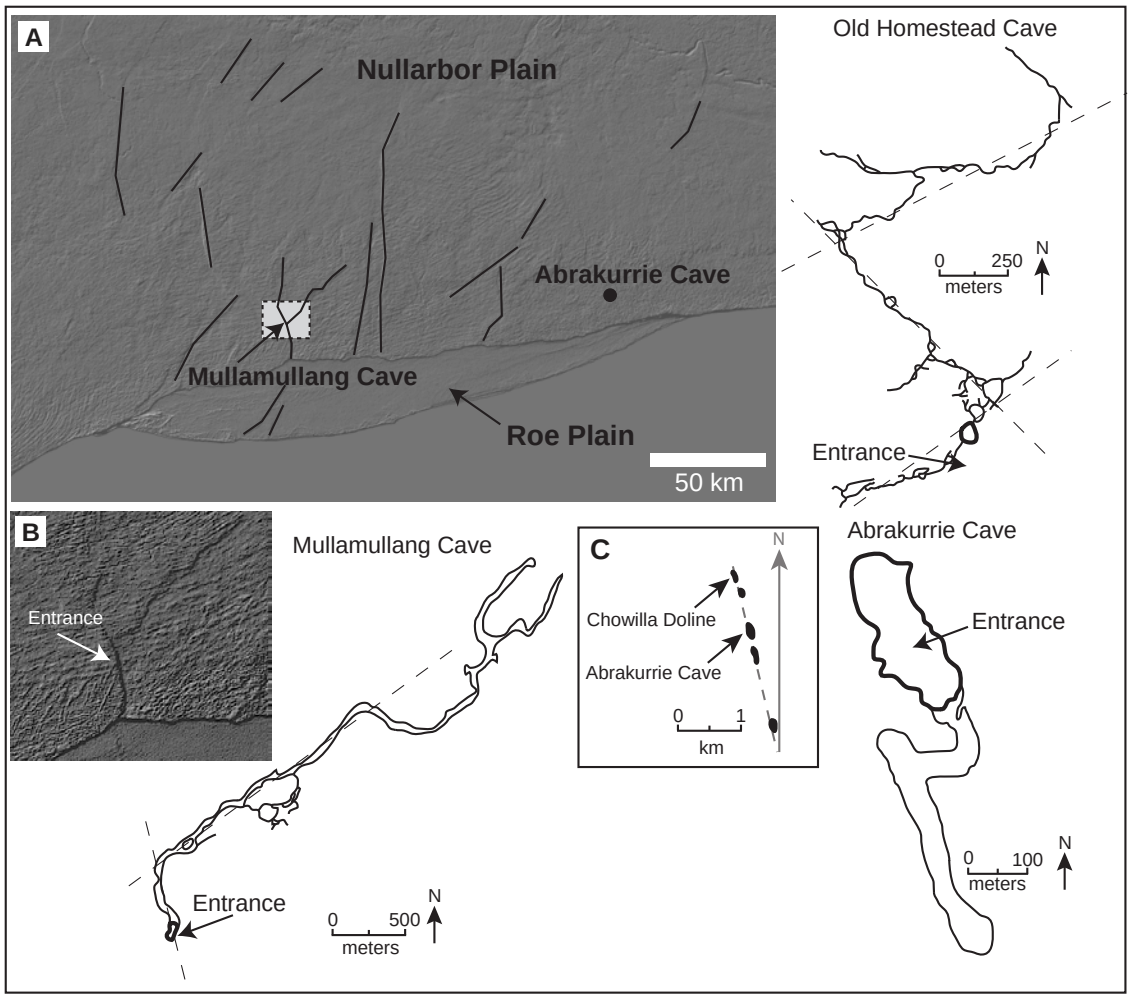


**Figure 2.7.** Diagrammatic illustration outlining surface lineations to stage 4 deep cave passage orientations. A) Digital Elevation Model (DEM) of the Nullarbor Plain showing subtle NNW/SSE and E/W variations in surface topography interpreted to represent structural lineaments. Inset is a map of the passages in Old Homestead Cave showing a preferred alignment (dashed lines) along the structural orientation presented in the DEM image. B) Map of passages in Mullamullang Cave showing the preferred alignment of cave passages to the orientation of structurally controlled surface lineations (dashed lines). C) Illustration showing alignment of deep cave entrances along the same orientation of Abrakurrie Cave's main passage. This alignment also parallels the structural lineations shown on the Nullarbor Plain surface. (Cave maps modified from C.E.G.S.A. 1986)

*Stage 5 - Shallow caves & precipitates*

*Description*

**Caves.—**Shallow caves, in the form of horizontal tubes and vertical shafts or chambers occur in the Nullarbor Limestone across the entire Plain, and are well exposed in the dolines of larger deep cave entrances and in quarry walls. The features typically extend 6 – 12 m below the modern ground surface, range in size from 0.25 – 20 m, and occur as isolated clusters of chambers and passages (0.05 – 0.20 m in diameter) (Fig. 2.6B). Shallow caves in the north are at a slightly higher elevation than those near the southern coast. Most chambers connect to the paleo-exposure surface through narrow (0.15 – 0.75 m) vertical to sub-vertical feeder conduits. Dissolution is neither fabric- nor lithology-selective and cross-cuts all pre-existing phases.

**Paleo-phreatic Precipitates.—**Isopachous low-Mg calcite precipitates line shallow cave walls as multigenerational, radial-fibrous, dendritic, and botryodial calcite coatings that vary in thickness from 2 – 15 cm. Such cements completely fill the basal parts of cavities. These radial-fibrous precipitates have sweeping extinction under cross polarized light and are clear, with a speckled appearance under plane polarized light (Fig. 2.6C). Botryoidal calcite cements are less numerous and typically occur in isolated clusters surrounded by radial-fibrous cements. Dark inclusions along growth layers are common in all of the phreatic cement stages (Fig. 2.6C). Isolated zones of dendritic or “shrubs” of branching and layered plates of low-Mg calcite tufa cements are commonly found at the bases of shallow caves, with extensive porosity (Fig. 2.6D).

**Paleo-vadose Precipitates.—**Low-Mg calcite, in the form of speleothems, flowstones, and crystal rafts, occur in the upper sections of shallow cave systems, abruptly overlying the previous forms. Such cements are light brown to moderate brown in colour and occur as

multigenerational layers. Stalagmites and stalactites are rare in the smaller caves, but when present are exceptionally well preserved (Fig. 2.6E). Cement morphologies are dominantly radial-fibrous in speleothems and flowstones. Elongate blocky and sparry calcite raft precipitates are encased in thin laminations of dark brown micrite and concentrated in distinct high porosity layers (Taylor and Chafetz 2004). These calcite cement fabrics are locally crusted with later halite and gypsum causing destruction of many previous calcite forms.

*Interpretation*

**Shallow caves.—**Shallow caves occur across the Nullarbor Plain and thus indicate a regional dissolution event. The regional similarity in cave depth below the surface, together with both phreatic tubes and vadose cavities indicate that corrosion occurred at a relatively shallow and stable water table (cf. Esteban and Klappa, 1983; James and Choquette, 1990). This would indicate a low north to south hydraulic gradient, much like the modern day Nullarbor Plain (Webb and James, 2006). The high water table is probably closely related to the Pliocene sea level highstand event coinciding with formation of the coastal Roe plain and deposition of the Roe Calcarenite (cf. James et al., 2006).

**Cave precipitates.—**Precipitation of calcite cement within the shallow caves occurred in two stages. Earliest precipitates are interpreted to have formed in phreatic cave environments. The presence of phreatic cements lining the basal sections of shallow cave chambers with stalactites directly covering them define falling paleo-water tables (Fig. 2.6B). These represent the highest water table positions preserved in the Nullarbor Plain dated to be 2.9 to 4.09 Ma (Woodhead et al. 2006; Blyth et al. 2010).

Speleothems, flowstones, and other vadose cements always encrust phreatic cements

and decrease in abundance as the cave depth increases. The abrupt transition between phreatic and vadose cement fabrics and the relative immaturity of vadose precipitates implies a relatively rapid drop in water table levels coupled with a decrease in groundwater $CaCO_3$ saturation. Alternations between dark brown and tan colours in Nullarbor calcite cements has been linked to high concentrations of intensely coloured humic compounds, sourced from overlying vegetation (Caldwell et al. 1982; Blyth et al. 2010).

## PHASE 3 – PLEISTOCENE TO RECENT ARID PALEOSOLS

The most recent phase of diagenesis on the Nullarbor Plain records the trend towards increasing aridity in central Australia. This phase includes 3 progressively more arid stages of diagenesis: 1) surface hollows filled with black limestone clasts, 2) shallow dolines filled with distinctive moderate red sediment composed of colluvium and larger deep dolines that form the entrances to deep caves, and finally 3) pedogenic calcrete, which forms the present day surface of the Nullarbor and Roe Plains.

### *Stage 6 Subsoil Hollows*

#### *Description*

Nullarbor Plain subsoil hollows are isolated and shallow depressions, 1 – 2 m in depth and diameter that are of consistent size everywhere. Their distribution is random and are scattered through doline and quarry walls, and on the surface in low rocky ridges where calcrete is thin or absent. The hollows have sharp, well defined dissolution edges that cross-cut all previous diagenetic phases (Fig. 2.8A). Promontories of Nullarbor Limestone locally protrude into the cavities leading to irregular boundaries (Fig. 2.8B).

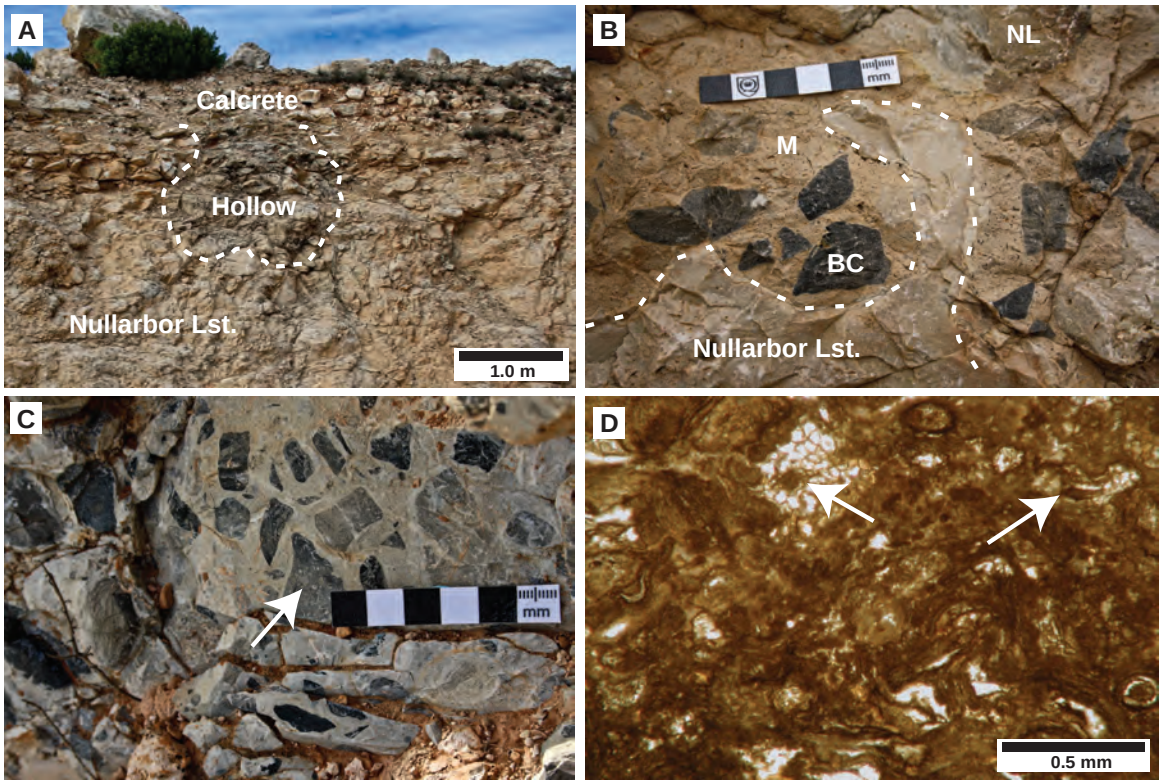


**Figure 2.8.** Stage 6. A) Subsoil hollow in Nullarbor Limestone with infill of blackened limestone clasts. B) The boundary of hollow showing the sharp margins and a promontory of parent lithology sticking into the cavity (dashed line). Components of the fill are comprised of blackened limestone clasts (BC), Nullarbor Limestone clasts (NL) and dense micritic matrix (M); Eucla Quarry. C) Blackened clasts in a subsoil hollow that show an assortment of black colouration in different clasts inside the same hollow. Arrow points to one such clast that has a differential degree of blackening across its width; Forrest. D) Photomicrograph (PPL) of a blackened clast in Eucla Quarry subsoil hollow showing a complex and contorted internal fabric. Honeycomb shaped structures (arrow) are common in the internal fabric of blackened clasts.

Hollows are filled with a distinctive breecia whose components are similar across the Nullarbor Plain. The breecia is matrix supported with floating angular, poorly sorted, 1 – 10 cm size clasts of blackened limestone, parent Nullarbor Limestone, and rare terrestrial pulmonate gastropods. The matrix is structureless to laminated micrite and fine to very fine grained quartz.

**Blackened Clasts.—**Black limestone clasts comprise 40 – 90% of the breecia infill (Fig. 2.8B, C). Most clasts are thin (5 – 25 mm thick) plates. They are locally surrounded by micrite laminations, creating large 1 – 2 cm diameter pisoids. Clasts range from completely black with no visible internal fabric to a spectrum of grey shades with visible internal fabric (Fig. 2.8C). They have a complex and contorted internal texture with common clotted fabrics, alveolar textures, and extremely fine laminations visible in transmitted light petrography (Fig. 2.8D).

**Matrix.—**Matrix sediment varies widely in colour and texture, although composition is similar throughout. Colours range from medium gray, to moderate reddish brown, to yellowish gray. Moderate to well rounded, very fine grained quartz with frosted margins is evenly dispersed throughout the micrite matrix. This is the first appearance of quartz grains or any other siliciclastic material in karst filling sediment; all previous sediments are quartz-free.

*Interpretation*

**Subsoil Hollow Formation.—**These karrens are subsoil dissolution features associated with subaerial exposure of carbonate rocks (cf. Esteban and Klappa, 1983; James and Choquette, 1988). The uniform size and nature of the hollows across the Nullarbor Plain suggest a common method of dissolution. Such hollows are generally interpreted to

have formed by stem flow drainage, which is caused by trees concentrating rainfall and enhancing the acidity of associated dissolving fluids (Herwitz 1993; Vanstone 1998). This process allowed focused water flow to penetrate the underlying limestone, resulting in the formation of karst solution pans up to 1 – 2 m in depth and diameter. The subsoil karst characterized by this phase of diagenesis is interpreted to represent the last large trees on the Nullarbor Plain. These remnants suggest that the climate was somewhat arid and could only support a low density flora.

**Blackened Clasts.—**Blackened clasts have been linked to subaerial unconformities across the globe, although their origin(s) is still poorly understood (Strasser and Davaud 1983; Strasser 1984; Shinn and Lidz 1988; Tucker 1990; Vera and Jimenez de Cisneros 1993) and is the focus of additional research. Current hypotheses include forest fires (Shinn and Lidz 1988), deposition in organic rich tidal, lacustrine, and hypersaline lake environments (Ward et al. 1970; Strasser 1984), microbial communities (Folk et al. 1973), and decayed terrestrial plant matter staining the surrounding limestone (Leinfelder 1987).

**Sediment Infill.—**The variety of clasts and grains show that there were multiple sources for the fill sediment, whereas the angular nature of the particles suggest that they were not transported far. Lack of blackened clasts outside the pits and their angular nature further implies that they developed close to or inside the subsoil hollows.

The sediment that was transported long distances is the fine to very fine grained quartz. The uniform fine grain size and frosted particle margins suggest that the quartz is aeolian. The closest sources of quartz are the northern dune fields of the Great Victoria Desert, Ooldea Range, and the Miocene paleochannels and drainages along the northern reaches of the Nullarbor Plain, implying transport distances of 100 km to 300 km via aeolian processes (Lowry and Jennings 1974; Benbow 1990; Alley et al. 1999; Pell et al.

1999). Aeolian transport of this magnitude indicates that much of the surface vegetation across the source area and Nullarbor Plain at this time was low and sparse, allowing surface winds to transport the quartz grains over long distances.

### *Stage 7 Dolines & Colluvium*

#### *Description*

Dolines on the Nullarbor Plain occur in two varieties: 1) shallow dolines that are near the surface and filled with fine calcium carbonate colluvium and 2) deep dolines are not completely filled with colluvium and connect to deep cave systems (stage 4). Colluvium-filled shallow dolines range in size from 2 – 15 m deep and 1 – 20 m wide (Fig. 2.9A – B). They cross-cut all previous phases and signal a new or rejuvenated period of dissolution. Undulatory boundaries of the sinks are sharp with little to no alteration of the host Nullarbor Limestone. There are no calcite or salt precipitates along the steep margins of adjacent dolines. Stoping features are present in most dolines with wide openings to the paleo-surface.

Most shallow dolines are partially to completely filled with moderate red colluvium composed of fine calcium carbonate with fine quartz, rhizoliths, limestone clasts, box-work textures, gypsum layers, and minor kaolinite and hematite (Fig. 2.9A). The sediment is extensively mottled by 2 – 5 mm diameter and 10 – 30 mm long tubes filled with lighter coloured sediment. Box-work textures comprise 1 – 2 mm thick vertical and horizontal resistant calcite walls that create a rectangular pattern in the colluvium. Gypsum layers, 2 – 5 cm thick, mostly in eastern portions of the Nullarbor Plain, drape down across some of the sink fills. The multitude of fabrics, structures and lithologies give the colluvium a heterogeneous fabric. Most dolines have 5 – 10 cm angular clasts of Nullarbor Limestone

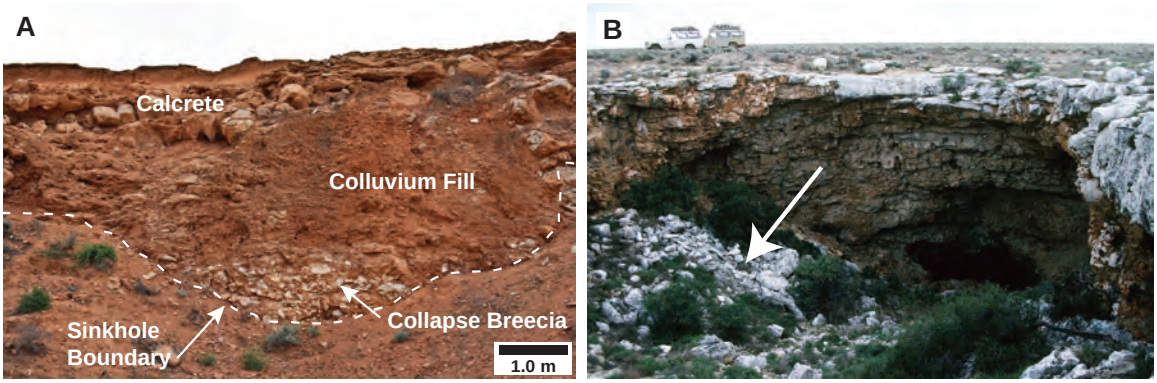


**Figure 2.9.** Stage 7. A) Pedogenic calcrete (stage 8) overlying a shallow collapse doline (stage 7) filled with red colluvium. Dashed line outlines the boundaries of the karstic sinkhole. The arrow points to parent breecia clasts at the base of the colluvium fill. Located at Cook Quarry. B) Chowilla Doline connecting to a deep cave, with steep overhanging boundaries and abundant karst breecia of Nullarbor Limestone (arrow). Vehicles for scale.

at their base. Colluvium at the base of the dolines is more lithified than later near surface sediment.

Deep dolines that connect large cave systems to the surface share similar morphologies to the shallow dolines described above, but they lack colluvium fill. These dolines have a wide range of diameters (10 m – 100 m) depending on the size of the underlying deep cave chamber. Such dolines commonly have steep Nullarbor Limestone walls that overhang several meters (Fig. 2.9B). Deep dolines are partially filled with 1 – 3 m diameter blocks of Nullarbor Limestone karst breecia and fine grained material that is overgrown with low bushes.

*Interpretation*

Collapse dolines opened numerous caves on the Nullarbor Plain and host fossilized remains of an extinct Pleistocene (>780 kya) megafauna (Prideaux et al. 2007; Prideaux and Warburton 2008), suggesting that the features are relatively recent. The presence of a large and varied community of grazing and arboreal marsupials points to a semi-arid woodland and shrub mosaic, including plants with palatable leaves and fleshy fruits, all supporting an interpretation of a dry and relatively open savannah environment (Prideaux et al. 2007; Prideaux and Warburton 2008).

The shallow colluvium-filled dolines are interpreted to have formed from the collapse of shallow caves (stage 5), whereas deeper dolines that are still open today formed from the collapse of larger deep cave systems (stage 4). The process of salt wedging is thought to have degraded the roofs of select shallow and deep caves to the point where they collapsed into the void below (Webb and James 2006). Pre-existing calcite cave decorations were destroyed in the collapse event and dissolved by meteoric waters.

Abundant rhizoliths in the colluvium confirm that there was vegetation either growing in the colluvium or washing into the dolines. By contrast, gypsum layers that drape down across the dolines with crystals growing upwards from a sub-planar base, suggests intermittent conditions of high evaporation in the colluvium and are interpreted as evidence for a dry climate with a distinct wet season, that supported grasslands and small shrubs. Colluvium was probably washed into the dolines during the wet season. The larger dolines that form entrances to deep cave passages are not filled with colluvium. This is interpreted to represent the larger hydrologic system of deep caves that allowed rainwater to transport the colluvium into the expanses of cave passages. Such a system was absent in the much more localized and smaller shallow caves and subsequently they were filled with colluvium.

### *Stage 8 – Accretionary Pedogenic Calcrete*

#### *Description*

Calcrete ranges from two meters in thickness where it is fully preserved to absent where it has been removed by erosion. Colour is a combination of moderate red and moderate reddish brown. The calcrete has a sharp basal contact with the underlying parent Nullarbor Limestone and a recurring vertical profile (Fig. 2.10A, D). The lower part comprises elongate plates of Nullarbor Limestone coated by several generations of thinly (0.25 – 1.5 mm) laminated micrite. Laminated sections are 1 – 5 cm thick and are much thicker on the top sides of the plates (Fig. 2.10B). The platy nature of the calcrete profile grades into a more nodular fabric up section where there is little to no parent material preserved. This upper part is entirely lithified calcrete pisoids with micrite laminations in a dense micrite matrix. Pisoids and ooids are 0.5 – 50 mm in size and coalesce as they become larger to

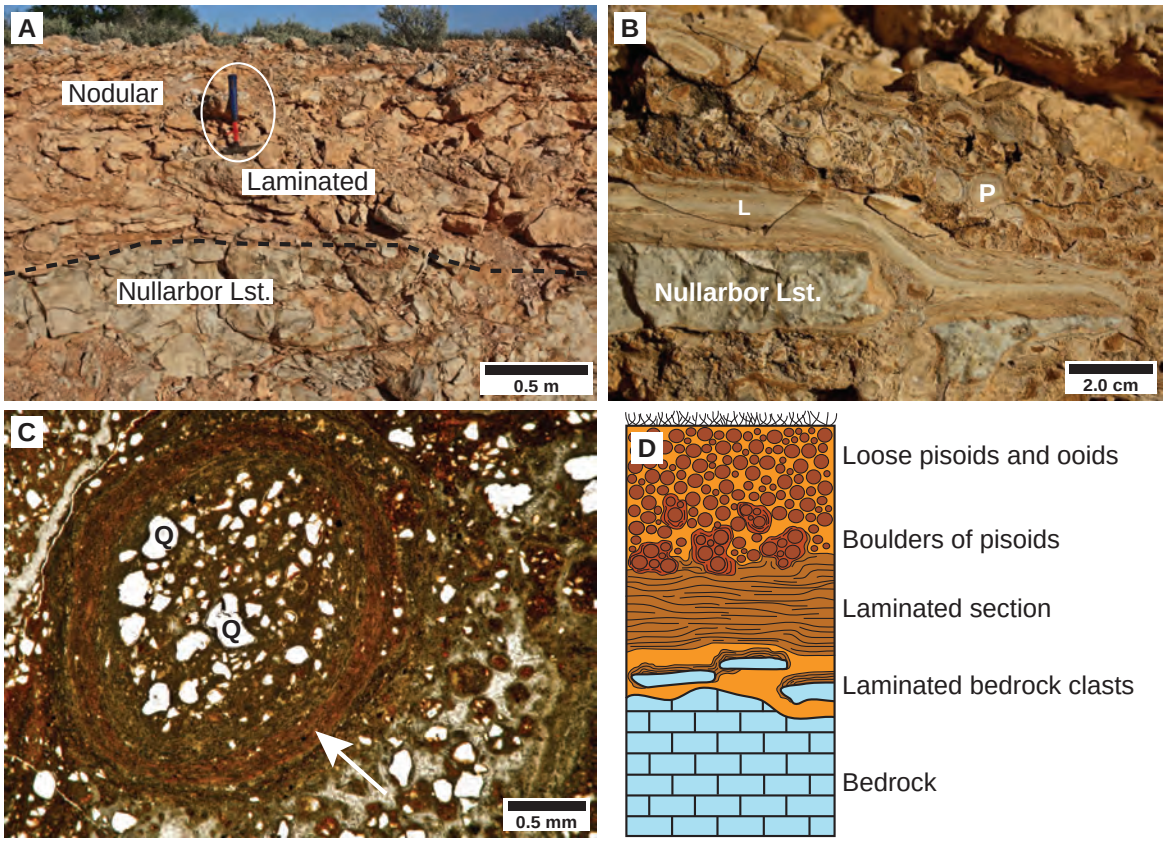


**Figure 2.10.** Stage 8. A) Pedogenic calcrete profile at Watson Quarry showing a sharp contact with the underlying Nullarbor Limestone, the basal laminated platy horizon (Laminated), and the upper nodular horizon (Nodular). B) Plate of Nullarbor Limestone with micrite laminations (L) preferentially on the upper surface. Surrounding the laminated plates are calcrete pisoids (P); Watson Quarry. C) Photomicrograph (PPL) of a calcrete pisoid showing the quartz (Q) rich nucleus and surrounding matrix with a cortex of micrite laminations (arrow), which are free of quartz grains; Cook Quarry. D) Diagrammatic profile of the pedogenic calcrete found across the surface of the Nullarbor Plain.

form pisolites and oolites. Pisoids have a dense micrite nucleus with abundant very fine grained quartz and a cortex that ranges from 0.25 – 10 mm in thickness and comprises alternating laminations of variably coloured and textured micrite. Cortical laminations are slightly undulatory, occasionally have bands of sparry meteoric calcite cement separating them, and only rarely contain quartz grains (Fig. 2.10C). Circumgranular cracking occurs in <5 % of micrite rich pisoids and such particles are outlined by clear calcite cement. These grains differ from those of palustrine ooids by being larger in size, moderate red in colour, having fewer circumgranular cracks, and a quartz rich nucleus. Pisolites are cemented into boulder-size clasts (20 – 50 cm) with a marked decrease in such lithification upwards with large boulders gradually becoming smaller and finally gravel sized at the top of the section. The very top of the section is characterized by individual calcrete pisoids and loose, fine grained burnt orange colluvium (Fig. 2.10D).

*Interpretation*

Nullarbor calcrete correlates with other coeval calcretes across southern Australia during this time of widespread regional aridity (Warren 1983; Phillips et al. 1987; Phillips and Self 1987; Wasson and Clark 1988; Lintern et al. 2004; Lintern et al. 2006). The modern arid to semi-arid climate of southern Australia today (Australian Water Resources Council 1976; White 1994) is favourable for the generation of accretionary calcrete. Nullarbor Plain laminar calcretes share attributes with numerous other examples worldwide that form via complex interactions between roots, physical processes, evaporation, and micro-organisms (Hay and Reeder 1978; Wright et al. 1988; Wright 1989; Mack and James 1992; Verrecchia et al. 1995; Alonso-Zarza and Arenas 2004; Zhou and Chafetz 2009). Calcrete pisoids across the Nullarbor and Roe Plains are macroscopically and microscopically similar to

microbially coated grains and calcrete pisoids described by previous authors (Read 1974; Calvet and Julia 1983; Phillips et al. 1987; Wright 1989; Alonso-Zarza and Arenas 2004), suggesting a parallel origin.

## STABLE ISOTOPE GEOCHEMISTRY

Samples were selected for stable oxygen and carbon isotope analyses from all diagenetic phases (Table 2.2). Their values define two distinct fields interpreted to represent humid to temperate and arid climates (Fig. 2.11). The highly negative $\delta^{13}C$ and $\delta^{18}O$ field comprises stages 1 – 7. $\delta^{13}C$ values of these calcites are indicative of fluids that have flowed through organic-rich soils (Salomons and Mook 1986; Armenteros and Daley 1998; Hoefs 2004). These values are interpreted to represent surface vegetation of C3 floral varieties, typical of a cool humid Neogene climate (Cerling 1984; Paulsen et al. 2003). Negative $\delta^{18}O$ values (-3 to -6 ‰) suggest that open meteoric water systems were prevalent during this period with accompanying high precipitation and low evaporation rates (Fleitmann et al. 2004; Fairchild et al. 2006).

By contrast, Nullarbor and Roe Plain calcretes (stage 8) have the least negative $\delta^{18}O$ and positive $\delta^{13}C$ isotope values of all calcites (Fig. 2.11). High rates of evaporation lead to preferential evaporation of the lighter oxygen isotope $^{16}O$, which subsequently yields higher $\delta^{18}O$ values in calcrete precipitates (Behrensmeyer et al. 2007). The more positive $\delta^{13}C$ values in Nullarbor Plain calcrete samples are interpreted to be representative of C4 vegetation, typical of sparse dry grasslands under an arid to semi-arid Neogene climate (Alonso-Zarza and Arenas 2004; Behrensmeyer et al. 2007). Roe Plain calcrete samples are thought to have lower $\delta^{13}C$ values because of more dominant C3 vegetation closer to the

**Table 2.2**
Stable Carbon and Oxygen Isotope Data

| Phase | Location | Description | $\delta C^{13}$ (‰ PDB) | $\delta O^{18}$ (‰ PDB) |
|---|---|---|---|---|
| **Phase 3 – Arid Paleosols** | | | | |
| Stage 8 Accretionary Pedogenic Calcrete | 1 – Eucla quarry | Micrite matrix of calcrete pisolite | -5.3 | -0.0 |
| | 2 – Watson quarry | Basal micrite calcrete laminations | -4.0 | -1.5 |
| | 3 – Madura quarry | Micrite matrix of unlithified calcrete | -1.8 | -1.6 |
| | 4 – Madura Pass | Blackened clast in poorly lithified calcrete | -5.5 | -1.5 |
| | 5 – Unnamed quarry | Calcrete pisoid lamination (possible contamination) | -9.3 | -1.9 |
| Stage 7 Dolines & Colluvium | 6 – Madura Pass | Poorly lithified calcium carbonate colluvium | -10.7 | -5.4 |
| | 7 – Eucla Pass | Poorly lithified calcium carbonate colluvium | -11.7 | -5.3 |
| | 8 – Watson quarry | Lithified calcium carbonate colluvium | -8.5 | -4.0 |
| Stage 6 Subsoil Hollows | 9A – Eucla quarry | Black limestone clast | -10.4 | -3.1 |
| | 9B – Eucla quarry | Breecia matrix | -7.9 | -3.7 |
| | 10A – Cook quarry | Black limestone clast | -9.8 | -4.8 |
| | 10B – Cook quarry | Breecia matrix | -9.9 | -4.6 |
| | 11 – Rawlinna quarry | Black limestone clast | -6.5 | -2.5 |
| **Phase 2 – Caves** | | | | |
| Stage 5 Shallow Caves & Precipitates | 12 – Eucla quarry | Earliest phreatic fibrous calcite phase | -9.4 | -6.0 |
| | 13 – Madura Pass | Earliest phreatic fibrous calcite cement | -11.7 | -5.5 |
| | 14 – Cook quarry | Late fibrous phreatic calcite | -8.7 | -4.9 |
| | 15 – Rawlinna quarry | Speleothem, youngest lamination | -9.4 | -5.0 |
| | 16 – Watson quarry | Earliest phase of vadose fibrous calcite cement | 7.0 | -4.0 |
| **Phase 1 – Microkarst and Sedimentation** | | | | |
| Stage 3 Post-Karst Sedimentation | 17 – Cocklebiddy Cave | Palustrine ooid in a cavity | -10.5 | -3.5 |
| | 18 – Cook quarry | Palustrine ooid on the surface | -8.9 | -4.3 |
| | 19 – Old Homestead Cave | Palustrine ooid in a cavity | -9.6 | -4.1 |
| | 20 – Watson quarry | Palustrine ooid in a cavity | -9.6 | -4.0 |
| | 21 – Eucla Pass | Palustrine ooid in a cavity | -11.1 | -4.5 |
| Stage 1 Fabric Specific Diagenesis | 22 – Cook quarry | Nullarbor Lst. with meteoric calcite spar | -6.9 | -3.1 |
| | 23 – Rawlinna quarry | Nullarbor Lst. with meteoric calcite spar | -6.6 | -3.2 |

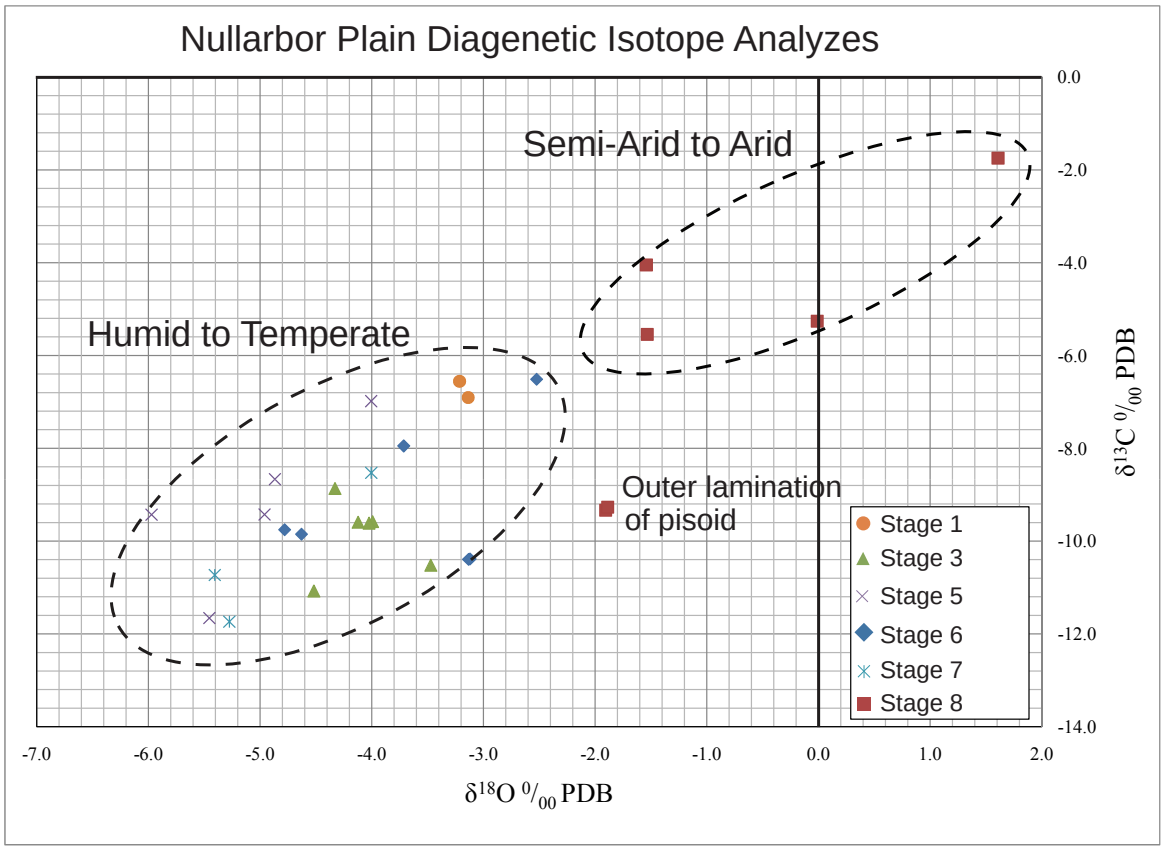


**Figure 2.11.** Carbon and oxygen isotope data series for selected Nullarbor Plain samples from diagenetic Stages 1 – 8. The data groups into two fields representing formation in an arid to semi-arid climate and in a humid to temperate climate.

coast, where rainfall was higher.

## SYNTHESIS

The Nullarbor Plain is an exceptional example of how paragenetic changes at unconformities can be directly related to evolving climate, a undertaking that is nearly impossible in the rock record. Preservation of eight distinct stages of diagenesis during 3 climate periods allow for the interpretation of a complex geohistory that illustrates what diagenetic traits should be expected under known climate change (Fig. 2.12). A multidisciplinary approach using several events as pinning points (Goldstein and Franseen 1995) allows the whole diagenetic succession to be put in an approximate temporal framework. The following proposed geohistory (Fig. 2.13) is based on an integration of this information with previously described field relationships and known climate regimens.

### *Middle Miocene (Phase 1) – Microkarst and Sedimentation*

Earliest vegetation on the newly uplifted middle Miocene Nullarbor Plain is thought to have been dominated by myrtle beech trees and ferns of cool temperate rainforest affinity (Drexel and Preiss 1995; Alley et al. 1999; Johnson 2009). Microkarst, lacustrine deposition, and palustrine modification formed during this period. With the exception of Cook quarry the only preservation of these deposits is hidden in underlying stage 2 microkarst cavities. This points to a subsequent prolonged period of weathering wherein these terrestrial deposits were largely removed by erosion during phase 2.

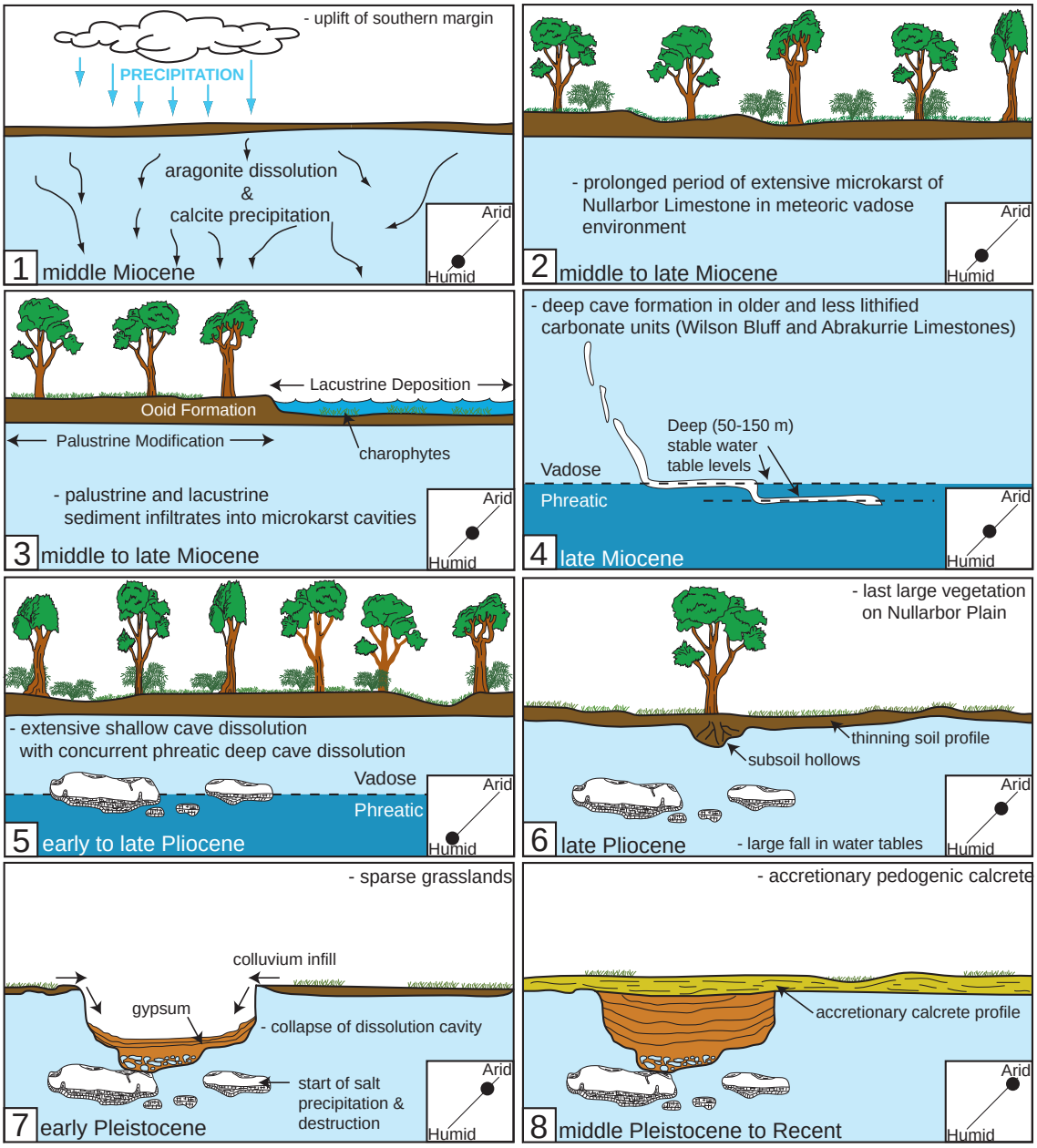


**Figure 2.12.** Paleoenvironment diagram illustrating the surface and subsurface processes and climate involved with the formation of the eight diagenetic phases. (1) Stage 1 – Uplift of the Nullarbor Plain and exposure to subaerial conditions. Rapid dissolution of aragonite skeletons and corresponding precipitation of sparry calcite cements lithified the Nullarbor Limestone. (2) Stage 2 – Microkarst dissolution is widespread under lacustrine and palustrine surfical environments. (3) Stage 3 – Large scale lacustrine system deposits are slowly modified in a pedogenic palustrine setting as the climate became drier. (4) Stage 4 – Deep cave formation at deep water tables in underlying less lithified limestone formations. Dissolution pathways follow tectonic lineations. (5) Stage 5 – Introduction of a humid climate interlude, rising water tables and allowing for the dissolution of shallow caves. Phreatic dissolution in deep caves heightens during this period. (6) Stage 6 – The climate becomes increasingly arid and through stem flow drainage the dissolution of subsoil hollows occur under the few eucalypt trees remaining on the plain. (7) Stage 7 – The formation and then infill of shallow dolines with colluvium rich in roots and grasses. This time also corresponds to the opening of dolines to deep cave passages. (8) Stage 8 – The heightened arid climate leads to the formation of a thick pedogenic calcrete horizon, which caps the modern surface of the Nullarbor Plain.

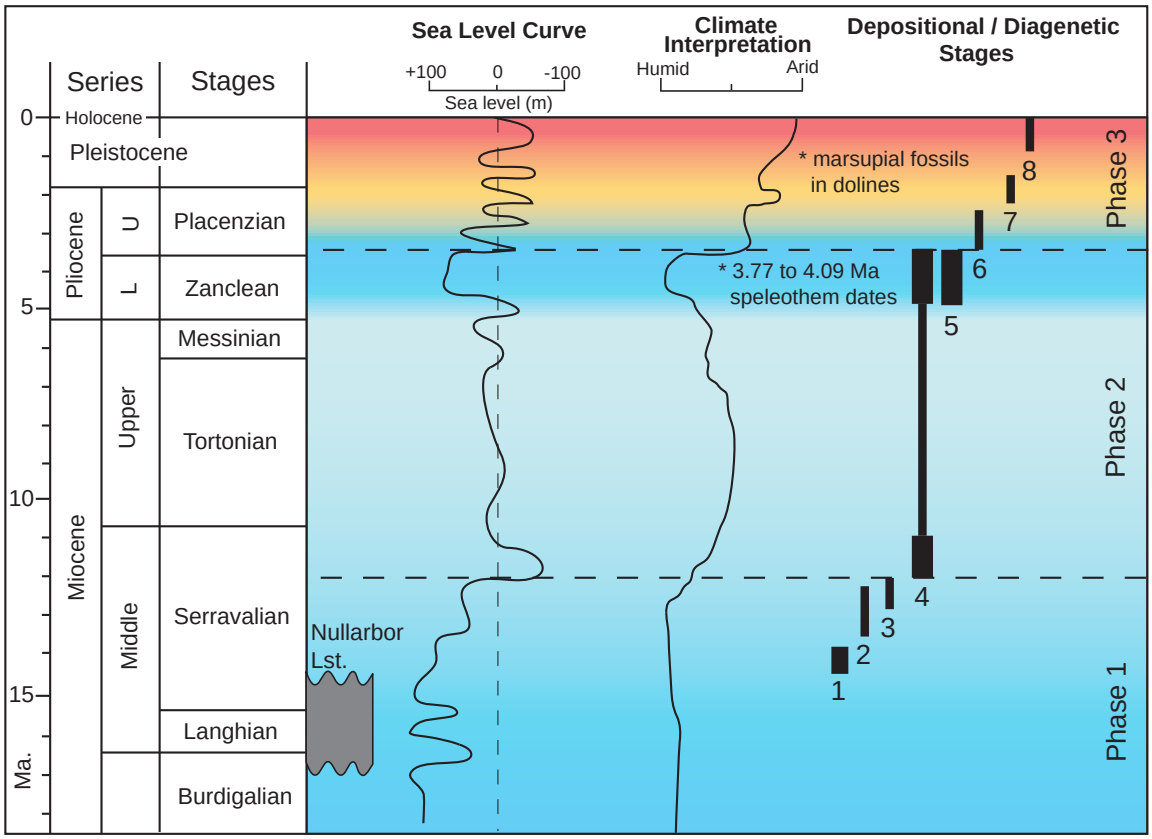


**Figure 2.13.** Summary chart showing the timeline of the depositional and diagenetic stages that have affected the Nullarbor Plain since exposure in the middle Miocene. The width of lines in the timeline of diagenetic phases illustrates the relative strength of the processes (a wider line represents more intensive processes). Climate is represented by a colour spectrum, dark blue colours represent humid climates with lighter blues being less humid, whereas yellow to red represents increasing aridity. The relative timing of each stage is determined from the relative sea level, known dates of diagenetic events (indicated by an *) and climate indicators. The relative sea level curve is derived from Haq et al. (1987).

*Late Miocene to late Pliocene (Phase 2) – Caves*

The late Miocene landscape supported a limited sclerophyll flora coincident with the onset of more temperate conditions and a pronounced wet and dry season that was increasingly arid inland (White, 1994). Deep cave dissolution (stage 4) is herein interpreted to have started shortly after phase 1 (late Miocene). The profoundly lowered sea level during the late middle Miocene (Fig. 2.13) (Haq et al. 1987) would have been accompanied by a dramatic depression of the water table. This enabled dissolution in the underlying less resistant lithologies (especially the Abrakurrie and particularly the Wilson Bluff limestones) to occur along joint set fractures related to faults for over 8 m.y. This proposed timing of deep cave formation contradicts previous theories that argue the majority of dissolution occurred in the Oligocene when the climate was interpreted to be more humid (Webb and James, 2006). Such an event would have occurred before deposition of the thick marine successions of the Abrakurrie and Nullarbor Limestones. These caves should have been infilled with sediments or undergone substantial collapse upon marine transgression, which they did not. Furthermore, the roofs of many deep caves hosted in the Wilson Bluff Limestone are composed of Abrakurrie Limestone, with minimal collapse present inside the chambers, and many of these larger caves are also themselves hosted in the Abrakurrie Limestone.

The early Pliocene is generally considered a warm and humid time across southern Australia (Benbow et al. 1995; Johnson 2009). This is when the more widespread stage 5 development of shallow caves formed during a sea level highstand (Haq et al. 1987) resulting in elevated water tables and increased dissolution (Fig. 2.13). Earlier deep cave passages, forming since the late Miocene, were subject to turbid phreatic groundwater flow, resulting in dramatic passage dissolution and enlargement (White 2002). Limited geochemical

dating of speleothems in shallow Nullarbor cave systems range from ~ 4 Ma (Woodhead et al. 2006) to ~2.9 Ma (Blyth et al. 2010). Calcite precipitation in the Nullarbor caves appears to have stopped at ~ 400 kya and was replaced by halite and gypsum precipitation and wedging, which is still ongoing (Goede et al. 1990; Goede et al. 1992).

### *Latest Pliocene to Recent (Phase 3) – Arid Paleosols*

When sea level began to fall in the late Pliocene to early Pleistocene because of polar icecap readvancement, the humid climate across the Nullarbor Plain changed rapidly to an increasingly arid one, with attendant lowering of water table levels and reduced carbonate dissolution (White 1994; Drexel and Preiss 1995; Alley et al. 1999; Johnson 2009). This is manifest as subsoil hollows indicative of an open savannah. Subsequent doline formation and colluvium fill took place after stage 6 as dry and wet seasons alternated with periods of infilling and evaporation in the dolines. The climate of southern Australia has become increasingly arid since the middle Pleistocene (~ 700 kya) (Goede et al. 1990; White 1994; Benbow et al. 1995; Johnson 2009). Pedogenic calcrete extends today across all of the Nullarbor Plain and past karst systems are largely moribund and in decay.

## DISCUSSION AND IMPLICATIONS

### *Surfical Erosion Rates*

In spite of the excellent preservation of multiphase diagenesis over ~ 14 m.y. it is unclear how much of the Nullarbor Limestone and early products of subaerial exposure have been removed by erosion. Lowry and Jennings (1974) estimate that erosion of the southern Plain has been 60 m and on the northern Plain 29 m, because of their differences in

aridity. Modern surface erosion of the Nullarbor, estimated from cosomgenic chlorine-36 in calcite, is ~ 4.5 m $Ma^{-1}$ or 63 m over the total length of exposure time (Stone et al. 1994). Although it is difficult to estimate the amount of erosion because of lack of evidence, these rates, on the basis of this study and other evidence, appear too high.

The Eocene Ooldea Range, a 40 – 180 m high suite of siliciclastic dunes, along with associated middle Miocene beach ridges of reworked Ooldea Sandstone, wave cut scarps into the underlying carbonates, and paleovalleys extending far out onto the Plain along the north-eastern Nullarbor Plain are completely preserved (Fig. 2.1) (Benbow 1990; Drexel and Preiss 1995; Alley et al. 1999; Johnson 2009). Preservation of these landscapes indicates that erosion rates have been persistently slow since the Eocene (Bunting et al. 1974; Benbow 1990).

Middle Miocene palustrine sediments, formed via pedogenic processes, extend down 10 – 15 m into microkarst cavities. If there had been extensive sections of sediment above then these roots and other pedogenic mechanisms would had to have extended many more tens of meters below the paleomarsh surface. This would not have been possible since many modern *Mallee* eucalypts roots are limited to depths of 8 – 10 m within 7 years of planting (Robinson et al. 2006). This depth is likely to have been only slightly deeper on the Plain since they would have extended down into the underlying microkarst cavities to access water.

Finally, the meter-scale bed of palustrine ooids at Cook quarry would, if erosion rates on the order of many tens of meters were accurate, would have been at least that thick (~ 20 – 100 m). However, the surface is sub-horizontal with no evidence of irregular erosion which would be expected if over 80 % of the palustrine succession had been removed. This expected irregular erosion is not seen across the Nullarbor Plain. Individual early

diagenetic fabrics illustrate this relationship, most importantly stage 5 shallow caves can be traced over many hundreds of kilometres without change in depth from the surface that should not be expected if substantial erosion had taken place.

On the basis of the preceding and the exceptionally well preserved nature of the diagenetic features, karst, palustrine sediments, speleothems, and pedogenic deposits, we suggest that surface erosion has been minor and much less than previously suggested. Instead, water seeped into the underlying limestones and subsequently focused dissolution in the subsurface.

### *Terrestrial Record of Sea Level*

The relationship between sea level change and the stratigraphic record is traditionally deciphered using marine successions (Haq et al. 1987). Yet, the water table is tied to the position of sea level at the shoreline (Hanshaw and Back 1980). Thus, to a first degree, acknowledging that the water table is also a function of limestone characteristics, inland precipitation rates, and recharge rates (Fetter 1994), the position of the water table through time is a reflection of eustasy: high water table equals high sea level and visa versa. If the hypothesis presented here that the excavation of deep caves was during the middle Miocene then it can be tied to the global low sea level at that time. Likewise the later stage of shallow Pliocene caves coincides with the coeval eustatic highstand at that time. In short, fluctuations of sea level not only affect marine carbonate deposition but also profoundly control meteoric diagenesis by determining the movement of the water table. This relationship is also well documented on the Yucatan Peninsula, another flat lying carbonate terrain (Stallard 1988; Worthington et al. 2000).

### *Palustrine Carbonates*

Lacustrine and palustrine sedimentation should be expected at long-term carbonate subaerial exposure surfaces; however, they are relatively rare at pre-Cenozoic surfaces (Wright 1994; Alonso Zarza 2006; MacNeil and Jones 2006; Alonso-Zarza and Wright 2010b). Palustrine ooids, the pedogenic alteration products of earlier lacustrine sediments are common across the Nullarbor Plain and so could be expected at prolonged unconformities, especially in post-Devonian successions. This does not seem to be the case, as the majority of unconformities in the rock record do not have any interpreted preserved lacustrine or palustrine deposits. Such an absence could be explained by the low preservation potential of such surfical sediments along coastal environments or that such deposits may have been misinterpreted in the past as overlying marine ooid transgressive systems tract (TST) deposits.

### *The Record of Subaerial Exposure*

The Nullarbor Plain, the most extensive areal karst in the modern world, has surprisingly few speleothems or other cave precipitates. The dearth of such features has been ascribed to the onset of aridity and a semi-arid climate (Jennings 1963; Dunkley and Wigley 1967; Lowry and Jennings 1974; Webb and James 2006). If this study is correct, most cave formation occurred during the middle and late Miocene and early Pliocene under a more humid climate than today, then this explanation is not viable. There is still the conundrum, however, as to why there are few speleothems. The answer is thought to be that the cave systems must have been closed and deep, associated with the profoundly depressed water table. The low surface gradient that probably prevented much surface erosion also focused karst development underground (Webb and James, 2006; Frisia and

Borsato, 2010). The consequence of this lack of speleothems and yet profound subsurface cavern formation is an aspect that can be applied to many ancient karst systems and carbonate unconformities; speleothems should not be an expected attribute of subaerial exposure.

## CONCLUSIONS

The present day Nullarbor Plain represents an ~ 14 m.y. exposure surface. Subaerial diagenetic history can be resolved into 3 regional phases of alteration, each of which comprises several discrete stages that can be related to subsurface and subaerial karst formation, lacustrine and palustrine deposition, and calcrete development.

Phase 1 – Humid climate – Stage 1 resulted in mineralogical equilibration with fresh waters, cementation, extensive mouldic porosity and subsequent widespread microkarst (stage 2). An extensive lacustrine and palustrine system (stage 3) developed in the late middle Miocene but all deposits except those that filtered into pre-existing karst cavities have since been removed by surfical erosion. Phase 2 – Temperate to humid climate – the longest period of diagenesis (stage 4), took place over a period of ~ 8 m.y. during the late Miocene and early Pliocene. Deep cave systems along the coast were created concurrent with late Miocene sea level lowstands and a depressed regional water table. A humid Pliocene interlude created secondary shallow cave systems (stage 5) coincident with a sea level highstand, high water table, phreatic dissolution, and enlargement of deep caves. During phase 3 – Semi-arid to arid climate – subsoil hollows interpreted to be generated by stem flow drainage related to large trees were filled with black pebbles (stage 6), followed by the generation of numerous collapse dolines and

attendant colluvium and gypsum infill (stage 7) occurred over a relatively short period of time in the latest Pliocene and early Pleistocene when the climate was becoming increasingly arid. The final phase, accretionary pedogenic calcrete developed under a wholly arid to semi-arid climate (stage 8), over the last 500 kya.

The Nullarbor exposure surface and attendant diagenetic paragenesis illustrates the wide variety of interpretable features that can be expected to accompany prolonged exposure under an evolving humid to arid climate. Extensive studies such as this can offer criteria for use in identifying ancient unconformities and also provide a better understanding of the climate in which they formed.

## ACKNOWLEDGEMENTS

This research is funded by the Natural Sciences and Engineering Research Council of Canada (NSERC) Discovery Grant to NPJ, and the Geological Survey of Western Australia (GSWA). We thank the helpful staff at GSWA and Laura O'Connell for field assistance, S. Milner for the use of an underground cave image, and K. Kyser and K. Klassen for their valued assistance and contributions with stable isotope geochemistry. R. Renaut generously shared his expertise with charophytes and lacustrine depositional systems. We thank B. Jones, P. Smart, F. Whitaker, and P. Wright for numerous stimulating discussions that helped in the writing of this manuscript. The authors are also thankful for the comments of two anonymous reviewers and the editor, Brian Jones, which greatly improved the manuscript.

## REFERENCES


Alley, N.F., Clarke, J.D.A., Macphail, M., and Truswell, E.M., 1999, Sedimentary infillings and development of major Tertiary palaeodrainage systems of south-central Australia: Special Publication of the International Association of Sedimentologists, v. 27, p. 337-366.

Alonso Zarza, A.M., 2006, Paleoenvironmental record and applications of calcretes and palustrine carbonates: Special Paper - Geological Society of America, v. 416, p. 239.

Alonso Zarza, A.M., Calvo, J.P., and Garcia del Cura, M.A., 1992, Palustrine sedimentation and associated features--grainification and pseudo-microkarst--in the middle Miocene (Intermediate Unit) of the Madrid Basin, Spain: Sedimentary Geology, v. 76, p. 43-61.

Alonso-Zarza, A.M., 2003, Palaeoenvironmental significance of palustrine carbonates and calcretes in the geological record: Earth-Science Reviews, v. 60, p. 261-298.

Alonso-Zarza, A.M., and Arenas, C., 2004, Cenozoic calcretes from the Teruel Graben, Spain; microstructure, stable isotope geochemistry and environmental significance: Sedimentary Geology, v. 167, p. 91-108.

Alonso-Zarza, A.M., and Wright, V.P., 2010a, Calcretes, *in* Alonso-Zarza, A.M., and Tanner, L.H., eds., Carbonates in Continental Settings: Facies, Environments and Processes: Developments in Sedimentology: Oxford, Elsevier, p. 225-267.

Alonso-Zarza, A.M., and Wright, V.P., 2010b, Palustrine Carbonates, *in* Alonso-Zarza, A.M., and Tanner, L.H., eds., Carbonates in Continental Settings: Facies, Environments and Processes: Developments in Sedimentology: Oxford, Elsevier,

p. 103-131.

Armenteros, I., 2010, Diagenesis of Carbonates in Continental Settings, *in* Alonso-Zarza, A.M., and Tanner, L.H., eds., Carbonates in Continental Settings: Geochemistry, Diagenesis and Applications: Developments in Sedimentology: Oxford, Elsevier, p. 61-151.

Armenteros, I., and Daley, B., 1998, Pedogenic modification and structure evolution in palustrine facies as exemplified by the Bembridge Limestone (Late Eocene) of the Isle of Wight, southern England: Sedimentary Geology, v. 119, p. 275-295.

Australian Water Resources Council, 1976, Review of Australia's water resources: Canberra, Australian Government Publishing Service, p. 170.

Bathurst, R.G.C., 1975, Carbonate sediments and their diagenesis, v. 12: Amsterdam, Elsevier Sci. Publ. Co., 658 p.

Behrensmeyer, A.K., Quade, J., Cerling, T.E., Kappelman, J., Khan, I.A., Copeland, P., Roe, L., Hicks, J., Stubblefield, P., Willis, B.J., and Latorre, C., 2007, The structure and rate of late Miocene expansion of C (sub 4) plants; evidence from lateral variation in stable isotopes in paleosols of the Siwalik Group, northern Pakistan: Geological Society of America Bulletin, v. 119, p. 1486-1505.

Benbow, M.C., 1990, Tertiary coastal dunes of the Eucla Basin, Australia: Geomorphology, v. 3, p. 9-29.

Benbow, M.C., Alley, N.F., Callen, R.A., and Greenwood, D.R., 1995, Geological History and Paleoclimate, *in* Drexel, J.F., and Preiss, W.V., eds., The geology of South Australia; Volume 2, The Phanerozoic: Adelaide, Geological Survey of South Australia, p. 208-217.

Blyth, A.J., Watson, J.S., Woodhead, J., and Hellstrom, J., 2010, Organic compounds

preserved in a 2.9 million year old stalagmite from the Nullarbor Plain, Australia: Chemical Geology, v. 279, p. 101-105.

Brasier, A.T., 2011, Searching for travertines, calcretes and speleothems in deep time: Processes, appearances, predictions and the impact of plants: Earth-Science Reviews, v. 104, p. 213-239.

Brown, J.S., 1970, Mississippi valley type lead-zinc ores: Mineralium Deposita, v. 5, p. 103-119.

Budd, D.A., Saller, A.H., and Harris, P.M., 1995, Unconformities and porosity in carbonate strata: American Association of Petroleum Geologists, v. Memoir 63, 313 p.

Bunting, J.A., Van de Graaff, W.J.E., and Jackson, M.J., 1974, Palaeodrainages and Cainozoic palaeogeography of the Eastern Goldfields, Gibson Desert and Great Victoria Desert, Geological Survey of Western Australia Report, p. 45-50.

Caldwell, J.R., Davey, A.G., Jennings, J.N., and Spate, A.P., 1982, Colour in some Nullarbor Plain speleothems: Helictite, v. 20, p. 3-10.

Calvet, F., and Julia, R., 1983, Pisoids in the caliche profiles of Tarragona (NE Spain): Coated grains, p. 456-473.

Carlisle, D., 1983, Concentration of uranium and vanadium in calcretes and gypcretes: Special Publication - Geological Society of London, v. 11, p. 185-195.

Cerling, T.E., 1984, The stable isotopic composition of modern soil carbonate and its relationship to climate: Earth and Planetary Science Letters, v. 71, p. 229-240.

Clari, P.A., Dela Pierre, F., and Martire, L., 1995, Discontinuities in carbonate successions; identification, interpretation and classification of some Italian examples: Sedimentary Geology, v. 100, p. 97-121.

Climent-Domènech, H., Martín-Closas, C., and Salas, R., 2009, Charophyte-rich

microfacies in the Barremian of the Eastern Iberian Chain (Spain): Facies, v. 55, p. 387-400-400.

Dickinson, J.A., Wallace, M.W., Holdgate, G.R., Gallagher, S.J., and Thomas, L., 2002, Origin and timing of the Miocene-Pliocene unconformity in Southeast Australia: Journal of Sedimentary Research, v. 72, p. 288-303.

Drexel, J.F., and Preiss, W.V., 1995, The geology of South Australia; Volume 2, The Phanerozoic: Bulletin - Geological Survey of South Australia, v. 54, Geological Survey of South Australia, Adelaide, South Aust., Australia, 347 p.

Dunkley, J.R., and Wigley, T.M.L., 1967, Caves of the Nullarbor; a review of speleological investigations in the Nullarbor plain, southern Australia, Speleol. Res. Counc.; (Sydney University, Speleological Society-Cave Exploration Group, South Australia), 61 p.

Esteban, M., and Klappa, C.F., 1983, Subaerial exposure environment, *in* Scholle, P.A., Bebout, D.G., and Moore, C.H., eds., Carbonate Depositional Environments: Tulsa, American Association of Petroleum Geologists, p. 1-54.

Esteban, M., and Wilson, J.L., 1993, Introduction to karst systems and paleokarst reservoirs Paleokarst Related Hydrocarbon Reservoirs, SEPM (Society for Sedimentary Geology), p. 1-9.

Fairchild, I.J., Smith, C.L., Baker, A., Fuller, L., Spoetl, C., Mattey, D., and McDermott, F., 2006, Modification and preservation of environmental signals in speleothems: Earth-Science Reviews, v. 75, p. 105-153.

Fetter, C.W., 1994, Applied Hydrogeology: New Jersey, Prentice Hall, 681 p.

Fleitmann, D., Burns, S.J., Neff, U., Mudelsee, M., Mangini, A., and Matter, A., 2004, Palaeoclimatic interpretation of high-resolution oxygen isotope profiles derived

from annually laminated speleothems from southern Oman: Quaternary Science Reviews, v. 23, p. 935-945.

FOLK, R.L., ROBERTS, H.H., and MOORE, C.H., 1973, Black Phytokarst from Hell, Cayman Islands, British West Indies: Geological Society of America Bulletin, v. 84, p. 2351-2360.

FORD, D., 1988, Characteristics of dissolutional cave systems in carbonate rocks, *in* James, N.P., and Choquette, P.W., eds., Paleokarst: New York, Springer-Verlag, p. 25-57.

FREEMAN, T.O.M., ROSELL, J., and OBRADOR, A., 1982, Oncolites from lacustrine sediments in the Cretaceous of north-eastern Spain: Sedimentology, v. 29, p. 433-436.

FREYTET, P., and VERRECCHIA, E.P., 2002, Lacustrine and palustrine carbonate petrography; an overview: Journal of Paleolimnology, v. 27, p. 221-237.

FRISIA, S., and BORSATO, A., 2010, Karst, *in* Alonso-Zarza, A.M., and Tanner, L.H., eds., Carbonates in Continental Settings: Facies, Environments and Processes: Developments in Sedimentology: Oxford, Elsevier, p. 269-318.

GIERLOWSKI-KORDESCH, E.H., 2010, Lacustrine Carbonates, *in* Alonso-Zarza, A.M., and Tanner, L.H., eds., Carbonates in Continental Settings: Facies, Environments and Processes: Developments in Sedimentology: Oxford, Elsevier, p. 1-101.

GOEDE, A., ATKINSON, T.C., and ROWE, P.J., 1992, A giant late Pleistocene halite speleothem from Webbs Cave, Nullarbor Plain, southeastern Western Australia: Helictite, v. 30, p. 3-7.

GOEDE, A., HARMON, R.S., ATKINSON, T.C., and ROWE, P.J., 1990, Pleistocene climatic change in southern Australia and its effect on speleothem deposition in some Nullarbor caves: Journal of Quaternary Science, v. 5, p. 29-38.

GOLDSTEIN, R.H., and FRANSEEN, E.K., 1995, Pinning points: a method providing quantitative

constraints on relative sea-level history: Sedimentary Geology, v. 95, p. 1-10.

HALLEY, R.B., 1977, Ooid fabric and fracture in the Great Salt Lake and the geologic record: Journal of Sedimentary Petrology, v. 47, p. 1099-1120.

HANSHAW, B.B., and BACK, W., 1980, Chemical mass-wasting of the northern Yucatan Peninsula by groundwater dissolution: Geology (Boulder), v. 8, p. 222-224.

HAQ, B.U., HARDENBOL, J., and VAIL, P.R., 1987, The new chronostratigraphic basis of Cenozoic and Mesozoic sea level cycles: Special Publications - Cushman Foundation for Foraminiferal Research, v. 24, p. 7-13.

HARDY, R., and TUCKER, M., 1988, X-ray powder diffraction of sediments, *in* Tucker, M., ed., Techniques in sedimentology: Oxford, Blackwell Sci. Publ., p. 191-228.

HAY, R.L., and REEDER, R.J., 1978, Calretes of Olduvai Gorge and the Ndolanya Beds of northern Tanzania: Sedimentology, v. 25, p. 649-672.

HERWITZ, S.R., 1993, Stemflow influences on the formation of solution pipes in Bermuda eolianite: Geomorphology, v. 6, p. 253-271.

HILLGAERTNER, H., 1998, Discontinuity surfaces on a shallow-marine carbonate platform (Berriasian, Valanginian, France and Switzerland): Journal of Sedimentary Research, v. 68, p. 1093-1108.

HILLGÄRTER, H., DUPRAZ, C., and HUG, W., 2001, Microbially induced cementation of carbonate sand; are micritic meniscus cements good indicators of vadose diagenesis?: Sedimentology, v. 48, p. 117-131.

HOCKING, R.M., 1990, Eucla Basin: Geological Survey of Western Australia, v. Memoir 3, p. 548-561.

HOEFS, J., 2004, Stable isotope geochemistry: Berlin, Springer-Verlag 244 p.

HOU, B., FRAKES, L.A., SANDIFORD, M., WORRALL, L., KEELING, J., and ALLEY, N.F., 2008,

Cenozoic Eucla Basin and associated palaeovalleys, southern Australia; climatic and tectonic influences on landscape evolution, sedimentation and heavy mineral accumulation: Sedimentary Geology, v. 203, p. 112-130.

James, N.P., and Bone, Y., 1991, Origin of a cool-water, Oligo-Miocene deep shelf limestone, Eucla Platform, southern Australia: Sedimentology, v. 38, p. 323-341.

James, N.P., Bone, Y., Carter, R.M., and Murray-Wallace, C.V., 2006, Origin of the late Neogene Roe Plains and their calcarenite veneer; implications for sedimentology and tectonics in the Great Australian Bight: Australian Journal of Earth Sciences, v. 53, p. 407-419.

James, N.P., and Choquette, P.W., 1988, Paleokarst: New York, Springer-Verlag, 416 p.

James, N.P., and Choquette, P.W., 1990, Limestones - The meteoric diagenetic environment, *in* McIlreath, I.A., and Morrow, D.W., eds., Diagenesis: Ottawa, Geological Association of Canada, p. 35-74.

Jennings, J.N., 1963, Some geomorphological problems of the Nullarbor plain: Transactions of the Royal Society of South Australia, v. 87, p. 41-62.

Johnson, D., 2009, The geology of Australia, Cambridge University Press, 355 p.

King, D., 1950, Geological notes on the Nullarbor cavernous limestone: Transactions of the Royal Society of South Australia, v. 73, p. 52-58.

Klappa, C.F., 1978, Biolithogenesis of Microcodium; elucidation: Sedimentology, v. 25, p. 489-519.

Klappa, C.F., 1979, Calcified filaments in Quaternary calcretes; organo-mineral interactions in the subaerial vadose environment: Journal of Sedimentary Petrology, v. 49, p. 955-968.

Kyser, T.K., 1987, Stable isotope geochemistry of low temperature processes: Short Course

Handbook, v. 13: Toronto, Mineralogical Association of Canada, 452 p.

LEINFELDER, R.R., 1987, Formation and significance of black pebbles from the Ota Limestone (Upper Jurassic, Portugal): Facies, v. 17, p. 159-170.

LINTERN, M.J., SHEARD, M.J., and CHIVAS, A.R., 2006, The source of pedogenic carbonate associated with gold-calcrete anomalies in the western Gawler Craton, South Australia: Chemical Geology, v. 235, p. 299-324.

LINTERN, M.J., SHEARD, M.J., and GOUTHAS, G., 2004, Key findings from the South Australian regolith project: Regolith 2004; proceedings of the CRC LEME regional regolith symposia 2004, p. 220-224.

LOWRY, D.C., 1970, Geology of the Western Australian part of the Eucla Basin: Bulletin - Geological Survey of Western Australia, v. 122: Perth, Geological Survey of Western Australia, 199 p.

LOWRY, D.C., and JENNINGS, J.N., 1974, The Nullarbor karst Australia: Zeitschrift fuer Geomorphologie, v. 18, p. 35-81.

MACK, G.H., and JAMES, W.C., 1992, Calcic Paleosols of the Plio-Pleistocene Camp Rice and Palomas formations, southern Rio Grande Rift, USA: Sedimentary Geology, v. 77, p. 89-109.

MACNEIL, A.J., and JONES, B., 2006, Sequence stratigraphy of a Late Devonian ramp-situated reef system in the Western Canada Sedimentary Basin: dynamic responses to sea-level change and regressive reef development: Sedimentology, v. 53, p. 321-359.

MILLER, C.R., and JAMES, N.P., in review, Autogenic microbial genesis of middle Miocene palustrine ooids: Nullarbor Plain, Australia: Journal of Sedimentary Research.

MILROY, P.G., and WRIGHT, V.P., 2002, Fabrics, facies control and diagenesis of lacustrine ooids and associated grains from the Upper Triassic, Southwest England: Geological

Journal, v. 37, p. 35-53.

O'Connell, L.G., James, N.P., and Bone, Y., 2012, The Miocene Nullarbor Limestone, southern Australia; deposition on a vast subtropical epeiric platform: Sedimentary Geology, v. 253-254, p. 1-16.

Paulsen, D.E., Li, H.-C., and Ku, T.-L., 2003, Climate variability in central China over the last 1270 years revealed by high-resolution stalagmite records: Quaternary Science Reviews, v. 22, p. 691-701.

Pell, S.D., Chivas, A.R., and Williams, I.S., 1999, Great Victoria Desert; development and sand provenance: Australian Journal of Earth Sciences, v. 46, p. 289-299.

Phillips, S.E., Milnes, A.R., and Foster, R.C., 1987, Calcified filaments; an example of biological influences in the formation of calcrete in South Australia: Australian Journal of Soil Research, v. 25, p. 405-428.

Phillips, S.E., and Self, P.G., 1987, Morphology, crystallography and origin of needle-fibre calcite in Quaternary pedogenic calcretes of South Australia: Australian Journal of Soil Research, v. 25, p. 429-444.

Platt, N.H., 1989, Climatic and tectonic controls on sedimentation of a Mesozoic lacustrine sequence; the Purbeck of the western Cameros Basin, northern Spain: Palaeogeography, Palaeoclimatology, Palaeoecology, v. 70, p. 187-197.

Platt, N.H., and Wright, V.P., 1992, Palustrine carbonates and the Florida Everglades; towards an exposure index for the fresh-water environment?: Journal of Sedimentary Petrology, v. 62, p. 1058-1071.

Popp, B.N., and Wilkinson, B.H., 1983, Holocene lacustrine ooids from Pyramid Lake, Nevada, *in* Peryt, T.M., ed., Coated grains: Berlin, Springer-Verlag, p. 142-153.

Prideaux, G.J., Long, J.A., Ayliffe, L.K., Hellstrom, J.C., Pillans, B., Boles, W.E.,

Hutchinson, M.N., Roberts, R.G., Cupper, M.L., Arnold, L.J., Devine, P.D., and Warburton, N.M., 2007, An arid-adapted middle Pleistocene vertebrate fauna from south-central Australia: Nature, v. 445, p. 422-425.

Prideaux, G.J., and Warburton, N.M., 2008, A new Pleistocene tree-kangaroo (Diprotodontia: Macropodidae) from the Nullarbor Plain of south-central Australia: Journal of Vertebrate Paleontology, v. 28, p. 463-478.

Read, J.F., 1974, Calcrete Deposits and Quaternary Sediments, Edel Province, Shark Bay, Western Australia: Memoir - American Association of Petroleum Geologists, v. 22, p. 250-282.

Renaut, R.W., 2010, Personal Communication.

Renaut, R.W., and Gierlowski-Kordesch, E.H., 2010, Lakes, *in* James, N.P., and Dalrymple, R.W., eds., Facies Models 4: St. John's, Geological Association of Canada, p. 541-575.

Robinson, N., Harper, R., and Smettem, K., 2006, Soil water depletion by *Eucalyptus* spp. integrated into dryland agricultural systems: Plant and Soil, v. 286, p. 141-151.

Salomons, W., and Mook, W.G., 1986, Isotope geochemistry of carbonates in the weathering zone, *in* Fritz, P., and Fontes, J.C., eds., The terrestrial environment: Amsterdam, Elsevier, p. 239-269.

Sandiford, M., 2007, The tilting continent; a new constraint on the dynamic topographic field from Australia: Earth and Planetary Science Letters, v. 261, p. 152-163.

Sandiford, M., Quigley, M., de Broekert, P., and Jakia, S., 2009, Tectonic framework for the Cenozoic cratonic basins of Australia: Australian Journal of Earth Sciences, v. 56, p. 5-18.

Sattler, U., Immenhauser, A., Hillgaertner, H., and Esteban, M., 2005, Characterization,

lateral variability and lateral extent of discontinuity surfaces on a carbonate platform (Barremian to lower Aptian, Oman): Sedimentology, v. 52, p. 339-361.

SHINN, E.A., and LIDZ, B.H., 1988, Blackened limestone pebbles; fire at subaerial unconformities, *in* James, N.P., and Choquette, P.W., eds., Paleokarst: New York, Springer-Verlag, p. 117-131.

SIESSER, W.G., 1973, Diagenetically formed ooids and intraclasts in South African calcretes: Sedimentology, v. 20, p. 539-551.

STALLARD, R.F., 1988, Weathering and erosion in the humid tropics, *in* Lerman, A., and Meybeck, M., eds., Physical and Chemical Weathering in Geochemical Cycles, Kluwer Academic Publishers, p. 225-246.

STONE, J., ALLAN, G.L., FIFIELD, L.K., EVANS, J.M., and CHIVAS, A.R., 1994, Limestone erosion measurements with cosmogenic chlorine-36 in calcite - preliminary results from Australia: Nuclear Instruments and Methods in Physics Research Section B: Beam Interactions with Materials and Atoms, v. 92, p. 311-316.

STRASSER, A., 1984, Black-pebble occurrence and genesis in Holocene carbonate sediments (Florida Keys, Bahamas, and Tunisia): Journal of Sedimentary Petrology, v. 54, p. 1097-1109.

STRASSER, A., and DAVAUD, E., 1983, Black pebbles of the Purbeckian (Swiss and French Jura); lithology, geochemistry and origin: Eclogae Geologicae Helvetiae, v. 76, p. 551-580.

TAYLOR, P.M., and CHAFETZ, H.S., 2004, Floating rafts of calcite crystals in cave pools, central Texas, U.S.A; crystal habit vs. saturation state: Journal of Sedimentary Research, v. 74, p. 328-341.

TUCKER, M., 1990, Diagenetic processes, products and environments, *in* Tucker, M.E.,

Wright, V.P., and Dickson, J.A.D., eds., Carbonate Sedimentology: Oxford, Blackwell Sci. Publ., p. 314-364.

TURNEY, C.S.M., BIRD, M.I., and ROBERTS, R.G., 2001, Elemental 13C at Allen's Cave, Nullarbor Plain, Australia: Assessing post-depositional disturbance and reconstructing past environments: Journal of Quaternary Science, v. 16, p. 779-784.

VANSTONE, S.D., 1998, Late Dinantian palaeokarst of England and Wales; implications for exposure surface development: Sedimentology, v. 45, p. 19-37.

VERA, J.A., and JIMENEZ DE CISNEROS, C., 1993, Palaeogeographic significance of black pebbles (Lower Cretaceous, Prebetic, southern Spain): Palaeogeography, Palaeoclimatology, Palaeoecology, v. 102, p. 89-102.

VERRECCHIA, E.P., FREYTET, P., VERRECCHIA, K.E., and DUMONT, J.-L., 1995, Spherulites in calcrete laminar crusts; biogenic CaCO (sub 3) precipitation as a major contributor to crust formation: Journal of Sedimentary Research, Section A: Sedimentary Petrology and Processes, v. 65, p. 690-700.

WARD, W.C., FOLK, R.L., and WILSON, J.L., 1970, Blackening of eolianite and caliche adjacent to saline lakes, Isla Mujeres, Quintana Roo, Mexico: Journal of Sedimentary Petrology, v. 40, p. 548-555.

WARREN, J.K., 1983, Pedogenic calcrete as it occurs in Quaternary calcareous dunes in coastal South Australia: Journal of Sedimentary Research, v. 53, p. 787-796.

WASSON, R.J., and CLARK, R.L., 1988, The Quaternary in Australia - past, present and future: Quaternary Australasia, v. 6, p. 17-22.

WEBB, J.A., and JAMES, J.M., 2006, Karst evolution of the Nullarbor Plain, Australia, *in* Harmon, R.S., and Wicks, C.M., eds., Perspectives on Karst Geomorphology, Hydrology, and Geochemistry - A tribute volume to Derek C. Ford and William B.

White: Boulder, Geological Society of America p. 65-78.

WHITE, M.E., 1994, After the greening: The browning of Australia: Kenthurst, Kangaroo Press Pty Ltd., 288 p.

WHITE, W.B., 1988, Models for karst processes; old and new paradigms: Geo (super 2), v. 15, p. 34.

WHITE, W.B., 2002, Karst hydrology; recent developments and open questions: Engineering Geology, v. 65, p. 85-105.

WOODHEAD, J., HELLSTROM, J., MAAS, R., DRYSDALE, R., ZANCHETTA, G., DEVINE, P., and TAYLOR, E., 2006, U-Pb geochronology of speleothems by MC-ICPMS: Quaternary Geochronology, v. 1, p. 208-221.

WORTHINGTON, S.R.H., FORD, D.C., and BEDDOWS, P.A., 2000, Porosity and permeability enhancement in unconfined carbonate aquifers as a result of solution, *in* Klimchouk, A.B., Ford, D.C., Palmer, A.N., and Dreybrodt, W., eds., Speleogenesis evolution of karst aquifers: Huntsville, National Speleological Society, p. 463-472.

WRIGHT, V.P., 1986, The role of fungal biomineralization in the formation of Early Carboniferous soil fabrics: Sedimentology, v. 33, p. 831-838.

WRIGHT, V.P., 1988, Paleokarsts and Paleosols as indicators of paleoclimate and porosity evolution; a case study from the Carboniferous of South Wales, *in* James, N.P., and Choquette, P.W., eds., Paleokarst: New York, Springer-Verlag, p. 329-341.

WRIGHT, V.P., 1989, Terrestrial stromatolites and laminar calcretes; a review: Sedimentary Geology, v. 65, p. 1-13.

WRIGHT, V.P., 1994, Paleosols in shallow marine carbonate sequences: Earth-Science Reviews, v. 35, p. 367-395.

WRIGHT, V.P., ALONSO ZARZA, A.M., SANZ, M.E., and CALVO, J.P., 1997, Diagenesis of late

Miocene micritic lacustrine carbonates, Madrid Basin, Spain: Sedimentary Geology, v. 114, p. 81-95.

Wright, V.P., Platt, N.H., and Wimbledon, W.A., 1988, Biogenic laminar calcretes: evidence of calcified root-mat horizons in paleosols: Sedimentology, v. 35, p. 603-620.

Zhou, J., and Chafetz, H.S., 2009, Biogenic caliches in Texas; the role of organisms and effect of climate: Sedimentary Geology, v. 222, p. 207-225.

# CHAPTER 3

# AUTOGENIC MICROBIAL GENESIS OF MIDDLE MIOCENE PALUSTRINE OOIDS; NULLARBOR PLAIN, AUSTRALIA

Cody R. Miller and Noel P. James

## ABSTRACT

Miocene palustrine ooids located in the Nullarbor Plain, southern Australia, illustrate the importance of microbes and soil processes in the formation of these spherically laminated grains in pedogenic settings. These particles are composed of dense minimicrite and include a wide assortment of microbially produced structures. Such biogenicity includes interpreted extracellular polymers (EPS), algal filaments, palygorskite and sepiolite nano-fiber mats, bacterial spores, and meniscate fabrics. Ooid nuclei are peloids that are interpreted to have formed via microbial binding of lacustrine sediment in a subsequent palustrine environment, both at the surface and inside underlying karst cavities. The peloids are encapsulated in multigenerational micrite laminations that form the spherical cortex. Individual cortical laminae are made up of degraded minimicrite crystals and complex encrusting mats of palygorskite and sepiolite nano-fibers. Cortex generation is interpreted to have been an annual process involving alternating soil hydration states. In this conceptual model, during the wet season, ooids were covered in bacterial mucus that bound ions from solution and produced hydrated Mg-Si gels that evenly surrounded the entire ooid. Gel dehydration during the following dry season resulted in fibrous palygorskite and sepiolite precipitation.

Succeeding seasonal variations in moisture produced numerous laminae that ultimately resulted in a multigenerational ooid cortex. This annual microbial process provides a new mechanism involving an autogenic formation of ooids that may be applied to a wide variety of pedogenic sediments. Unlike the more common marine ooids that require constant movement to achieve cortical precipitation, the process of grainification, combined with microbial mediated mineral precipitation under different soil hydration states, results in the in-place formation of terrestrial ooids.

## INTRODUCTION

Ooids and pisoids have been ubiquitous components of sedimentary rocks since the Archean (Peryt 1983a; Wright 1990; Flügel 2004). The majority of these spherically coated carbonate grains are generated in shallow marine environments, although they can also form in a wide variety of terrestrial settings such as caves, lakes, rivers, and calcareous soils (Peryt 1983a; Barton 2006; Barton and Jurado 2007; Zhou and Chafetz 2009; Alonso-Zarza and Wright 2010; Gierlowski-Kordesch 2010; Jones 2011a). Marine ooids have been studied extensively, whereas their terrestrial counterparts have garnered much less attention.

Perhaps the most common terrestrial ooids appear in pedogenic environments (Calvet and Julia 1983; Wright 1994; Alonso-Zarza 2006; Alonso-Zarza and Wright 2010). These terrestrial coated grains are increasingly being found to have microbial affinities, suggesting a biogenic influence during their formation (James 1972; Calvet and Julia 1983; Phillips et al. 1987; Alonso-Zarza et al. 1992; Armenteros and Daley 1998; Loisy et al. 1999; Folk and Rasbury 2007; Zhou and Chafetz 2009; Alonso-Zarza and Wright 2010). Palustrine ooids

(those formed in pedogenically overprinted lacustrine sediments) are known to occur in organic soil environments where the presence of microbes are thought to have far-reaching effects on their genesis (Alonso-Zarza et al. 1992; Armenteros and Daley 1998; Alonso-Zarza and Wright 2010). Whereas these microbial attributes are recognized in pedogenic sediments, there is less certainty as to how microbial processes contribute to the formation of these spherically laminated grains. Current hypotheses involve complicated mechanisms of grain rolling akin to their counterparts in marine realms (Wright 1994), microbial binding and precipitation of calcite (Jones 1991; Folk and Lynch 2001), and capillary pore water movement (Siesser 1973).

Well-preserved and widely exposed middle Miocene interpreted palustrine ooids associated with prolonged subaerial exposure of the Nullarbor Plain in southern Australia (Fig. 3.1) offer the opportunity to explore the formation of these conspicuous grains. This multi-scale study uses multiple petrographic and geochemical techniques to arrive at a new mechanism for terrestrial ooid formation. The purposes of this paper are to: 1) document the Miocene palustrine ooids on the Nullarbor Plain, 2) ascertain the role of microbes in the formation of these grains, and 3) propose a microbial mechanism for the *in situ* genesis of pedogenic coated grains that may be applicable to other ancient examples worldwide.

## TERMINOLOGY

A wide variety of terms have been used to classify coated grains developed in terrestrial carbonate environments (Appendix E). These include ooids (Braithwaite 1983; Brasier 2011), vadose ooids (Harrison 1977), vadoids (Peryt 1983b), pedogenic coated grains (Wright 1989), terrestrial oncoids (Jones 1991; Jones 2011a), and peloids (Alonso-

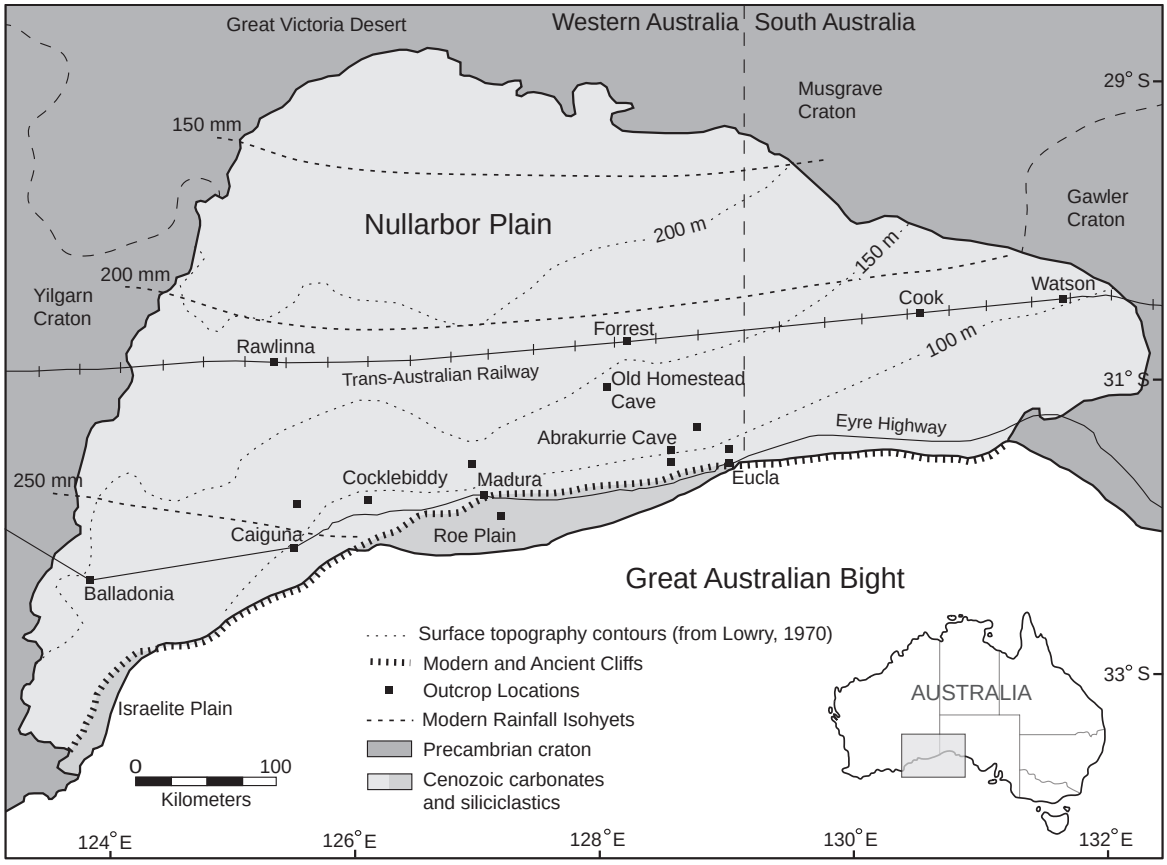


**Figure 3.1.** Nullarbor Plain location map showing outcrops, modern rainfall isohyets, surface elevation contours, important geographic features, and villages.

Zarza et al. 1992; Alonso-Zarza 2003). Herein, the unadorned term "ooid" is applied to all spherically laminated carbonate grains across the Nullarbor Plain. Use of this term acknowledges the widely accepted definition of the term ooid, which is a biotic or abiotic spherically coated grain with a well-defined laminated cortex, nucleus, commonly less than 2 mm in size, and usually formed of calcium carbonate but may be of other mineralogy (Newell et al. 1960; Flügel 1982; Wright 1990; Flügel 2004).

The crystal size of minimicrite and micrite has been fraught with inconsistencies (Jones 2011a). The term "micrite" has been most widely used to describe Mg-calcite and calcite crystals 1 – 4 μm in size, whereas "minimicrite" describes crystal sizes < 1 μm (Folk 1974; Flügel 2004). Herein, these crystal dimensions will be used to differentiate between the two types of microcrystalline calcite. Minimicrite appears as a dense fabric in thin section but in SEM it has a regular crystal size and structure, with planar crystal boundaries and high intercrystalline porosity (Flügel 2004).

## SETTING

The Nullarbor Plain, located on the southern margin of Australian continent, is a vast featureless (approximately 240,000 $km^2$) landscape that comprises the world's largest areal karst. Cenozoic marine limestones underlying the plain are part of the Eucla Basin, a shallow epicratonic depression that developed on the boundaries of the Yilgarn, Musgrave, and Grawler cratons (Hocking 1990) (Fig. 3.1). The Plain has been subaerially exposed since the middle Miocene (~ 14 m.y.) resulting in extensive diagenetic alteration of the underlying marine limestone, particularly in the Nullarbor Limestone, which forms the modern surface of the Plain (King 1950; Lowry and Jennings 1974; Webb and James 2006;

Miller et al. 2012).

Three broad phases of alteration are recognized in the Nullarbor Limestone (Fig. 3.2) (Miller et al. 2012). The focus of this study is on components in the earliest phase of diagenesis and includes: microkarst, lacustrine sediments, and subsequent palustrine pedogenetic deposits. These processes are interpreted to have taken place during the middle Miocene when the regional climate was humid to temperate (Miller et al. 2012). During this time the plain is thought to have hosted a cool temperate rainforest, with large inland lakes and marshes, akin to those of modern day northern Tasmania (White 1994; Drexel and Preiss 1995; Johnson 2009; Miller et al. 2012).

Today, the Nullarbor Plain lies under an arid to semi-arid climate with marked annual temperature differences, with mean temperatures from 23° – 26° C in summer to 10° – 12° C in winter (Goede et al. 1990). Annual rainfall is between 150 – 250 mm, increasing towards coastal regions, whereas potential evaporation exceeds 2500 – 3000 mm (Australian Water Resources Council 1976). These arid conditions allow only sparse vegetation that is dominated by shrubby salt brush and isolated groves of small eucalypts near the coast (Dunkley and Wigley 1967; Lowry and Jennings 1974).

## METHODS

Twenty-one locations were studied across the Nullarbor Plain with samples collected at sixteen of the sites. Outcrops are restricted to dolines, caves, quarries, and road cuts (Fig. 3.1). Forty-two polished thin sections were prepared from these samples and analyzed with standard transmission light microscopy. Eleven samples used for scanning electron microscopy (SEM) analyses were chosen based on fabric orientation

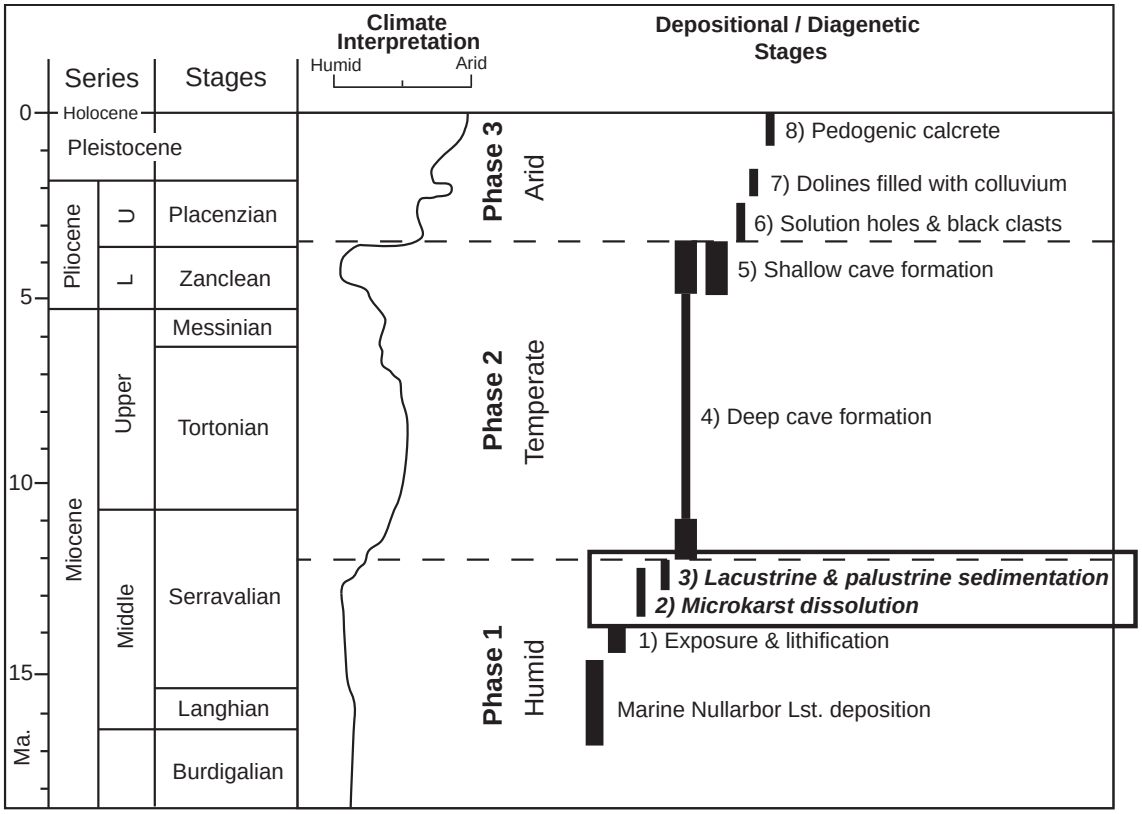


**Figure 3.2.** Paragenetic history of the Nullarbor Plain since initial subaerial exposure in the middle Miocene (~14 my). Width of lines in the timeline of diagenetic phases illustrates the relative intensity of the processes (a wider line represents more intensive processes). (Modified from Miller et al. 2012)

and features in thin section. They were mounted on stubs using silver conductive glue and sputter coated with gold prior to examination on a JOEL Field Emission SEM (JOEL 6301FE) at the University of Alberta. An accelerating voltage of 5 kV was used to obtain high magnification images, whereas 20 kV was used while completing energy-dispersive X-ray (EDX) analyses. These analyses obtained from the Princeton Gamm-Tech X-ray analysis system (attached to the SEM) were used for elemental content determination. The minimum beam diameter is 1 µm, which is larger than most of the microbial fabrics in the samples. This challenge was overcome by analyzing large mats of microbes rather than single filaments and ensuring that the thickest portions were investigated, as outlined in Jones (2010b). Multiple analyses were used to limit error in establishing the elemental components in each fabric. Mineralogy of various diagenetic fabrics was determined using x-ray diffraction (XRD) with a Co anode and zero background plate (Hardy and Tucker 1988). Clay mineralogy was determined from samples that had their calcium carbonate fraction dissolved. The samples were dissolved in 20 % HCl, with the remaining insoluble residue being rinsed with de-ionized water to ensure sample purity and consistency.

## MIDDLE MIOCENE MICROKARST

The Nullarbor Limestone was lithified shortly after uplift and subaerial exposure via dissolution and equilibration of metastable carbonate minerals with meteoric fluids, resulting in extensive diagenetic low-Mg calcite cement precipitation and numerous dissolution molds (Miller et al. 2012). Extensive fabric-selective microkarst dissolution occurred in the upper 20 m of the Nullarbor Limestone shortly after lithification (Fig. 3.3). These microkarst features are widespread and occur across the Nullarbor Plain except at

Cook quarry (Fig. 3.1) (Miller et al. 2012). Cook quarry lacks microkarst and instead the Nullarbor Limestone at this location is still friable with high porosity and permeability. Elsewhere on the plain, dissolution was destructive with an estimated 25 % of the Nullarbor Limestone being dissolved, locally increasing to 75 %. Resultant cavities lack speleothems but are instead filled with sediment.

## MIDDLE MIOCENE POST-KARST SEDIMENTATION

Miller et al. (2012) document the general aspects of this diagenetic phase and offer interpretations for its position in the paragenetic sequence, geologic age, and depositional history. Sediment that formed after the period of karsting comprises a suite of muddy and grainy carbonates that are now only preserved in the microkarst cavities except for one bed at the top of Cook quarry (Fig. 3.1). These deposits include two distinct lithologies 1) oolites (packstone to grainstone fabrics) and 2) laminated micrite whose components include, in order of abundance, ooids, alveolar and filamentous micrite, peloids, structureless micrite, low-Mg calcite cement, charophytes, and ostracods. Sediment composition is consistent across the Nullarbor Plain with oolites forming the majority of these deposits. Ooids are the focus of this study and are located in both the microkarst cavities and on the surface at Cook quarry.

### *Oolite*

Post-karst sediments are dominated by spherical, sand size (0.5 – 2.0 mm) ooids (Fig. 3.4A). The grains are poorly sorted (Fig. 3.4B) with rare inverse grading present in microkarst cavities. Grains are almost entirely micrite with a well-defined nucleus and

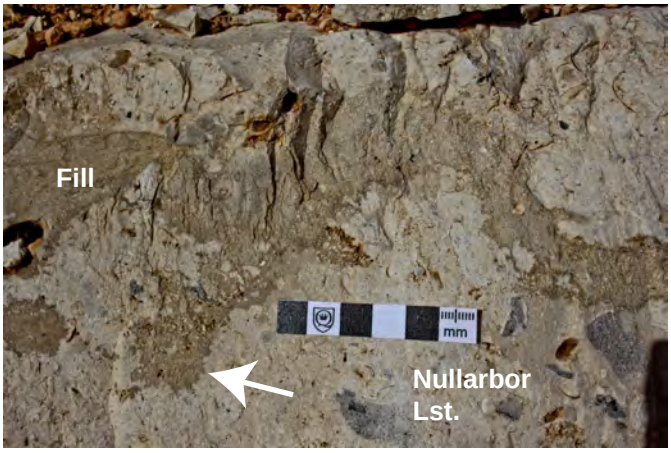


**Figure 3.3.** Middle Miocene microkarst – Watson Quarry outcrop showing microkarst cavities. The cavities have digitate boundaries and are filled with micritic sediment, which is in stark contrast to the surrounding Nullarbor Limestone grainstone lithology.

laminated cortex (Fig. 3.4C, D). They are light gray to yellowish gray color in outcrop and moderate brown under plane-polarized light (PPL), with rare black nuclei. Inverse graded beds are thin (< 10 cm), isolated to specific cavities, and typically bounded above and below by micrite laminations or ungraded ooids. The ooid nucleus and cortex each have a suite of recurring characteristics and morphologies.

Peloids are relatively minor constituents, although they increase in relative abundance in northern portions of the Nullarbor Plain. They are important, however, because they constitute ooid nuclei. Grains are small (typically < 2 mm), spherical, and composed of dense and commonly clotted low-Mg calcite micrite with a moderate brown color in standard transmitted light petrography. This structureless micrite can contain charophytes and unidentifiable fossil fragments.

### *Laminated Micrite*

Laminated micrite layers (5 – 15 cm in thickness) line the base of some microkarst cavities and contain poorly preserved charophytes and ostracods (Fig. 3.5A) (Miller et al. 2012). Laminations range in thickness from 50 μm to 500 μm and are composed of different colored dense micrite. Thin (100 - 300 μm) zones of multigenerational calcite cement commonly alternate with micrite laminations (Fig. 3.5B). Botryoidal calcite fans that radiate upward and branch into complex arrangements are a common morphology in the laminated layers (Fig. 3.5B). The calcite cement in these fans has a more cloudy and moderate brown hue in transmitted light microscopy than later pore-filling sparry calcite cement. Laminated micrite layers are not present at Cook quarry.

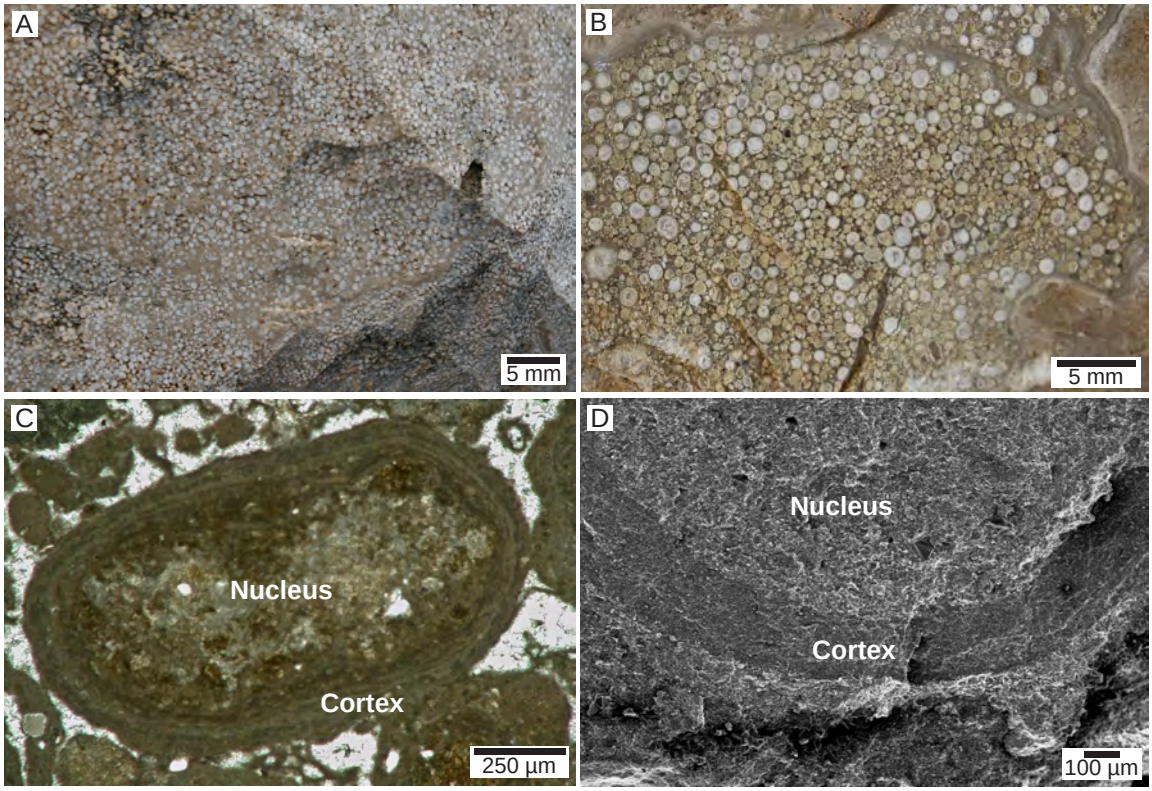


**Figure 3.4.** Ooids A) Microkarst cavity filled with spherical ooids of various sizes at Eucla Quarry. B) Ooids in a microkarst cavity at Eucla quarry illustrating their dominantly poorly sorted nature. C) Photomicrograph of an individual ooid with a clotted micrite nucleus and thinly laminated cortex; Rawlinna Quarry. D) SEM image of an ooid from Cook Quarry showing the subdivision between the nucleus and cortex.

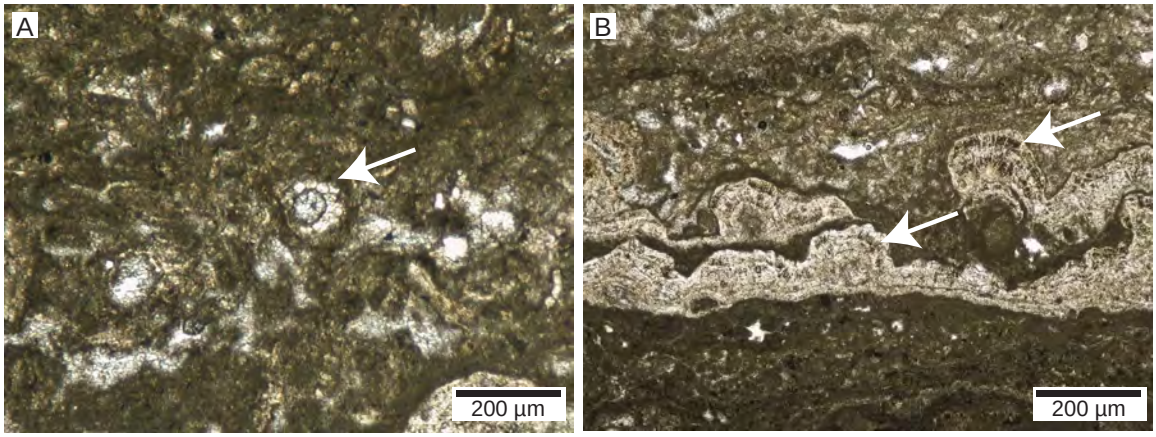


**Figure 3.5.** Laminated Micrite A) Photomicrograph of laminated micrite bed with partially preserved charophyte debris (arrow); Cook Quarry. B) Photomicrograph of botryoidal radial fibrous calcite (arrows) along laminations in dense micrite. The calcite cements have dark bands of inclusions in some portions, interpreted to represent incorporated organic stains. Way up is towards the top of the page.

*Paleoenvironmental Interpretation*

Miller et al. (2012) has demonstrated that microkarst cavities and post-karst lacustrine and palustrine sediments are uniform across the Nullarbor Plain indicating a widespread similarity of origin and common paleoenvironmental interpretation (Fig. 3.6). The karst cavities that immediately post-date the lithification of the Nullarbor Limestone lack any speleothems or other calcite precipitates indicating that the plain's surface was barren limestone (Fig. 3.6A), since soils would have incorporated $CO_2$ into the water system and through degassing in the cavities precipitated calcite (Miller et al. 2012).

Lacustrine environments are interpreted to have formed across the Nullarbor Plain following this extensive dissolution, depositing laminated micrite sediments with associated fresh to brackish water fossils. These sediments would have not only been deposited on the surface but also in the newly formed cavities (Fig. 3.6B). Laminated sections that are rarely preserved in isolated or basal sections of microkarst cavities represent this original lacustrine depositional event (Miller et al. 2012). The lacustrine systems progressively altered into established palustrine environments where extensive pedogenic modification destroyed almost all original bedding. These pedogenic settings extended from the surfical sediment down into the underlying microkarst sediment. Such palustrine settings are interpreted to have been the sites for *in situ* peloid and ooid development outlined in the proceeding sections (Fig. 3.6C) (Alonso-Zarza et al. 1992; Armenteros and Daley 1998; Freytet and Verrecchia 2002; Alonso-Zarza 2006; Miller et al. 2012). Surface deposits have since been removed by subsequent erosion and diagenesis in all but one location at Cook quarry. The microkarst cavities offered increased preservation potential, whereas most surfical deposits were removed due to subsequent erosion and diagenesis (Fig. 3.6D).

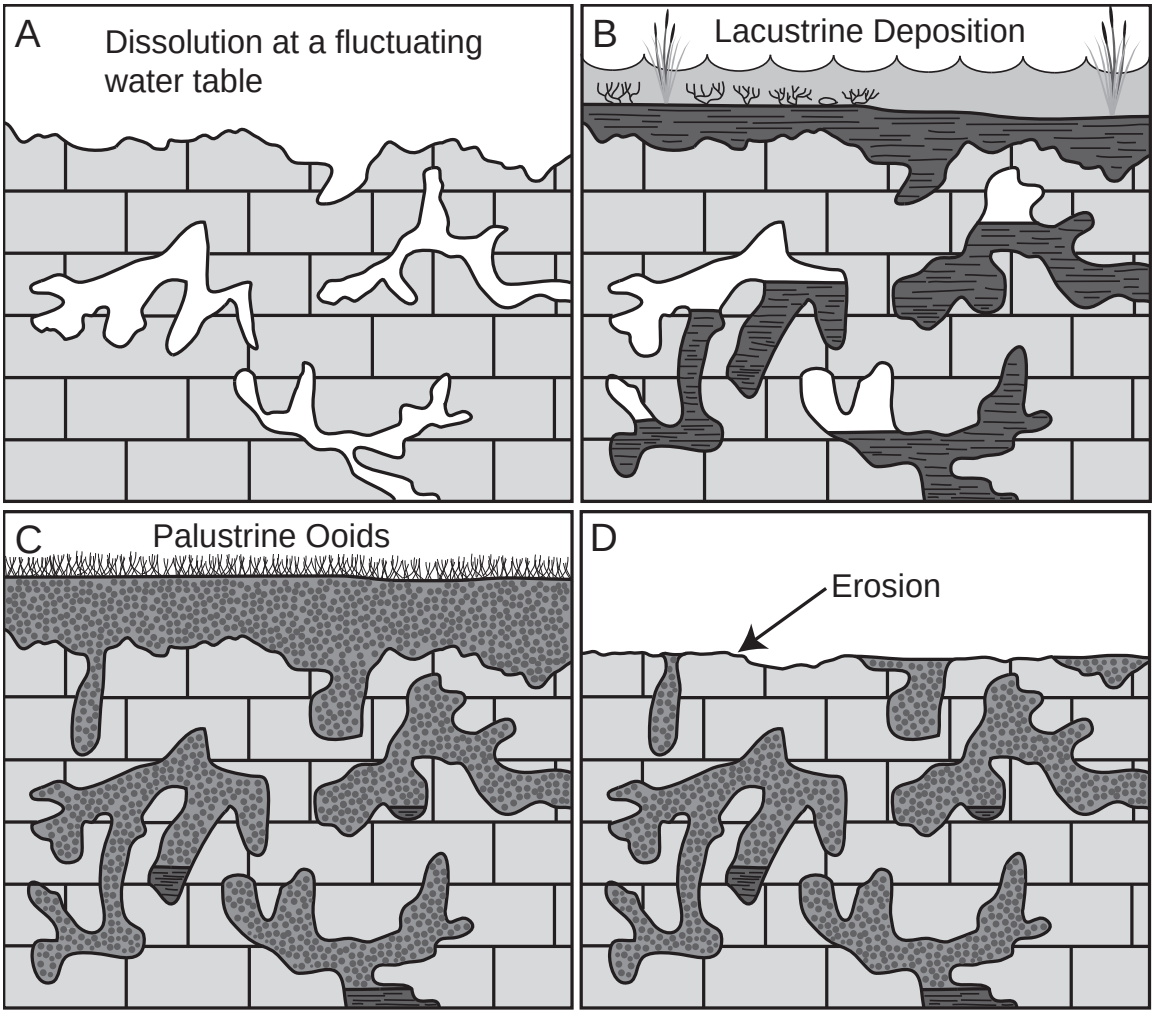


**Figure 3.6.** Evolution of microkarst and sedimentation A) Subdued surface and extensive subsurface karst of underlying Nullarbor Limestone. B) Introduction of lacustrine environments across the Nullarbor Plain and deposition of fine grained calcareous sediments on surface and in microkarst cavities. C) Extensive pedogenic processes in a palustrine environment alter the lacustrine sediment, producing ooids, in both the subsurface and surface environments. D) Subsequent erosion and diagenesis removes most surfical palustrine sediments, leaving the only evidence of such an environment in the underlying karst cavities.

## OOID PETROGRAPHY

Nullarbor Plain palustrine ooids have widespread and characteristic fabrics in their nucleus, cortex, and associated intergranular pore spaces (Fig. 3.7). Ooid nuclei are micritic peloids and rare blackened clasts that have a complex and repeatable suite of microstructural fabrics. Cortical laminations vary in thickness from 50 to 200 μm and encompass the entire nuclei, leading to their dominantly spherical shape. The entire ooid is dominated by structureless to partially clotted micrite and minimicrite. Circumgranular cracks, filled with sparry calcite cement, are a common attribute in the ooids and tend to be prevalent in all ooids where present.

### *Ooid Nucleus*

The nucleus consists of minimicrite and micrite, smooth calcareous coatings, and smooth calcareous strands. Minimicrite comprises > 90 % of the core together with micrite and local small unidentifiable bioclasts and fragmented charophyte debris. Minimicrite crystal size is variable, ranging from < 100 nm to 1 μm (Fig. 3.8A). Crystals have well-defined boundaries that become more distinct with increasing crystal size. The small crystal size and random crystal orientations lead to microporosity estimated at 10 % throughout the nucleus.

**Smooth Calcareous Coatings.—**Thin (<100 nm), localized, and uniform calcite coatings are common throughout the ooid nucleus. These coatings have a smooth surfical appearance that completely obscures the surfaces of minimicrite crystals and other fabrics (Fig. 3.8B). They occur as 5 – 15 μm wide zones throughout the ooid nucleus, with the areas between composed of minimicrite (Fig. 3.8C). The fabrics locally have linear and parallel sets

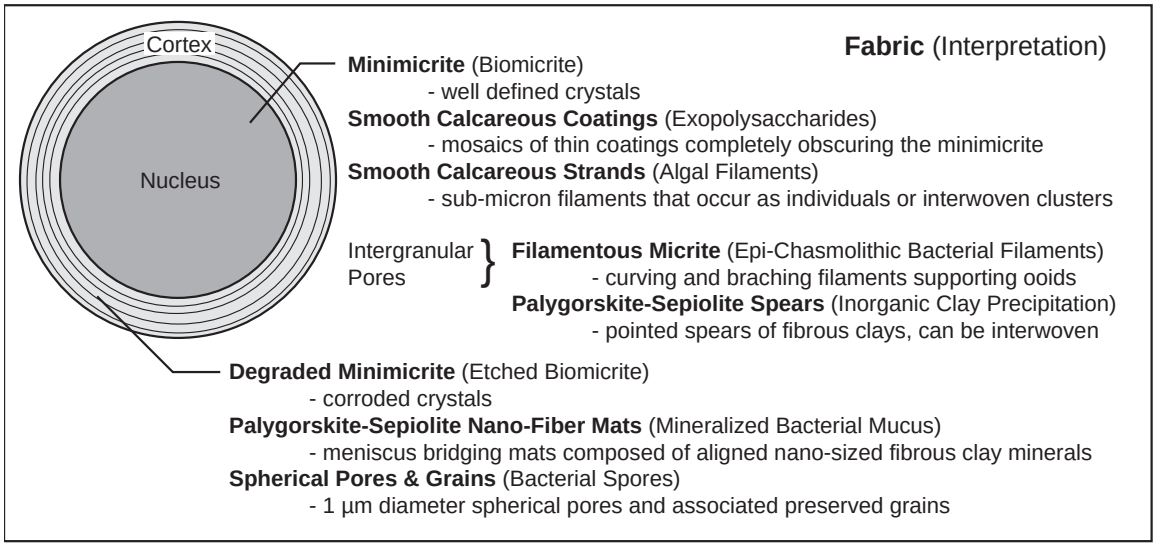


**Figure 3.7.** Diagrammatic illustration of an ooid showing the locations of the morphological characteristics that define the nucleus and cortex. Bold print is the structure or fabric, their interpretation is in parentheses immediately following, and listed below is a short description of the feature.

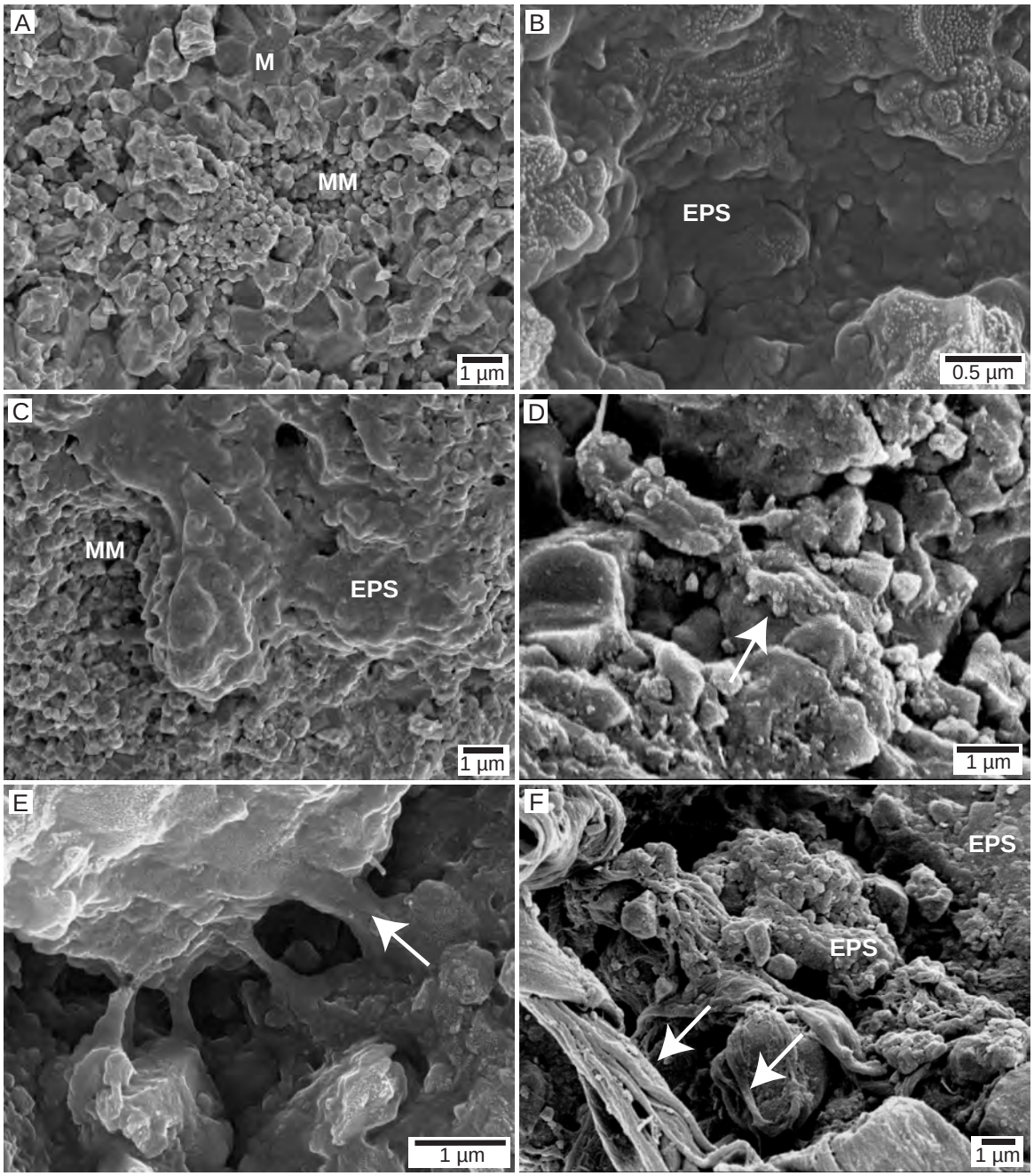


**Figure 3.8.** Ooid Nucleus A) SEM image showing the relationships between micrite (M) and minimicrite (MM) with abundant microporosity in an ooid nucleus from Cook Quarry. B) SEM image of interpreted exopolysaccharides (EPS) coatings in an ooid nucleus from Cook Quarry. The small 30 nm wide beads on areas of the interpreted EPS are interpreted to be an artifact from gold coating. C) SEM image of same ooid nucleus from Cook Quarry showing mosaics of interpreted EPS and minimicrite. This patchy relationship is widespread in ooid nuclei. D) Cascading façade of interpreted EPS (arrow) covering the sides of larger micrite crystals in an SEM image of an ooid nucleus; Rawlinna Quarry. E) SEM image of EPS bridges across a 1 µm pore. The bridges are narrowest at their midsections (arrow) and widen at their attachments; Cook Quarry. F) SEM image of algal filaments (arrow) entwining with neighboring filaments, minimicrite crystals, and EPS fabrics; Eucla Quarry.

of fissures that create an uneven surface. Coating mineralogy throughout ooid nuclei is mostly calcite with rare Mg and Si mineralization, as determined only by EDX analyses with the SEM because of the small size.

Smooth calcified fabrics commonly cover the tops and extend partially down the sides of larger grains, creating a cascading facade (Fig. 3.8D). These fabrics grade into the smooth fabrics to form bridges across small (1 - 3 μm) pores. The smooth calcareous bridges are typically < 1 μm thick at their midpoints and widen where they attach to neighboring grains or other smooth zones (Fig. 3.8E).

**Smooth Calcareous Strands.—**The nuclei have varying proportions of calcareous strands (0.3 – 0.5 μm wide and 2 – 10 μm in length) with smooth outer surfaces and a constant thickness through their length. They occur as isolated strands although small interwoven clusters of individual strands curl and entwine with themselves and neighboring strands (Fig. 3.8F). Most are entombed in the minimicrite matrix and have complex multifaceted terminal attachments to the substrate (Fig. 3.8F). Strands, especially where they attach to other grains, can be uncoated, partially coated, or fully covered by smooth calcareous coatings, suggesting that they are coeval.

### *Ooid Cortex*

Cortical laminations have a diverse assemblage of micro-scale and nano-scale fabrics including palygorskite-sepiolite nano-fiber mats, degraded minimicrite, and spherical pores and grains. These fabrics are unique to the cortex and do not occur in the ooid nucleus and similarly, smooth calcareous strands are absent from ooid cortices. As in the nucleus, the cortex has extensive minimicrite, although the crystals have a degraded, smoothed, and commonly pitted appearance when compared to similar well-defined crystals in the nucleus

(Fig. 3.9A).

**Palygorskite-Sepiolite Nano-Fiber Mats.—**Palygorskite and sepiolite nano-fibers, which create continuous mats enveloping the entire nucleus and appear to follow an underlying branching morphologic structure are the dominant feature in ooid cortices (Fig. 3.9B). These straight fibers are 15 – 30 nm wide, 0.5 – 5.0 μm long (Fig. 3.9C). Individual nano-fibers entwine and weave together to create an encrusting and scalloped mat (Fig. 3.9D). The nano-fiber mats surround and incorporate minimicrite grains, and create intricate fabrics that bridge across 1 - 2 μm wide pores. This bridging fabric creates interconnecting meniscus structures and mats that grow over each other (Fig. 3.9C, D). Meniscus structures have a gently curved morphology, with distinct boundaries that are progressively wider at the ends and thinner in the mid-section. Such fabrics form the laterally continuous, porous, and encrusting structure of these mats.

Nano-fibers have different morphologies depending on which cortex lamination they comprise; fibers near the nucleus generally have a rudimentary alignment and are flattened (Fig. 3.9D); fibers on the outermost cortex lamination have a “spiky” and pointed morphology. This transition of fiber morphology is gradational with respect to the nucleus surface and inter-ooid pore space (Fig. 3.9E).

XRD analyzes of bulk Nullarbor Plain ooid samples consistently yield a low-Mg calcite mineralogy (Fig. 3.10A). This low-Mg calcite mineralogy is, however, not as prevalent when nano-fiber mats are analyzed in greater detail with EDX elemental analyses performed on the SEM. The nano-fiber mats in the ooid cortex are predominantly composed of the elements Ca, Mg and Si, with lesser amounts of Al (Fig. 3.10B). Determination of nano-fiber mat mineralogy through XRD analysis was only viable if the calcium carbonate content was not high.

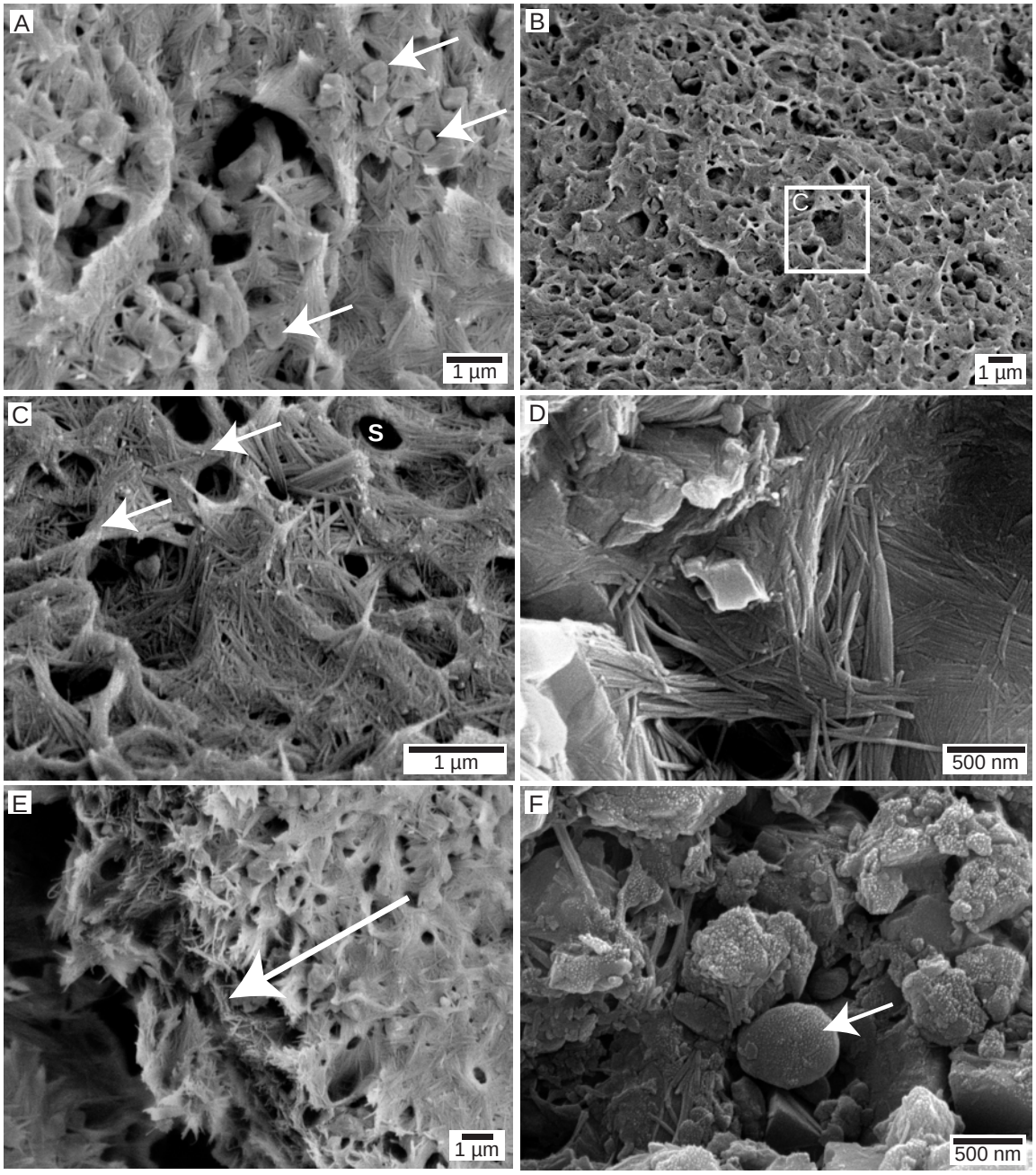


**Figure 3.9.** Ooid Cortex A) SEM image of nano-fiber mat in ooid cortex with degraded minimicrite crystals; Old Homestead Cave. B) Plan view in an SEM image of nano-fiber mat in an ooid cortex from Old Homestead Cave with an encrusting morphology, a multitude of bridging meniscus structures, and incorporated minimicrite crystals. C) Higher magnification SEM image of (C) illustrating the intricate network of intertwining and bridging nano-fibers to create laterally pervasive mats. Arrows point towards the abundant meniscus structures that outline the nano-fiber mats general structure; (S) represents the small and numerous voids left by a preexisting feature, interpreted to be organic. D) High magnification SEM image of a bridging nano-fiber mat at Cocklebiddy Cave showing the aligned nature of individual fibers and the interweaving of fibers at the ends of meniscus structures. E) SEM image of the changing morphology in nano-fibers across a portion of the ooid cortex. The arrow points towards the outside lamination and pore space and away from the ooid nucleus. Nano-fibers are flat nearer to the nucleus and become more fibrous the closer they get to the edge of the ooid cortex; Cook Quarry. F) High magnification SEM image of small spherical particle that is preserved and is similar size to the small pores shown in (C), interpreted to be a bacterial spore; Eucla Quarry.

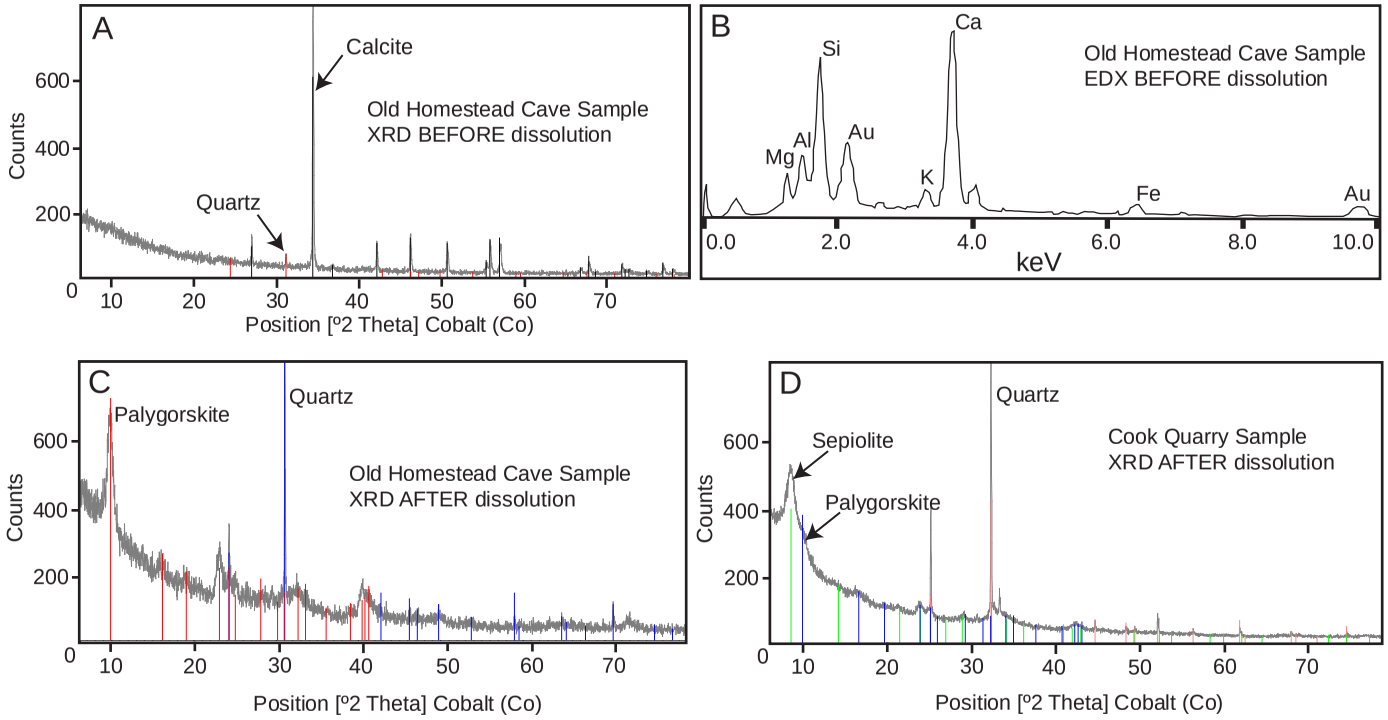


**Figure 3.10.** Mineralogy A) XRD profile for ooid sample from Old Homestead Cave showing the dominant low-Mg calcite mineralogy. B) EDX profile of a nano-fiber mat from same Old Homestead Cave ooid sample showing abundant elements suggesting mineralogy different than that obtained from XRD. C) XRD profile of same Old Homestead Cave ooid sample after dissolving all carbonate minerals, showing a dominant palygorskite and quartz mineralogy. D) XRD profile of a Cook Quarry ooid sample after calcite dissolution showing similar results to Old Homestead Cave although with both sepiolite and palygorskite present.

Calcium carbonate was removed from the ooids through dissolution in 20 % HCl, leaving a solid phase of cortical nano-fiber mats with no apparent corrosion or alteration via acid treatment. Matrix material and ooid nuclei were completely removed during dissolution, whereas all ooid cortices were preserved as thin, hollow spheres. XRD analyzes of the residual material determined that nano-fiber mats are composed of palygorskite and sepiolite clays and are ubiquitous in ooid cortices across the Nullarbor Plain (Fig. 3.10C, D). The nano-fibers that comprise the encrusting mats in ooids cortices represent the fibrous crystalline structure of palygorskite and sepiolite (Birsoy 2002). The lath and fibrous morphology has a crystallographic a-axis parallel to the fibers length (Gehring et al. 1995; Folk and Rasbury 2007). Small quantities of quartz are also present in all the dissolved ooid samples.

**Spherical Pores and Grains.—**Numerous small spherical pores (~ 0.5 μm) occur within the nano-fiber mats and are thought to represent a pre-existing feature that has since been removed (Fig. 3.9C). The size and circular shape of these pores remain consistent throughout the cortex lamination. Nano-fiber mats commonly wrap around these small features and do not bridge across them. Small spherical calcareous grains are rarely preserved with their uniform shape closely matching these pores (Fig. 3.9F). The grain's outer surface has a smooth texture and is commonly covered in smooth calcareous coatings, locally making contacts between individual spheres diffuse.

### *Intergranular Pores*

Pores in the oolite packstone to grainstone are filled with, in order of abundance, large filamentous micrite fabrics, low-Mg sparry calcite cement, palygorskite-sepiolite spears, and structureless micrite. These fabrics support the ooids with little original porosity

preserved in the oolite. Extensive porosity does occur in isolated microkarst cavities where filamentous micrite and clear calcite cements are absent. These zones are extensively weathered in both quarry and doline walls.

**Filamentous Micrite.—**Microkarst cavities locally have micrite linings that grade laterally into filamentous structures. These thin linings (0.5 – 2.0 mm thick) have complex laminated, clotted, and bulbous morphologies (Fig. 3.11A). These different morphologies commonly grade into each other in localized cavity linings. Dendritic fabrics are orientated either upward or downward in cavities, depending on the orientation of the cavity wall. The microstructure of these linings is composed of minimicrite and smooth calcareous coatings.

Filamentous micrite structures occur exclusively with ooids in microkarst cavity fills and at the surface in Cook quarry. Complex intergranular networks of anastomosing curved and branching micrite filaments (15 – 35 μm thick) (Fig. 3.11B) are commonly the only material in intergranular pore spaces. These larger filaments bridge between grains, such that they are supporting the ooids; there are very few ooid grain-to-grain contacts (Fig. 3.11C). Under high magnification (~ 2000x) they are composed dominantly of minimicrite crystals covered with smooth calcareous coatings, creating an even undulating surface (Fig. 3.11D). Zones of these smooth coatings amongst the minimicrite outline the slightly curved, 75 μm long and 10 μm wide, filament structure. Clear, sparry calcite cement fills intergranular pore spaces that are not occupied by these filaments and ooids.

**Palygorskite-Sepiolite Spears.—**Large intergranular pores between individual ooids have a distinctly different nano-fiber morphology when compared to those of the ooid cortex. The spaces between ooids not filled by filamentous micrite or sparry calcite cement have complex arrangements of acicular palygorskite and sepiolite (Fig. 3.11E). These structures resemble sea urchins with spines sticking out of a nucleation point, typically on micrite or the

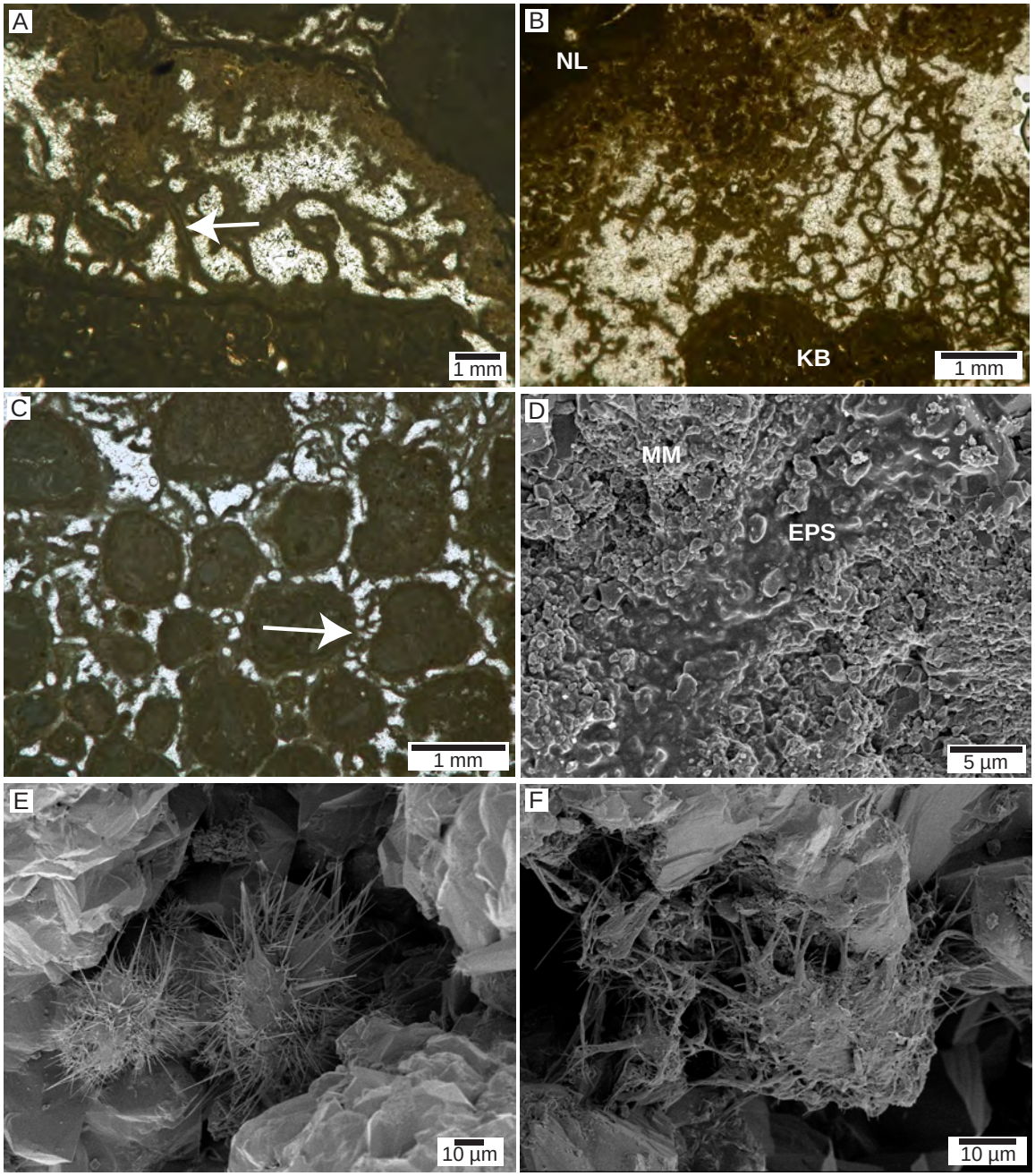


**Figure 3.11.** Intergranular Pores A) Photomicrograph of a microkarst cavity lining at Rawlinna Quarry. The lining grades from dendritic clotted micrite into branching individual filaments that have a curved appearance and double micrite walls (arrow). B) Lower magnification photomicrograph of the same Rawlinna Quarry cavity lining showing the complex curved and branching morphology of filamentous micrite suspending a karst breecia clast (KB). (NL represents Nullarbor Limestone) C) Photomicrograph of small ooids completely supported by filamentous micrite; few grain-to-grain contacts are observed; Cook Quarry. D) SEM image of the filamentous micrite in Rawlinna Quarry. Minimicrite (MM) and interpreted EPS outline the structure of the filaments, which are either surrounded by micrite or sparry calcite crystals. E) Fibrous palygorskite nucleating off small micrite grains in the intergranular pore spaces between ooids; Old Homestead Cave. F) Palygorskite fibers binding and suspending a small grain onto the sparry calcite crystals near the edge of an ooid; Cook Quarry.

ooid surface. The palygorskite and sepiolite crystals appear to have grown unimpeded into the pore space. Palygorskite-sepiolite nano-fibers locally coalesce, twist, and intertwine to form larger (~ 1 μm) rope-like chords. The nano-fibers also incorporate micrite grains onto the outer edges of ooids causing the grains to have a suspended appearance (Fig. 3.11F).

## MICROBIAL OOID GENESIS

Nullarbor Plain palustrine ooids have characteristics that imply formation via complex interactions between microbes and mineralization processes. High-resolution SEM images reveal numerous interpreted microscopic microbial fabrics including exopolysaccharides, epi- and chasmolithic bacterial filaments, algal filaments, bacterial mucus, and bacterial spores. This diverse abundance of interpreted microbial communities suggests that they had a systematic role in the formation of the palustrine ooids. Rapid mineralization processes that in turn produce the ooid fabrics also promote microbe preservation.

### *Palustrine Grainification*

Ooid nuclei are essentially micritic peloids produced by the pedogenic reworking of lacustrine sediment in a palustrine environment (Alonso-Zarza et al. 1992; Wright et al. 1997; Armenteros and Daley 1998; Alonso-Zarza 2003). This process is important to the production of peloids in terrestrial environments and formed through a complex interaction of physical, chemical, and biological components. The close relationships between smooth calcareous coatings and smooth calcareous strands that are found in ooid nuclei suggest that they were contemporaneous and thus formed via a common suite of processes.

The desiccation and aggregation of muddy sediment into peloids is termed

"grainification" and produces "diagenetic grainstones" that have been documented in palustrine deposits worldwide (Wright 1990; Alonso-Zarza et al. 1992; Alonso-Zarza and Wright 2010). The degree of grainification in palustrine environments can be directly related to advancing pedogenesis (Armenteros and Daley 1998). The widespread occurrences of peloids and ooids across the Nullarbor Plain suggest that long-term palustrine processes overprinted sediment originally deposited in the lake complex. Previous studies elsewhere confirm that grainification is due to wetting and drying cycles, root activities, and associated physical processes (James 1972; Wright 1990; Alonso-Zarza et al. 1992), whereas the abundance of microbial features in Nullarbor peloids suggests that microorganisms played a more important role in their formation. Microbial cells, faunal and bacterial secretions, root hair processes, and biologic mucus act as cementing agents in humic soils and help form such aggregates (grainification) in pedogenic settings (von Lützow et al. 2008). Furthermore, calcium carbonate precipitation and clay mineralization on organic matter locally aids in the formation of micritic peloids by limiting decay and promoting development of humus (Duchaufour 1982; Wright 1994). The following microstructures present in ooid nuclei are thought to have been responsible for the binding of lacustrine sediments and production of peloids.

**Smooth Calcareous Coatings.—**Smooth calcareous coatings are interpreted to represent calcified exopolysaccharides (EPS) (Jones 1995; Wingender and Flemming 1999; Folk and Chafetz 2000; Braissant et al. 2003; Jones 2011b). EPS can be produced by a wide array of microorganisms including photoautotrophic and heterotrophic bacteria as well as cyanobacteria (Folk and Chafetz 2000; Dupraz et al. 2009). These substances occur in numerous organic-rich terrestrial carbonate settings where microbes are interpreted to have strongly influenced the formation of many depositional and diagenetic fabrics (Phillips

et al. 1987; Jones 1995; Loisy et al. 1999; Jones 2011a). The widespread incorporation of interpreted EPS mosaics and algal filaments with minimicrite in Nullarbor ooid nuclei suggest that these organic substances acted as binding agents during formation of peloids in palustrine environments. Such substances are thought to originate as adhesive organic accumulations outside microbial cells that protect them and aid in attaching microbes to various substrates (Riding 2000). These accumulations, combined with algal filaments (see below), are interpreted to have bound minimicrite in the subsurface of middle Miocene palustrine soils, creating numerous peloids that were later coated to form ooids.

The interpreted EPS fabrics in Nullarbor ooids are calcified and thought to have precipitated in the original bacterial secretions; this process would have slowed down decay and promoted formation of humus (Duchaufour 1982). Remaining partially decomposed organics and stable humus was then readily and repeatedly calcified to create the variety of calcified microbial fabrics (Wright 1994; Braissant et al. 2003). The microbes responsible for these actions in palustrine settings are likely oxidative soil bacteria (Braissant et al. 2003).

**Smooth Calcareous Strands.—**These strands are interpreted to represent algal sheaths (filaments) that were calcified and preserved in only the ooid nucleus (Klappa 1979; Jones 1991; Folk 1993; Alonso-Zarza et al. 1998; Braissant et al. 2003; Flügel 2004; Jones 2010a). The interpreted algal filaments in ooid nuclei demonstrate that they were active sediment binders during the micritic peloid formation. Complex arrangements of filaments attached to the minimicrite and EPS mosaics demonstrate an active role in sediment grainification (Braissant et al. 2003; von Lützow et al. 2008). The presence of algal filaments would have also created favorable chemical conditions for calcification of the organic material and preservation of the peloidal grains (Wright 1994; Braissant et al. 2003).

*Cortical Lamination*

Cortex microstructure assemblages are different from those of the nucleus, suggesting a different suite of chemical and biological processes during its formation, although microbial fabrics are still common. EPS coatings and filaments, which were numerous in the nucleus, are replaced in the cortex by an abundance of 1) palygorskite and sepiolite nano-fiber mats, 2) meniscus bridging structures, 3) bacterial spheres, and 4) degraded minimicrite, all of which suggest microbial processes. Microstructures are most obvious with SEM techniques when the surface of a laminated cortex is analyzed, whereas cross-sections of the cortex typically yield minimicrite with rare zones (~ 5 μm) of nano-fibers. This observation suggests that the interpreted microbial mats encrusted the whole ooid nucleus as one continuous thinly laminated shell and through multiple generations leading to the laminated cortical structure.

**Palygorskite-Sepiolite Nano-Fiber Mats.—**Nano-fiber mats are only found in and dominate ooid cortex microstructure. They occur as multigenerational laminations enveloping the nucleus and create the concentric cortical laminations in ooids. Mats are constructed in an identical and repeatable configuration in cortex laminations across the Nullarbor Plain. Meniscus and bridging structures of the nano-fiber mats have an appearance analogous to those produced by modern organic mucus and microbial secretions (Folk 1993; Golubic et al. 2000; Merz-Preiß 2000; Folk and Lynch 2001; Kirkland et al. 2008). The similarity of structures is interpreted to represent an originally organic mucus substrate from which palygorskite and sepiolite nano-fibers later precipitated. These clays are common in Mg and Si rich environments such as alkaline lakes, soils, and deep sea sediments (Folk and Rasbury 2007). Such mineral precipitation is interpreted to have occurred early because extracellular polymers and mucus are very efficient at binding ions from fluid solutions,

serving as nucleation sites. This setting would have been enhanced by associated metabolic activity leading to conditions favorable for mineral precipitation (Fortin et al. 1997; Leveille et al. 2000b; Leveille et al. 2000a). Preservation of the original organic mucus morphology by nano-fiber mats also suggests that this mineralization occurred before decomposition of the organics. Organic mucus thus would have surrounded the ooid nucleus and repeatedly precipitated palygorskite and sepiolite, leading to formation of the laminated ooid cortices. The presence of palygorskite and sepiolite nano-fiber mats in the cortex rather than the nucleus suggests that the mucus envelope was unique to the system during cortex development. The nano-fibers could represent chemolithoautotrophic bacteria because they have a morphology similar to individual fibers (Cunningham et al. 1995; Armenteros and Daley 1998; Folk and Rasbury 2007). This relationship is difficult to ascertain because there is no organic material left in the structures to unequivocally justify a bacterial interpretation. A more plausible explanation is that the nano-fibers are representative of fibrous palygorskite and sepiolite crystallization, whereas the morphology of the meniscus bridging nano-fiber mat structure represents the original microbial precursor. These fibrous clay minerals in turn preserved the original organic meniscus structure as it provided a suitable substrate and composition for clay mineralization.

**Spherical Pores and Grains.—**The spherical pores inside nano-fiber mats are interpreted to represent particles that were originally organic, and have since decayed leaving a mold. Some of these calcified and preserved spherical grains suggest that they were present during formation of the cortical mats. The spherical grains are interpreted to be bacterial spores, similar in morphology to those described by Jones (2009) and Jones (2011a). The presence of such bacteria would be expected during a microbial-induced surfical coating process, as invoked in this study for the formation of laminated ooid cortices. Various forms

of bacterial secretions and other metabolic products have been documented to enhance mineral precipitation and sediment binding (Chafetz and Buczynski 1992; Fortin et al. 1997; Leveille et al. 2000b; Leveille et al. 2000a).

### *Intergranular Pores*

**Filamentous Micrite.—**The microstructures of matrix material between ooids are also interpreted as microbial. The curving and branching morphology of filaments are interpreted to represent various forms of cyanobacteria and fungi (Wright 1986; Hillgärter et al. 2001). Similar calcified epi- and chasmolithic filament networks of the bacteria *Bacinella irregularis* can form under vadose conditions, both in soils and in caves (Hillgärter et al. 2001). This microbial interpretation is supported by SEM evidence as the filaments show a long curving morphology that is outlined by dense minimicrite coated in EPS. These fabrics are present in smaller filaments that bridge between ooid grains, again suggesting that these bridges are microbial in origin. The microbes would have been present in the microkarst cavities as the ooids were being formed or shortly thereafter.

## DISCUSSION

### *Microbial Mineralization in the Ooid Cortex*

The complex process of microbially mediated mineralization of Mg-clay minerals, akin to those interpreted to have taken place in Nullarbor ooid cortices, has become an important aspect of carbonate diagenesis in the meteoric realm (Stotzky 1967; Coleman and Raiswell 1993; Leveille et al. 2007; Dupraz et al. 2009). These processes are known to take place in caves and palustrine pedogenic environments where Mg and Si are in solution

(Pozo and Casas 1999; Leveille et al. 2000b; Leveille et al. 2002; Jones 2010b). Hydrated Mg-Si gels, facilitated by mat-forming bacteria and associated extracellular polymers, are thought to have encompassed the Nullarbor peloid nuclei of ooids in palustrine soil settings during wet seasons. The bacteria would have decreased diffusion, concentrated and bound ions from solution, and provided nucleation sites that aided in overcoming the kinetic inhibition of mineral formation (Jones 1986; Leveille et al. 2002). Silica and magnesium in such settings are concentrated in the organic mucus until Mg-Si gels can form, which in turn mimics the pre-existing structure of the mucus, during high hydration states (Stotzky 1967; Weaver 1989; Pozo and Casas 1999). Ion concentration fluctuations in soil environments in ensuing dry seasons, caused by evaporative processes, would have created the necessary conditions leading to clay mineral precipitation. Evaporation and dehydration causes mineral crystallization by increasing the concentrations of $Mg^{2+}$ and $OH^{-}$ ions when silica reaches its saturation point (Weaver 1989; Pozo and Casas 1999). Such a cyclic process of changing hydration states is thought to be from strong seasonal variations of rainfall in a wet savanna climate regime. Wet seasons would have created a proliferation of Mg-Si gels that consequently would have led to the dehydration and mineralization during dry seasons (Fig. 3.12). This directly led to the multigenerational laminated fabric in ooid cortices across the Nullarbor Plain and suggests that the laminations were annual events. Such an annual process also provides a mechanism for *in situ* ooid formation, in that the movement of ooid grains is not necessary for the even laminations in their cortices. The flat and aligned fibers of palygorskite and sepiolite in the inner cortex are interpreted to represent the recurring envelopment of Mg-Si gel mucus that causes the fibers to flatten (Fig. 3.12). Such a process is not seen in the outer cortical lamination and intergranular pore spaces because the coating process had stopped, and thus the minerals could grow unimpeded.

Carbonate – silicate mineralization has been documented in Hawaiian basaltic sea caves (Leveille et al. 2000b), caves in Cayman Brac, British West Indies (Jones 2010b), and in modern palustrine environments (Pozo and Casas 1999). The source of Mg, Si, and Al for nano-fiber palygorskite and sepiolite mineralization in the Nullarbor is puzzling because the Cenozoic limestones in which they are found are deficient in these elements. Various transport mechanisms, both through the atmosphere and groundwater, might move these elements. The clay-forming elements could have been derived from the Archean cratons surrounding the Nullarbor Plain (Fig. 3.1). These cratons are composed of granites, greenstones, and granitic gneisses, all of which contain the elements necessary for clay mineral formation (Myers 1995). Groundwater flowing from these Proterozoic rocks or aeolian transport of weathered detrital grains derived from these rocks could have transported exotic elements onto the dominantly low-Mg calcite Nullarbor Plain. Volcanism in southeastern Australia during the Cainzoic is another possible source of Mg and Si (Wellman 1983). These mafic volcanics would have created westward flowing debris clouds that caused material to fallout and become incorporated in the soils across southern Australia. Finally, rainwater in southern Australia could have included high concentrations of these elements since it is derived from evaporation of ocean water, which has a composition that includes these elements.

### *Implications for* In Situ *Ooid Formation*

This conceptual model of ooid formation in palustrine settings offers an explanation for the heretofore-puzzling *in situ* formation of coated grains in pedogenic settings. Grainification of lacustrine sediments into peloids is known to take place in mature palustrine soils (Peryt 1983a; Alonso-Zarza et al. 1992; Platt and Wright 1992; Wright et al.

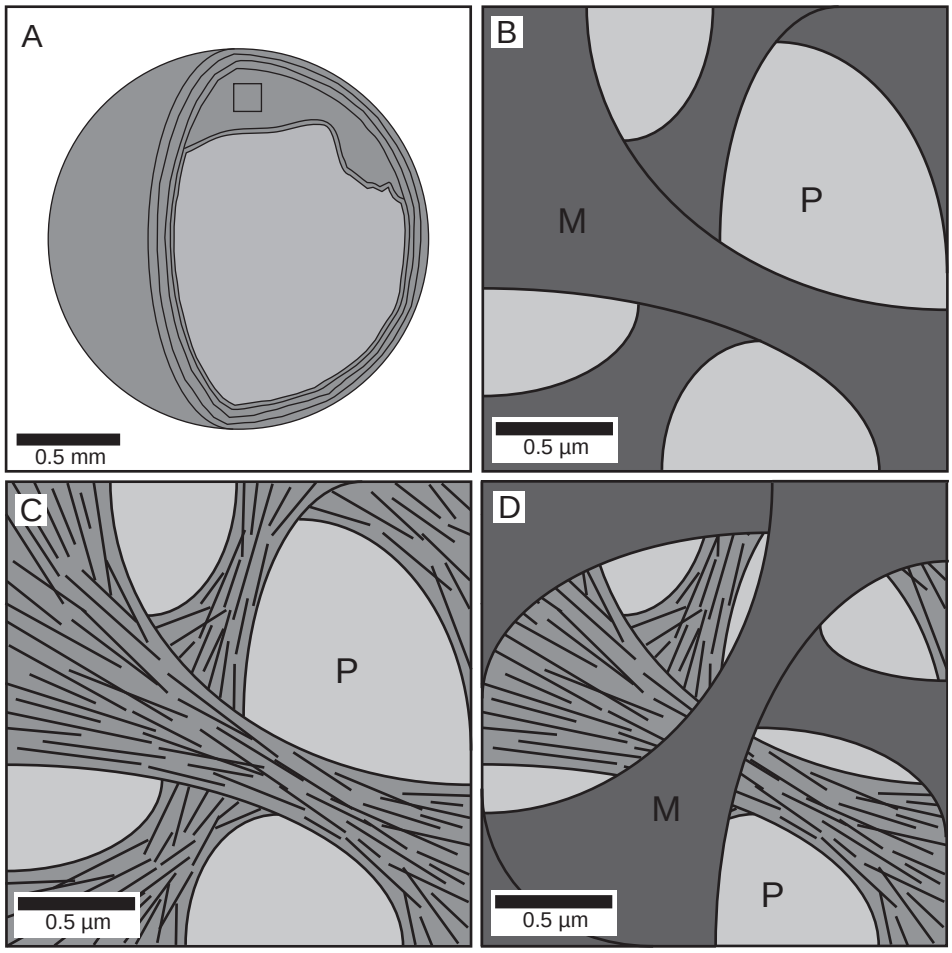


**Figure 3.12.** Microbial Ooid Cortex Genesis A) Overview of ooid, small box shows location of following illustrations, which are focused on the surface of an individual lamination. B) Interpreted illustration showing mucus forming meniscus structures (M) that encapsulate the micritic peloid (P) in a palustrine soil during high hydration states (wet season). C) The mucus coating then is mineralized during dehydration (dry season) where nano-fibers of palygorskite and sepiolite form and are flattened by succeeding generations of mucus envelopment. D) Successive growth of mucus coatings encompasses the ooid again during ensuing wet seasons to form another lamination in the ooid cortex. This annual process creates the finely laminated palygorskite/sepiolite ooid cortex.

1997; Armenteros and Daley 1998; Freytet and Verrecchia 2002; Alonso-Zarza and Wright 2010). Physical processes such as root activity and moisture changes were considered to be the major controls, but the results of this study suggest that microbial processes likely aided in the production of these grains through extensive sediment binding. Furthermore, microbially mediated mineral precipitation allows for spherical laminations to develop on these peloids, leading to the creation of ooids. The annual microbial processes invoked in this study to create such laminations can be used as a general model of genesis for many other coated grains in paleosols, regardless of mineralogy. These grains can include not only palustrine ooids but also calcrete pisoids, and other pedogenic coated grains. The seasonal alternations between hydrated microbial mucus coatings and their subsequent dehydration and clay crystallization led to the formation of evenly laminated spherical cortices. This mineralization process should be expected in soils that have seasonal variations in rainfall, and in which organics undergo changes in moisture content. Such a model helps to explain how grains can be coated with even laminations *in situ*, without having to utilize complicated mechanisms of rolling, soil creep, or other regular physical disturbances to evenly coat grains, a problem that has long baffled carbonate sedimentologists (Peryt 1983b; Wright 1994; Armenteros 2010).

The close similarities between palustrine and calcrete ooids with their marine counterparts can cause difficulties when attempting to differentiate depositional models that include oolites. Subtle characteristics in calcareous soil ooids can be used to differentiate them from their marine equivalents. Perhaps the most convincing argument would come from a convergence of evidence including the appearance of circumgranular cracking, abundant minimicrite, poor sorting, lack of bedding or rare inverse graded beds, fresh to brackish water fossil debris in nucleus (charophytes and ostracods), negative stable carbon

isotope values, and an abundance of microbial features in the nucleus and cortex that are preserved through mineralization of clays, such as palygorskite and sepiolite.

Palustrine ooids can further be differentiated from calcrete ooids by the abundance of circumgranular cracking, close lacustrine sediment associations, lack of oxidization, more positive oxygen isotope values, and a better defined laminated cortex. Palustrine ooids usually have more circumgranular cracking given that they form under fluctuating conditions of precipitation, typically in a more humid to temperate climate setting than calcrete ooids. Calcrete is more closely associated with semi-arid to arid climates and does not have the same changing hydromoprhic systems to cause such widespread circumgranular cracking. This climatic difference is also illustrated in more positive stable oxygen isotope values in view of the fact that evaporation is higher in calcrete soils (Hoefs 2004). Palustrine ooids are also closely associated with lacustrine sediments, with related fossil debris typically hosted within their nucleus. Finally, young calcrete soils and associated ooids commonly have a rusty orange color due to an abundance of iron oxides and in the case of Nullarbor Plain calcrete ooids an abundance of aeolian quartz grains (Miller et al. 2012). This situation is in stark contrast to palustrine ooids that lack this coloration due to commonly reducing environments because of high biologic metabolism in the soils. These subtle but critical dissimilarities can be applied to the rock record to understand better the depositional environments of oolitic deposits.

## CONCLUSIONS

Lacustrine and later palustrine environments covered the now arid to semi-arid Nullarbor Plain in southern Australia during the middle Miocene. These extensive

lacustrine and palustrine environments produced a suite of sediments, including palustrine ooids that are now preferentially preserved in underlying microkarst cavities and at the surface in Cook quarry. The palustrine ooids have a dense micritic peloidal nucleus and a multigenerational laminated cortex, similar in structure to their marine counterparts.

Oolite microstructures indicate an important microbial component in the formation of these distinctive grains. Peloidal nuclei are interpreted to be the products of dynamic biologic processes in soil environments where microbial activity produced EPS substances while algal filaments bound the lacustrine sediment together. Nano-fiber mats, composed of palygorskite and sepiolite, in the ooid cortex are interpreted to be the mineralized remains of organic mucus encapsulating the ooid nucleus. Microbes created Mg-Si gels that encompassed the ooid during periods of hydration (wet seasons) and as these gels dehydrated during intervening dry periods (dry seasons), they precipitate nano-fiber palygorskite and sepiolite minerals. Such seasonal processes of alternating hydration and dehydration states create a uniformly laminated structure in the ooid cortex that was produced *in situ*. Filamentous micrite fabrics are widespread in the ooid filled cavities, and typically form the only matrix. These structures are interpreted to represent calcified epi- and chasmolithic filaments of cyanobacteria and algae that bridge and support the ooids.

The microbial mechanism invoked for in-place formation of palustrine ooids in this study may be applicable to the genesis of many coated grains within calcretes and other calcareous soils without the necessity of particle movement. In this conceptual model, seasonal change in soil hydration provides the chemical and biological necessities for uniform grain coating.

## ACKNOWLEDGEMENTS

The Natural Sciences and Engineering Research Council of Canada (NSERC) Discovery Grant to NPJ and the Geological Survey of Western Australia (GSWA) funded this research. This study would have not been possible without the guidance, advice, and experience of Brian Jones and his SEM facility at the University of Alberta. We thank the helpful staff at GSWA (R. Hocking and the Carlislie staff), L. O'Connell, and Y. Bone for field assistance. The authors are also indebted to G. Braybrook and D. Rollings who were instrumental in the SEM analyzes and A. Grant for XRD analyzes.

## REFERENCES

ALONSO-ZARZA, A.M., 2003, Palaeoenvironmental significance of palustrine carbonates and calcretes in the geological record: Earth-Science Reviews, v. 60, p. 261-298.

ALONSO-ZARZA, A.M., 2006, Paleoenvironmental record and applications of calcretes and palustrine carbonates: Special Paper - Geological Society of America, v. 416, p. 239.

ALONSO-ZARZA, A.M., CALVO, J.P., and GARCIA DEL CURA, M.A., 1992, Palustrine sedimentation and associated features--grainification and pseudo-microkarst--in the middle Miocene (Intermediate Unit) of the Madrid Basin, Spain: Sedimentary Geology, v. 76, p. 43-61.

ALONSO-ZARZA, A.M., SANZ, M.E., CALVO, J.P., and ESTEVEZ, P., 1998, Calcified root cells in Miocene pedogenic carbonates of the Madrid Basin; evidence for the origin of Microcodium b: Sedimentary Geology, v. 119, p. 181.

Alonso-Zarza, A.M., and Wright, V.P., 2010, Palustrine Carbonates, *in* Alonso-Zarza, A.M., and Tanner, L.H., eds., Carbonates in Continental Settings: Facies, Environments and Processes: Developments in Sedimentology: Oxford, Elsevier, p. 103-131.

Armenteros, I., 2010, Diagenesis of Carbonates in Continental Settings, *in* Alonso-Zarza, A.M., and Tanner, L.H., eds., Carbonates in Continental Settings: Geochemistry, Diagenesis and Applications: Developments in Sedimentology: Oxford, Elsevier, p. 61-151.

Armenteros, I., and Daley, B., 1998, Pedogenic modification and structure evolution in palustrine facies as exemplified by the Bembridge Limestone (Late Eocene) of the Isle of Wight, southern England: Sedimentary Geology, v. 119, p. 275-295.

Australian Water Resources Council, 1976, Review of Australia's water resources: Canberra, Australian Government Publishing Service, p. 170.

Barton, H.A., 2006, Introduction to cave microbiology: a review for the non-specialist: Journal of Cave and Karst Studies, v. 68, p. 43-54.

Barton, H.A., and Jurado, V., 2007, What's up down there? Microbial diversity in caves: Microbe, v. 2, p. 132-138.

Birsoy, R., 2002, Formation of sepiolite-palygorskite and related minerals from solution: Clays and Clay Minerals, v. 50, p. 736-745.

Braissant, O., Cailleau, G., Dupraz, C., and Verrecchia, E.P., 2003, Bacterially induced mineralization of calcium carbonate in terrestrial environments; the role of exopolysaccharides and amino acids: Journal of Sedimentary Research, v. 73, p. 485-490.

Braithwaite, C.J.R., 1983, Calcrete and other soils in Quaternary limestones; structures, processes and applications: Journal of the Geological Society of London, v. 140, p.

351-363.

Brasier, A.T., 2011, Searching for travertines, calcretes and speleothems in deep time: Processes, appearances, predictions and the impact of plants: Earth-Science Reviews, v. 104, p. 213-239.

Calvet, F., and Julia, R., 1983, Pisoids in the caliche profiles of Tarragona (NE Spain), *in* Peryt, T.M., ed., Coated grains: Berlin, Springer-Verlag, p. 456-473.

Chafetz, H.S., and Buczynski, C., 1992, Bacterially induced lithification of microbial mats: Palaios, v. 7, p. 277-293.

Coleman, M.L., and Raiswell, R., 1993, Microbial mineralization of organic matter; mechanisms of self-organization and inferred rates of precipitation of diagenetic minerals: Philosophical Transactions - Royal Society of London, Physical Sciences and Engineering, v. 344, p. 69-87.

Cunningham, K.I., Northup, D.E., Pollastro, R.M., Wright, W.G., and LaRock, E.J., 1995, Bacteria, fungi and biokarst in Lechuguilla Cave, Carlsbad Caverns National Park, New Mexico: Environmental Geology (Berlin), v. 25, p. 2-8.

Drexel, J.F., and Preiss, W.V., 1995, The geology of South Australia; Volume 2, The Phanerozoic: Bulletin - Geological Survey of South Australia, v. 54, Geological Survey of South Australia, Adelaide, South Aust., Australia, 347 p.

Duchaufour, P., 1982, Pedology; pedogenesis and classification: London, Allen and Unwin, 448 p.

Dunkley, J.R., and Wigley, T.M.L., 1967, Caves of the Nullarbor; a review of speleological investigations in the Nullarbor plain, southern Australia, Speleol. Res. Counc.; (Sydney University, Speleological Society-Cave Exploration Group, South Australia), 61 p.

Dupraz, C., Reid, R.P., Braissant, O., Decho, A.W., Norman, R.S., and Visscher, P.T., 2009, Processes of carbonate precipitation in modern microbial mats: Earth-Science Reviews, v. 96, p. 141-162.

Flügel, E., 1982, Microfacies Analysis of Limestones: Berlin, Springer-Verlag, 633 p.

Flügel, E., 2004, Microfacies of carbonate rocks: analysis, interpretation and application: Berlin, Springer-Verlag, 976 p.

Folk, R.L., 1974, The natural history of crystalline calcium carbonate: effect of magnesium content and salinity: Journal of Sedimentary Petrology, v. 44, p. 40–53.

Folk, R.L., 1993, SEM imaging of bacteria and nannobacteria in carbonate sediments and rocks: Journal of Sedimentary Research, v. 63, p. 990-999.

Folk, R.L., and Chafetz, H.S., 2000, Bacterially induced microscale and nanoscale carbonate precipitates, *in* Riding, R.E., and Awramik, S.M., eds., Microbial sediments: Berlin, Springer, p. 40-49.

Folk, R.L., and Lynch, F.L., 2001, Organic matter, putative nannobacteria and the formation of ooids and hardgrounds: Sedimentology, v. 48, p. 215-229.

Folk, R.L., and Rasbury, E.T., 2007, Nanostructure of palygorskite/sepiolite in Texas caliche; possible bacterial origin: Carbonates and Evaporites, v. 22, p. 113-122.

Fortin, D., Ferris, F.G., and Beveridge, T.J., 1997, Surface-mediated mineral development by bacteria: Reviews in Mineralogy, v. 35, p. 161-180.

Freytet, P., and Verrecchia, E.P., 2002, Lacustrine and palustrine carbonate petrography; an overview: Journal of Paleolimnology, v. 27, p. 221-237.

Gehring, A.U., Keller, P., Frey, B., and Luster, J., 1995, The occurrence of spherical morphology as evidence for changing conditions during the genesis of a sepiolite deposit: Clay Minerals, v. 30, p. 83-86.

Gierlowski-Kordesch, E.H., 2010, Lacustrine Carbonates, *in* Alonso-Zarza, A.M., and Tanner, L.H., eds., Carbonates in Continental Settings: Facies, Environments and Processes: Developments in Sedimentology: Oxford, Elsevier, p. 1-101.

Goede, A., Harmon, R.S., Atkinson, T.C., and Rowe, P.J., 1990, Pleistocene climatic change in southern Australia and its effect on speleothem deposition in some Nullarbor caves: Journal of Quaternary Science, v. 5, p. 29-38.

Golubic, S., Lee, S.-J., and Browne, K.M., 2000, Cyanobacteria; architects of sedimentary structures, *in* Riding, R.E., and Awramik, S.M., eds., Microbial sediments: Berlin, Springer, p. 57-67.

Hardy, R., and Tucker, M., 1988, X-ray powder diffraction of sediments, *in* Tucker, M., ed., Techniques in sedimentology: Oxford, Blackwell Sci. Publ., p. 191-228.

Harrison, R.S., 1977, Caliche profiles: indicators of near-surface subaerial diagenesis, Barbados, West Indies: Bulletin of Canadian Petroleum Geology, v. 25, p. 123-173.

Hillgärter, H., Dupraz, C., and Hug, W., 2001, Microbially induced cementation of carbonate sand; are micritic meniscus cements good indicators of vadose diagenesis?: Sedimentology, v. 48, p. 117-131.

Hocking, R.M., 1990, Eucla Basin: Geological Survey of Western Australia, v. Memoir 3, p. 548-561.

Hoefs, J., 2004, Stable isotope geochemistry: Berlin, Springer-Verlag 244 p.

James, N.P., 1972, Holocene and Pleistocene calcareous crust (caliche) profiles, criteria for subaerial exposure: Journal of Sedimentary Petrology, v. 42, p. 817-836.

Johnson, D., 2009, The geology of Australia, Cambridge University Press, 355 p.

Jones, B., 1991, Genesis of terrestrial oncoids, Cayman Islands, British West Indies: Canadian Journal of Earth Sciences = Journal Canadien des Sciences de la Terre, v.

28, p. 382-397.

Jones, B., 1995, Processes associated with microbial biofilms in the twilight zone of caves; examples from the Cayman Islands: Journal of Sedimentary Research, Section A: Sedimentary Petrology and Processes, v. 65, p. 552-560.

Jones, B., 2009, Cave pearls; the integrated product of abiogenic and biogenic processes: Journal of Sedimentary Research, v. 79, p. 689-710.

Jones, B., 2010a, Microbes in caves; agents of calcite corrosion and precipitation: Geological Society Special Publications, v. 336, p. 7-30.

Jones, B., 2010b, Speleothems in a wave-cut notch, Cayman Brac, British West Indies; the integrated product of subaerial precipitation, dissolution, and microbes: Sedimentary Geology, v. 232, p. 15-34.

Jones, B., 2011a, Biogenicity of terrestrial oncoids formed in soil pockets, Cayman Brac, British West Indies: Sedimentary Geology, v. 236, p. 95-108.

Jones, B., 2011b, Stalactite growth mediated by biofilms; example from Nani Cave, Cayman Brac, British West Indies: Journal of Sedimentary Research, v. 81, p. 322-338.

Jones, B.F., 1986, Clay mineral diagenesis in lacustrine sediments: U. S. Geological Survey Bulletin, p. 291-300.

King, D., 1950, Geological notes on the Nullarbor cavernous limestone: Transactions of the Royal Society of South Australia, v. 73, p. 52-58.

Kirkland, B.L., Lynch, F.L., Folk, R.L., Owen, A.M., Mylroie, J.E., Culpepper, J.D., and Funderburk, W.K., 2008, Role of organic matter in precipitation of cement; examples from three different environments: Abstracts: Annual Meeting - American Association of Petroleum Geologists, v. 2008.

Klappa, C.F., 1979, Calcified filaments in Quaternary calcretes; organo-mineral interactions

in the subaerial vadose environment: Journal of Sedimentary Petrology, v. 49, p. 955-968.

Leveille, R.J., Fyfe, W.S., and Longstaffe, F.J., 2000a, Geomicrobiology of carbonate-silicate microbialites from Hawaiian basaltic sea caves: Chemical Geology, v. 169, p. 339-355.

Leveille, R.J., Fyfe, W.S., and Longstaffe, F.J., 2000b, Unusual secondary Ca-Mg-carbonate-kerolite deposits in basaltic caves, Kauai, Hawaii: Journal of Geology, v. 108, p. 613-621.

Leveille, R.J., Longstaffe, F.J., and Fyfe, W.S., 2002, Kerolite in carbonte-rich speleothems and microbial deposits from basaltic caves, Kauai, Hawaii: Clays and Clay Minerals, v. 50, p. 514-524.

Leveille, R.J., Longstaffe, F.J., and Fyfe, W.S., 2007, An isotopic and geochemical study of carbonate-clay mineralization in basaltic caves; abiotic versus microbial processes: Geobiology, v. 5, p. 235-249.

Loisy, C., Verrecchia, E.P., and Dufour, P., 1999, Microbial origin for pedogenic micrite associated with a carbonate Paleosol (Champagne, France): Sedimentary Geology, v. 126, p. 193-204.

Lowry, D.C., and Jennings, J.N., 1974, The Nullarbor karst Australia: Zeitschrift fuer Geomorphologie, v. 18, p. 35-81.

Merz-Preiss, M., 2000, Calcification in cyanobacteria, *in* Riding, R.E., and Awramik, S.M., eds., Microbial sediments: Berlin, Springer, p. 50-56.

Miller, C.R., James, N.P., and Bone, Y., 2012, Prolonged carbonate diagenesis under an evolving late Cenozoic climate; Nullarbor Plain, southern Australia: Sedimentary Geology, v. 261-262, p. 33-49.

Myers, J.S., 1995, The generation and assembly of an Archaean supercontinent: evidence from the Yilgarn craton, Western Australia: Geological Society, London, Special Publications, v. 95, p. 143-154.

Newell, N.D., Purdy, E.G., and Imbrie, J., 1960, Bahamian Oolitic Sand: The Journal of Geology, v. 68, p. 481-497.

Peryt, T.M., 1983a, Coated Grains: Berlin, Springer-Verlag, 655 p.

Peryt, T.M., 1983b, Vadoids, *in* Peryt, T.M., ed., Coated grains: Berlin, Springer-Verlag, p. 437-449.

Phillips, S.E., Milnes, A.R., and Foster, R.C., 1987, Calcified filaments; an example of biological influences in the formation of calcrete in South Australia: Australian Journal of Soil Research, v. 25, p. 405-428.

Platt, N.H., and Wright, V.P., 1992, Palustrine carbonates and the Florida Everglades; towards an exposure index for the fresh-water environment?: Journal of Sedimentary Petrology, v. 62, p. 1058-1071.

Pozo, M., and Casas, J., 1999, Origin of kerolite and associated Mg clays in palustrine-lacustrine environments; the Esquivias Deposit (Neogene Madrid Basin, Spain): Clay Minerals, v. 34, p. 395-418.

Riding, R., 2000, Microbial carbonates; the geological record of calcified bacterial-algal mats and biofilms: Sedimentology, v. 47, Suppl. 1, p. 179-214.

Siesser, W.G., 1973, Diagenetically formed ooids and intraclasts in South African calcretes: Sedimentology, v. 20, p. 539-551.

Stotzky, G., 1967, Clay minerals and microbial ecology: Transactions of the New York Academy of Sciences, v. 30, p. 11-21.

von Lützow, M., Kögel-Knabner, I., Ludwig, B., Matzner, E., Flessa, H., Ekschmitt,

K., GUGGENBERGER, G., MARSCHNER, B., and KALBITZ, K., 2008, Stabilization mechanisms of organic matter in four temperate soils: Development and application of a conceptual model: Journal of Plant Nutrition and Soil Science, v. 171, p. 111-124.

WEAVER, C.E., 1989, Clays, muds, and shales: Developments in Sedimentology, v. 44: Oxford, Elsevier, 819 p.

WEBB, J.A., and JAMES, J.M., 2006, Karst evolution of the Nullarbor Plain, Australia, *in* Harmon, R.S., and Wicks, C.M., eds., Perspectives on Karst Geomorphology, Hydrology, and Geochemistry - A tribute volume to Derek C. Ford and William B. White: Boulder, Geological Society of America p. 65-78.

WELLMAN, P., 1983, Hotspot volcanism in Australia and New Zealand: Cainozoic and mid-Mesozoic: Tectonophysics, v. 96, p. 225-243.

WHITE, M.E., 1994, After the greening: The browning of Australia: Kenthurst, Kangaroo Press Pty Ltd., 288 p.

WINGENDER, N.T., and FLEMMING, H.C., 1999, What are bacterial extracellular polymeric substances?, *in* J Wingender, T.N., H-C Fleming, ed., Microbial Ex- tracellular Polymeric Substances: Berlin, Springer, p. 93–112.

WRIGHT, V.P., 1986, The role of fungal biomineralization in the formation of Early Carboniferous soil fabrics: Sedimentology, v. 33, p. 831-838.

WRIGHT, V.P., 1989, Terrestrial stromatolites and laminar calcretes; a review: Sedimentary Geology, v. 65, p. 1-13.

WRIGHT, V.P., 1990, Carbonate sediments and limestones: constituents, *in* Tucker, M., and Wright, V.P., eds., Carbonate Sedimentology: Oxford, Blackwell Science Ltd., p. 1-27.

WRIGHT, V.P., 1994, Paleosols in shallow marine carbonate sequences: Earth-Science Reviews, v. 35, p. 367-395.

WRIGHT, V.P., ALONSO ZARZA, A.M., SANZ, M.E., and CALVO, J.P., 1997, Diagenesis of late Miocene micritic lacustrine carbonates, Madrid Basin, Spain: Sedimentary Geology, v. 114, p. 81-95.

ZHOU, J., and CHAFETZ, H.S., 2009, Biogenic caliches in Texas; the role of organisms and effect of climate: Sedimentary Geology, v. 222, p. 207-225.

# CHAPTER 4

# GENESIS OF BLACKENED LIMESTONE CLASTS AT LATE CENOZOIC SUBAERIAL EXPOSURE SURFACES; SOUTHERN AUSTRALIA

Cody R. Miller, Noel P. James, and T. Kurtis Kyser

## ABSTRACT

Black limestone clasts are present across the globe at modern and ancient subaerial exposure surfaces, and in intertidal and supratidal environments. These problematic clasts are particularly found in abundance at multiple subaerial exposure surfaces across southern Australia. The genesis of such exceptionally preserved clasts can be interpreted through universal fabrics across wide geographic regions and geologic ages. Regardless of location or age all blackened clasts have a similar microstructure that is dominated by porous micritic laminae and chambered tubules. Such laminae are interpreted to represent calcified root cells and occur in two different varieties; 1) micrite walled tubules with hollow centers that are thought to represent calcification in the rhizosphere or outer surfaces of the root and 2) tubules consistent with calcification of both the medulla and cortex, which preserved medulla, cortex, and parenchymatic cells along with xylem vessels. Preserved root fabrics are only present in the blackest clasts and are subsequently thought to be the main mechanism driving limestone blackening. The dark coloration in southern Australian clasts is derived from the impregnation of partially decayed terrestrial organics. These organics were trapped in the cellular structures of roots as they calcified and were subsequently

protected from further decay and oxidation. A threshold of approximately 7-weight % organic carbon is needed in the insoluble residue to produce the distinct black coloration in limestone. This process occurs at the base of slightly organic rich humic soil profiles where they interact with underlying carbonate bedrock (B-C soil horizon). Roots both physically and chemically (through acid secretion) corrode the underlying limestone and provide the calcium bicarbonate needed in the root calcification process. Current ideologies suggest that specific semi-arid flora have the ability to calcify their cellular structures, which could explain why blackened clasts do not occur at all unconformities. This means that the formation of blackened clasts via root calcification and entrapment of organics relies upon specific conditions of semi-arid plants and climate along with organic soils. Such conditions would be restricted to a specific climate regime and when combined with the new proposed blackening mechanism herein could help explain their limited distribution and occurrences worldwide.

## INTRODUCTION

Black limestone clasts are common constituents of calcareous breccias at modern and ancient carbonate subaerial exposure surfaces globally (Ward et al. 1970; Strasser and Davaud 1983; Strasser 1984; Leinfelder 1987; Shinn and Lidz 1988; Lang and Tucci 1997). The clasts themselves are characteristically angular, dark gray to black in color, and occur in specific carbonate settings, namely paleosols and karst depressions. Such clasts have been documented in carbonate successions as old as Ordovician, although they are most common in post-Carboniferous strata (Strasser 1984). Generation of this black coloration in limestone has puzzled carbonate researchers for decades with past

interpretations including forest fires (Shinn and Lidz 1988), decayed terrestrial plant matter staining the surrounding limestone (Leinfelder 1987), microbial communities (Folk et al. 1973), deposition in organic rich tidal, lacustrine, and hypersaline lake environments (Ward et al. 1970), manganese/iron oxides and sulfides (Tucker 1973; Lang and Tucci 1997), and incorporation of fine particulate organic substances (Strasser 1984).

Blackened limestone clasts are found in abundance across much of southern Australia at the surface and in the shallow subsurface with geologic ages ranging from middle Miocene to latest Pleistocene. Although the clasts have different depositional settings, they all share common physical and geochemical characteristics. The large lateral and temporal variations along with exceptional preservation in these deposits permit a comprehensive investigation into their origins and an interpretation of the mechanisms causing this unique black coloration.

The purpose of this study is to 1) document black limestone clast occurrences within the Neogene strata of southern Australia, 2) unravel the diagenetic fabrics in their microstructure and determine some of their geochemical attributes, and 3) outline the mechanism responsible for the genesis of these blackened limestone clasts that may be applied to the formation of other post-Devonian black limestone pebbles at subaerial exposure surfaces.

## SETTING

Blackened limestone clasts in this study come from three different geologic ages and geographic locations across southern Australia (Fig. 4.1). The Nullarbor Plain contains two distinctive varieties of clasts 1) bedded middle Miocene clasts located in Rawlinna Quarry and 2) late Pliocene black clasts within subsoil hollows across the entire Nullarbor Plain.

Pleistocene blackened clasts are also located on the surface and in the shallow subsurface at Cape Spencer in southern Yorke Peninsula.

### *Nullarbor Plain*

The Nullarbor Plain, the largest aerial karst system in the world, is a vast ~ 240 000 $km^2$ flat carbonate landscape situated along the southern margin of continental Australia (Fig. 4.1) (Miller et al. 2012). The Plain was subaerially exposed during the middle Miocene (~ 14 Ma) as a consequence of the northward movement of Australia and subduction beneath Indonesia at the Timor Trench (Sandiford 2007; Hou et al. 2008; Sandiford et al. 2009). Today, the region is under the influence of an arid to semi-arid climate with temperature differences of 23º - 26ºC in summer and 10º - 12ºC in winter (Goede et al. 1990; White 1994). Annual rainfall in the northern plain is below 150 mm and increases to 250 mm near the southern coast, however, this pales in comparison to the potential evaporation which exceeds 2500 – 3000 mm (Australian Water Resources Council 1976). These conditions limit vegetation to bluebush, saltbush, drought resistant shrubs, and small woodlands of *Myall acacias* in coastal settings (Lowry and Jennings 1974; Goede et al. 1990; White 1994).

Three Cenozoic marine limestone formations underlie the Plain as part of the much larger Eucla Basin, a broad shallow depression that extends offshore towards the south (Lowry 1970; Hocking 1990; James and Bone 1991; Feary and James 1998; Hou et al. 2008; O'Connell et al. 2012). The modern surface of the Nullarbor Plain is composed of the middle Miocene Nullarbor Limestone (maximum thickness 45 m) that has been extensively altered through three broad phases of diagenesis (Miller et al. 2012). The Nullarbor Limestone is composed of laterally continuous grainstones to rudstones that are

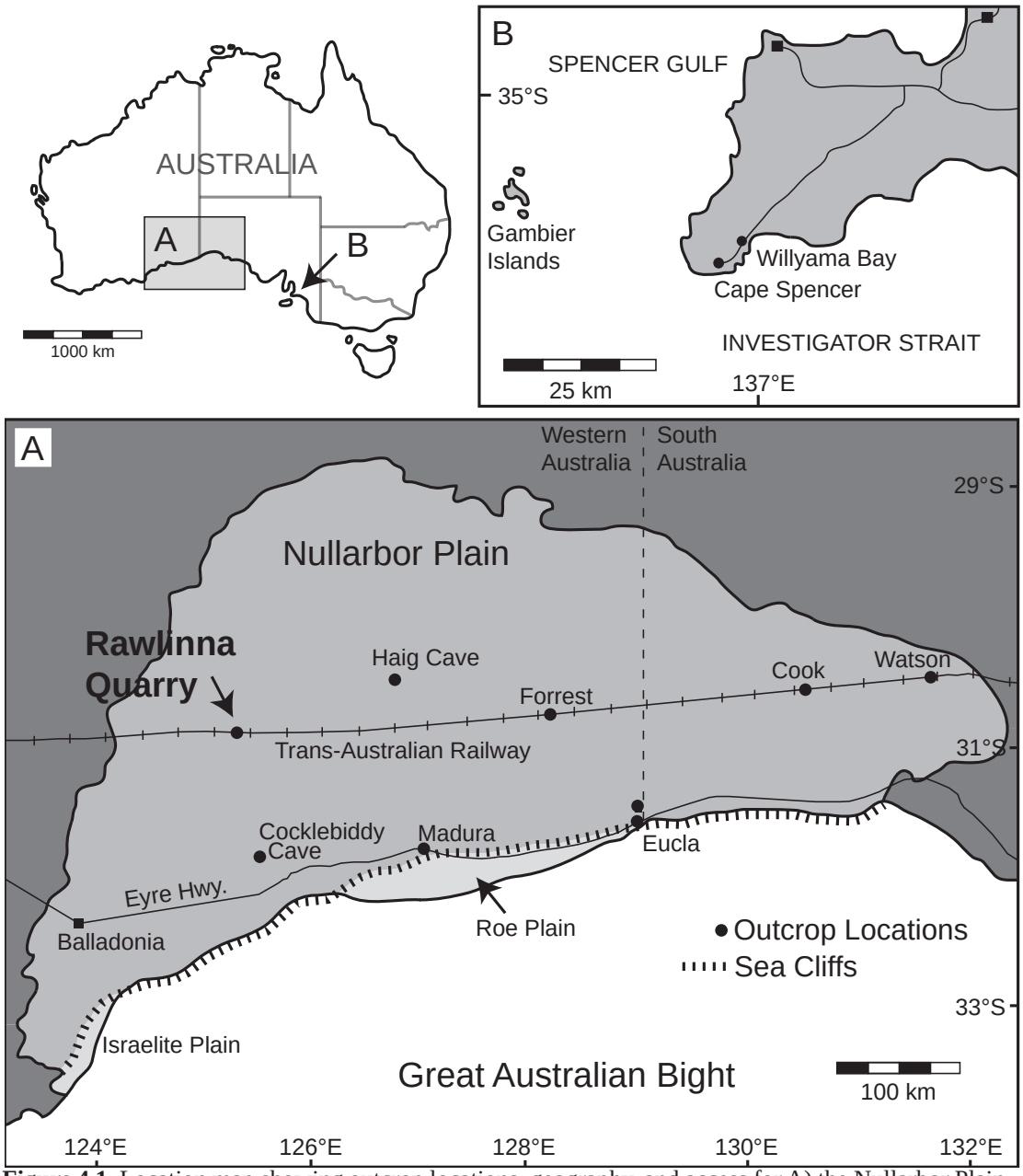


**Figure 4.1.** Location map showing outcrop locations, geography, and access for A) the Nullarbor Plain and Rawlinna Quarry and B) Cape Spencer.

dominated by benthic foraminifera, coralline red algae, corals, gastropods, bivalves, and echinoids (Lowry 1970; O'Connell et al. 2012).

Rawlinna quarry, located in the west central region of the Nullarbor Plain (Fig. 4.1A), contains three laterally continuous beds of blackened carbonate clasts that are interbedded with Nullarbor Limestone lithologies. The quarry is approximately 137, 500 $m^2$ and 20 m deep, offering exceptional outcrop exposure to determine three-dimensional relationships and lateral continuity of the middle Miocene black clast horizons.

### *Cape Spencer*

Black carbonate clasts are also common in coastal Pleistocene aeolianites across much of southern Australia. Cape Spencer, at the southern end of Yorke Peninsula (Fig. 4.1B), is composed of stacked calcareous aeolianites that have been eroded into ~74 m high formidable sea cliffs. These escarpments expose excellent sections of both the paleodunes and interdune paleosols (Crawford and Ludbrook 1965; Belperio et al. 1995).

The stratigraphy at Cape Spencer comprises a 54 m thick section of lower Bridgewater Formation bioclastic aeolianites and intervening terra rossa paleosols overlain by a 20 m thick section of upper Bridgewater Formation bioclastic aeolianites and calcrete paleosols. The upper unit is estimated to have been deposited during Pleistocene highstand Isotope Stage 5e (~ 125ka) and contains numerous black pebbles at paleosol intervals. This multi-dune succession passes laterally into interdune corridors.

## METHODOLOGY

Twenty-three locations were studied across the Nullarbor Plain and Cape Spencer

with blackened limestone clast samples obtained from fifteen of these outcrops. Samples were collected from ten of these sites with outcrops in dolines, road cuts, limestone quarries, and sea cliffs. Ten polished thin sections were prepared from these samples and analyzed through standard transmission light microscopy. Hand sample and petrographic colors are classified with respect to the Munsell color chart. Select samples were then analyzed with a scanning electron microscope (SEM) to determine microstructure relationships. Small fragments of the blackened clasts were mounted on stubs with double sided conductive tape and sputter coated with gold. They were analyzed at the University of Alberta with a JOEL Field Emission SEM (JOEL 6301FE) with an accelerating voltage of 5 kV used to obtain the highest resolution images. A 20 kV voltage was utilized to determine elemental content determination with energy-dispersive X-ray (EDX) analyses. Such elemental analyses were obtained from the Princeton Gamm-Tech X-ray analysis system (attached to the SEM). Mineralogy of blackened clasts was determined using x-ray diffraction (XRD) with a Cu anode and zero background plate (Hardy and Tucker 1988). Oxygen and carbon stable isotope analyses were completed on selected whole rock samples using techniques outlined by Kyser (1987). These are presented relative to the Pee Dee Belemnite (PDB) reference standard.

Blackened clast samples were then dissolved in 20% HCl, with the insoluble residue analyzed through different geochemical techniques. After dissolution the residue was thoroughly rinsed with de-ionized water, centrifuged, and placed in a vial to dry. These samples were then examined using XRD to determine the non-carbonate mineralogy using the same methods as the whole rock samples. Small quantities (0.1 – 0.3 mg) of residue were weighed and placed in tin buckets to be used for the determination of weight percent carbon and stable isotopic carbon ratios on a Costech Elemental Analyzer (EA) connected

to a Delta XL isotope ratio mass spectrometer at Queen's University. Finally, the insoluble residue was further analyzed with the SEM to better understand the microstructure and mineralogy of the different clays and organics. Samples were selected for analyses to ensure a spectrum in the degree of black coloration and location for geographic representation. The darkest samples yielded the most volume of insoluble residue with corresponding non-blackened clasts having very little to no material present after the dissolution process.

Short Wavelength Infrared Spectral Analyses (SWIR) obtained via a Portable Infrared Mineral Analyzer (PIMA) at Queen's University was used to quantitatively determine the darkness of each sample before it was dissolved and analyzed with the EA. Analyses were performed on clean, fresh, and dry blackened clast surfaces. Samples need to have a minimum surface area of 4 $cm^2$ to insure that the surrounding breccia matrix was not within the investigation radius. Normalized Hull Coefficient peak intensities (area of the curve inflection) for the carbon – oxygen bond at a wavelength of approximately 1320 nm provided a measure for the degree of blackness. Black samples absorb most or all of the incoming wavelength spectra, whereas partially blackened or non-blackened pebbles will reflect different C-O bond peak intensities that are dependent upon the degree of black coloration. Non-blackened samples yielded area under the C-O bond curve values of approximately 17 with black pebbles having values less than 3.

## DEPOSITIONAL & DIAGENETIC SETTINGS

Blackened limestone clasts from the Nullarbor Plain and Cape Spencer range not only in geologic age but also in terms of depositional setting. Whereas, the depositional setting of each location is different, the clasts themselves are identical throughout. The

following section outlines the depositional framework of each location and describes the nature and composition of the blackened clast breccia.

### *Nullarbor Plain*

Rawlinna Quarry, where the oldest clasts occur, is located in the western margin of the Nullarbor Plain and exposes three laterally continuous horizons of black limestone clast breccia. These beds are located in the upper 5 m of the quarry wall and occur at approximately the same depth below the surface throughout (Fig. 4.2A). Such 15 – 30 cm thick black clast bed overlies a pronounced undulatory surface with 30 – 50 cm wide and deep depressions (Fig. 4.2B). Such beds are separated by marine fossilferous grainstones/ rudstones belonging to the middle Miocene Nullarbor Limestone. These marine sediments are also the matrix for the blackened clast breccia. This matrix sediment is however, more abraded and better sorted than the intervening Nullarbor Limestone (Fig. 4.2C).

The black clasts themselves are angular, fragmented, poorly sorted, and have different degrees of blackening. Particles range from 1 – 10 cm in diameter to 1 – 5 cm in thickness and commonly have insitu fracturing. The majority of clasts, independent of coloration, contain numerous small marine fossils that are dominated by benthic foraminifera and coralline algae (Fig. 4.2C). Such fossils also compose the prevailing Nullarbor Limestone lithologies and breccia matrix.

Breccia horizons also contain unique laminated micrite pebbles and boulders that are yellowish gray in color with more intensive black coloration along their margins (Fig. 4.2D). They range from ~ 3 – 35 cm in diameter and occur clustered together in the lower most black clast horizon. Laminations inside these clasts are < 1 mm thick, wavy, and have inter-layered coarser grained sediments. Most of these clasts have dissolution voids that

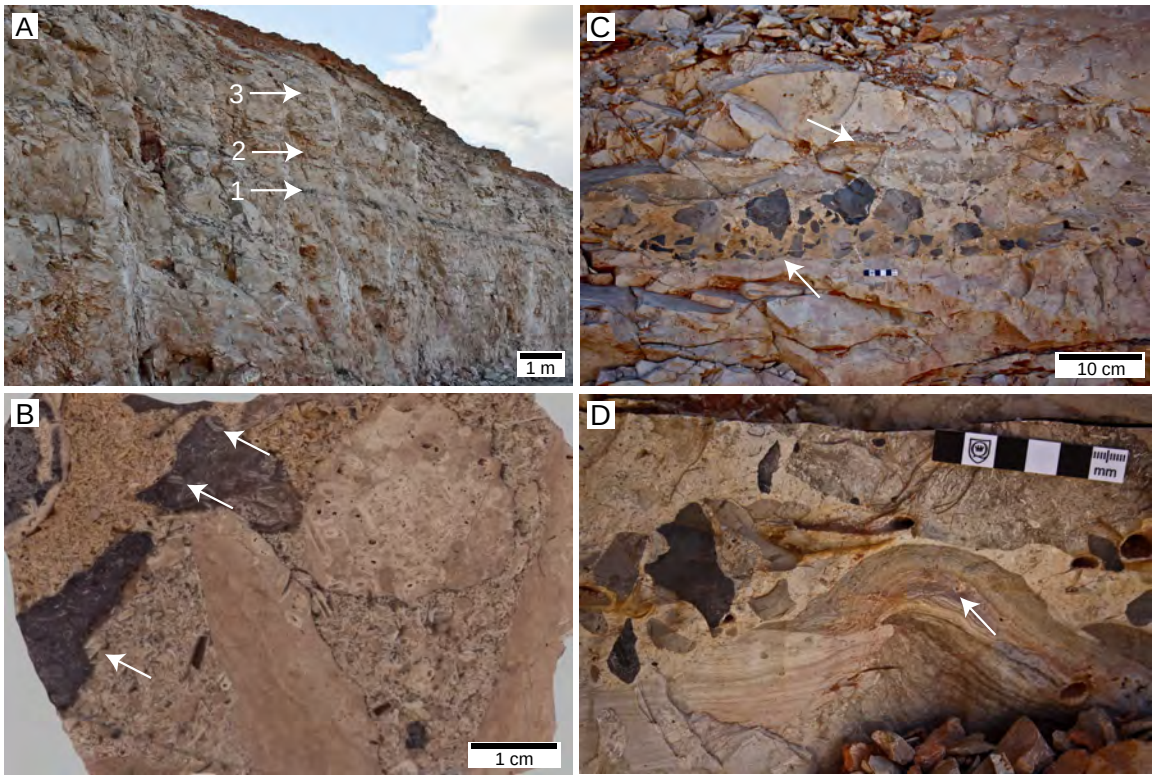


**Figure 4.2.** Rawlinna Quarry A) Photograph of a vertical quarry wall illustrating the horizontal orientation of planar bedded blackened clast horizons. Three horizons consistent in terms of depth and bedding characteristics are found throughout the quarry with the lowermost horizon the most developed. B) Lowermost blackened clast bed illustrating the underlying contact with the Nullarbor Limestone (arrow). The contact is undulatory and is defined by a prominent dissolution surface into the Nullarbor Limestone. The bed has a gradual upper contact with the intervening Nullarbor Limestone beds (arrow). C) Bedded horizon sample showing blackened and non-blackened clasts amongst a matrix of fossiliferous grainstones that are solely composed of marine bioclasts. The blackened clasts have some of these bioclasts preserved inside their internal fabric (arrows). D) Lowermost blackened clast bed that has common laminated micrite clasts and boulders (LM). These components commonly have contorted internal fabrics and domal structures (arrow).

are filled with fossiliferous matrix sediment.

Black limestone clast breccias elsewhere on the Nullarbor Plain are hosted in a singular diagenetic setting; isolated subsoil hollows that have been excavated into the underlying Nullarbor Limestone (Fig. 4.3A). These latest Pliocene isolated shallow depressions are of constant size, 0.5 – 2 m deep and 0.5 – 3 m in diameter, and occur throughout dolines, quarries, and on the surface where calcrete is thin or absent (Miller et al. 2012). Such depressions have smooth boundaries, lack any alteration rims with the surrounding limestones, and have wide openings to the surface, forming a broad bowl shape.

These subsoil hollows are filled with a calcareous breccia composed of, in order of abundance, variably blackened limestone clasts, Nullarbor Limestone clasts, micrite, fine to very fine grained quartz sand, pisoids (with black nuclei), and pulmonate gastropods (Fig. 4.3B). Black clasts dominate these fills making up approximately 60 – 75% of the breccia components. Such clasts have a varying degree of blackness and some display a distinct internal progression of black coloration from dark at the surface to light gray inward (Fig. 4.3C). The darkest clasts have a structureless appearance, whereas, partially colored clasts have parent rock fabrics wherein even fragmented bioclasts are visible.

The blackened clasts are 0.5 cm – 15 cm in diameter, 0.5 – 5 cm thick, angular, and poorly sorted. Small (< 1 cm diameter) black clasts can locally form the nucleus of soil pisoids that have an evenly laminated micrite cortex (Fig. 4.3D). These pisoids are commonly clustered in cavities that cross cut the larger dissolution hollows. Matrix sediment supporting the black clast breccia in the hollows is dominantly micritic, ranging in color from light gray to moderate reddish brown. Fine-grained quartz with frosted margins is also a common constituent in all matrix sediment.

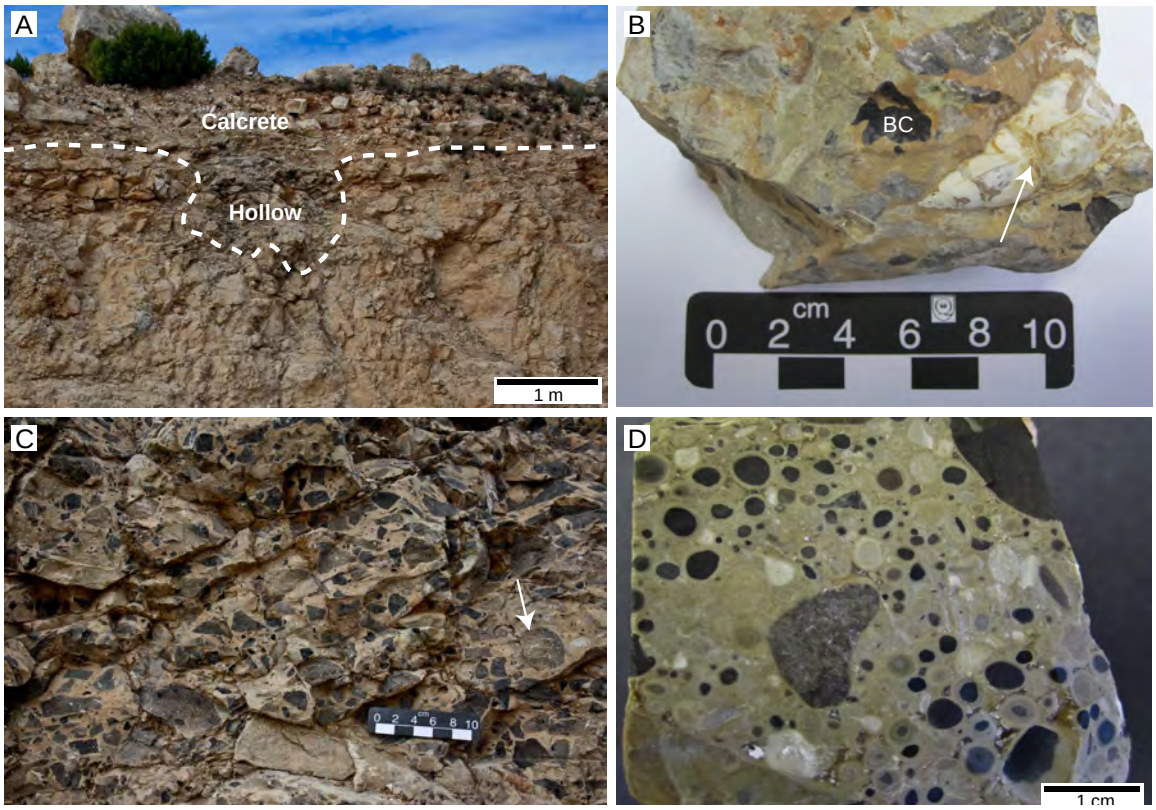


**Figure 4.3.** Nullarbor Plain A) Subsoil hollow karstic depression at Eucla Quarry that hosts a blackened limestone clast breecia. Hollows are of consistent size across the Plain and are always filled with the characteristic breecia. B) Breecia fill with blackened clasts (BC) and a large aragonitic terrestrial pulmonate gastropod (arrow); Cocklebiddy Cave. C) Blackened clasts in Eucla Quarry (from same subsoil hollow as in A) illustrating their characteristic angular, poorly sorted, and matrix supported nature. Most clasts are completely blackened although some show an internal progression of blackening (arrow). D) Blackened clasts in a subsoil hollow at Forrest showing a later event of diagenesis that forms small pisoids with blackened limestone nuclei; Forrest.

*Cape Spencer*

The Bridgewater Formation at Cape Spencer hosts numerous paleosols that are replete with black pebbles, both at dune crests and particularly in interdune corridors (Fig. 4.4A). Samples were collected both at the top of the dune sequence that is the modern surface and in the paleosols lying on depressions between dunes. These paleosols occur within both the Lower and Upper Bridgewater Formations.

Black clasts occur throughout subsurface Lower Bridgewater Formation terra rossa paleosols (Fig. 4.4A). These clasts are 1 – 5 cm in diameter and are the dominant component in a matrix-supported calcareous breccia, along with larger lithified clasts of the underlying aeolian sediments. The angular clasts have differential black colorations and commonly possess darker margins than the central parts. Black pebbles locally can be coated by thin moderate reddish brown colored cortical micrite laminations (< 1 cm) forming pisoids. They commonly occur in association with uncoated black pebbles and lithified limestone clasts. The matrix sediment is moderate reddish brown in color and fine grained, typical of other semi-arid paleosols in southern Australia (Lintern et al. 2004; Lintern et al. 2006; Miller et al. 2012).

The Upper Bridgewater Formation also contains 1 – 5 cm diameter black limestone clasts at multiple paleosol horizons (Fig. 4.4A). The black clasts are associated with calcrete horizons at dune crests and are similar in morphology to the clasts located below in the terra rossa paleosols described above (Fig. 4.4B). The hardened calcrete surface at Cape Spencer is also covered with loose blackened clasts and is commonly embedded in the underlying limestone. Such clasts are characteristically more resistant to weathering than the surrounding calcareous aeolianites and calcretes (Fig. 4.4C). The surfaces of these clasts show extensive dissolution features dominated by micro-runnel fabrics.

The loose surface pebbles share attributes with those of underlying paleosol horizons, whereas the clasts still embedded in the limestone have dissimilarities. Embedded clasts are commonly 5 – 25 cm in diameter and < 3 cm thick. Such platy morphologies occur in shallow rounded depressions (~ 20 – 120 cm in diameter and 5 – 10 cm deep) on the surface (Fig. 4.4D). The edges of these hollows are differentially more blackened and weather in relief compared to the center of (Fig. 4.4C, D). These large plates of blackened limestone fragment and contribute to the much more abundant pebble gravel covering the surface.

## BLACKENED LIMESTONE CLAST MICROSTRUCTURE

Despite differences in their geographic location and geologic age, black limestone clasts in this study have comparable macroscopic and microscopic features. These include 1) fragments of underlying limestone, very fine grained quartz, and clotted minimicrite, 2) porous micritic laminae, 3) calcareous coatings, 4) calcareous filaments, 5) microtubules, 6) calcareous spheres, 7) illite clay, 8) common stable carbon isotope values, and 9) organic carbon.

### *General Characteristics*

Black limestone clasts are completely composed of dense micrite and minimicrite that has a distinctive grayish brown color with a clotted, mottled, and commonly laminated microfabric. Small (< 300 μm) quartz grains are locally common in these micritic fabrics. The dense micrite of many clasts is locally porous and is crosscut by < 2 mm wide veins, both of which are variably filled with sparry calcite cement.

Small-corroded (0.5 – 3 mm diameter) particles of the underlying limestone are

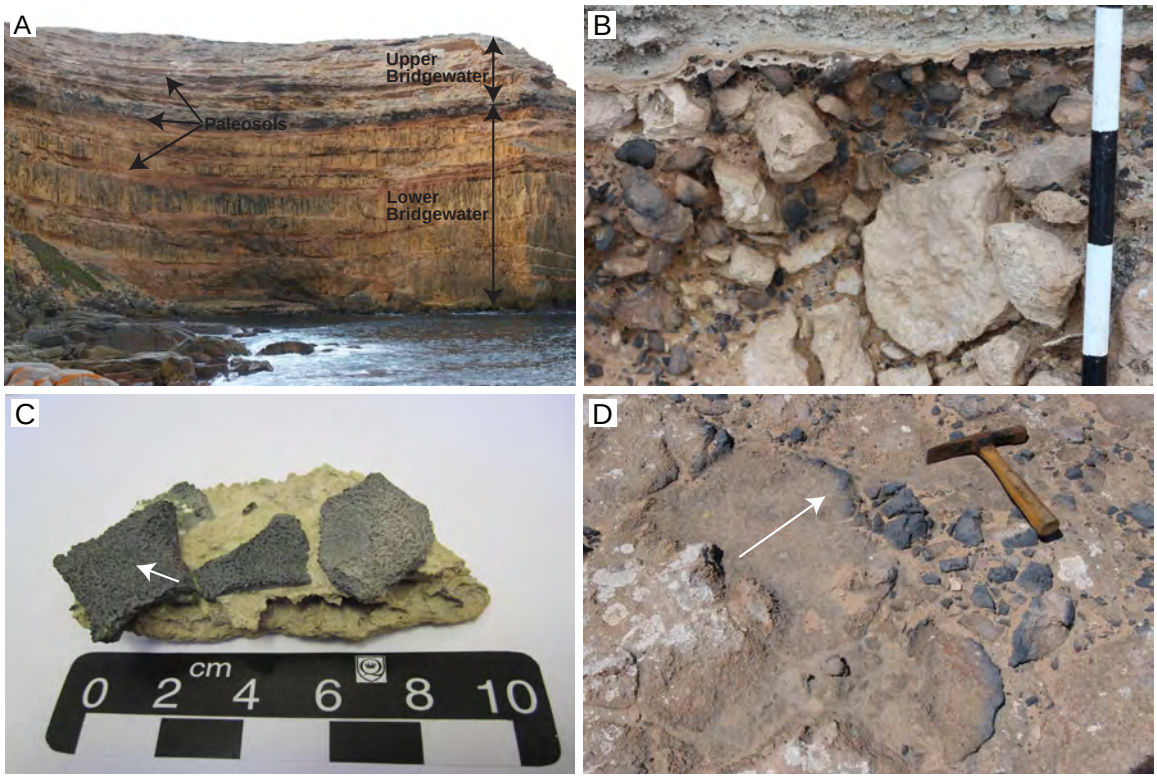


**Figure 4.4.** Cape Spencer A) Sea cliff at the edge of Cape Spencer illustrating the stratigraphy of the Bridgewater Formation. The resistant layers are the terra rossa paleosols of the Lower Bridgewater Formation and calcretes of the Upper Bridgewater Formation. B) Fragmented blackened clasts in a calcrete paleosol horizon within the Upper Bridgewater Formation; Willyama Bay. C) Sample from Innes National Park illustrating the differential weathering between the more resistant blackened clasts and least resistant fine grained calcarenites. The surface of the blackened clasts also shows micro-runnel dissolution fabrics (arrow). D) Ground surface at Innes National Park illustrating the numerous shallow karstic pits in the underlying limestone. The limestone in these pits has a distinct progression of blackening towards their outer edges (arrow) where the blackened limestone fragments into clasts.

commonly incorporated in the black clast microstructure (Fig. 4.5A). These fragments contain benthic foraminifera, coralline red algae, echinoderms, and pelagic foraminifera bioclasts. The amount of original fossiliferous material is directly related to the degree of black coloration in the clast. Intensely blackened clasts have substantially fewer or no fossil particles incorporated, whereas, lighter colored clasts numerous biofragments. This mixing of fossilferous particles is most evident at Rawlinna Quarry and on the surface of Cape Spencer.

### *Porous Micritic Laminae*

Porous micritic laminae are anastomosing networks of millimeter- to submillimeter-size tubules that have ~ 20 μm thick dark micritic walls (Fig. 4.5B). The ~ 100 – 400 μm diameter and <1 mm long tubules are delicately contorted and form crudely laminated fabrics that make up the whole microstructure in black clasts. The tubes are filled with sparry calcite cement and usually have alveolar structures and *Microcodium* aggregates between them (cf. Klappa 1979; Klappa 1980; Wright 1994; Alonso-Zarza 2003; Kosir 2004). Small (< 2 mm diameter) coated grains and micritic ooids are also locally present between these laminae and are most numerous at Cape Spencer. There are two different types of tubules that occur separately and are not found in association with one another.

**Partitioned tubules.—**The most common tubiform is a long ellipsoidal and spherical micritic cylinder with internal partitions that creates a series of small calcite spar filled chambers (Fig. 4.5C, D). The size and shape of these chambers are different in the central portion of the tubule as opposed to the outer walls. Thin micritic walls (< 10 μm thick) that intersect one another in a regular pattern form all chambers. The central portions of tubules are composed of isodiametric micritic walls that create a honeycomb texture (Fig. 4.5C, D).

These chambers are ~ 25 μm in diameter and change shape at a prominent boundary toward the outside margins of the tubule. The outer wall has similar micritic partitions, however, the chambers are elongate with an ~ 2:1 length to width ratio (Fig. 4.5D).

**Hollow tubules.—**The other tubules are hollow linear (~ 100 μm in length) cylinders or 100 – 150 μm wide spheres. Such tubules have ~ 15 μm thick exterior micritic walls and are either occluded by sparry calcite cement or are porous. The microstructures of hollow tubules have a distinct absence of any internal micritic partitions or chambers and subsequently have less microporosity than partitioned tubules.

### *Calcareous Coatings*

Ultrathin (<100 nm), uniform, and smooth coatings are prevalent in all black pebble samples. These coatings completely to partially cover the surfaces of micrite and minimicrite crystals, leading to regions of obscured original microcrystalline calcite fabrics and undulating heterogeneous coating draperies (Fig. 4.6). Such coatings are calcareous but can have low levels of Mg and Si (rarely detected in EDX analyses).

The variation in coating thickness creates a mosaic of smooth and uneven surfaces. More laterally continuous areas of thickened coatings are smooth in appearance although locally the surface becomes undulatory where they are thin. These coatings fill all original microporosity between micrite and minimicrite crystals, whereas zones that lack this coating material have well developed rhombohedral microcrystalline calcite and microporosity. Coatings also form meniscus-bridges across pores and between micrite/minimicrite crystals (Fig. 4.6).

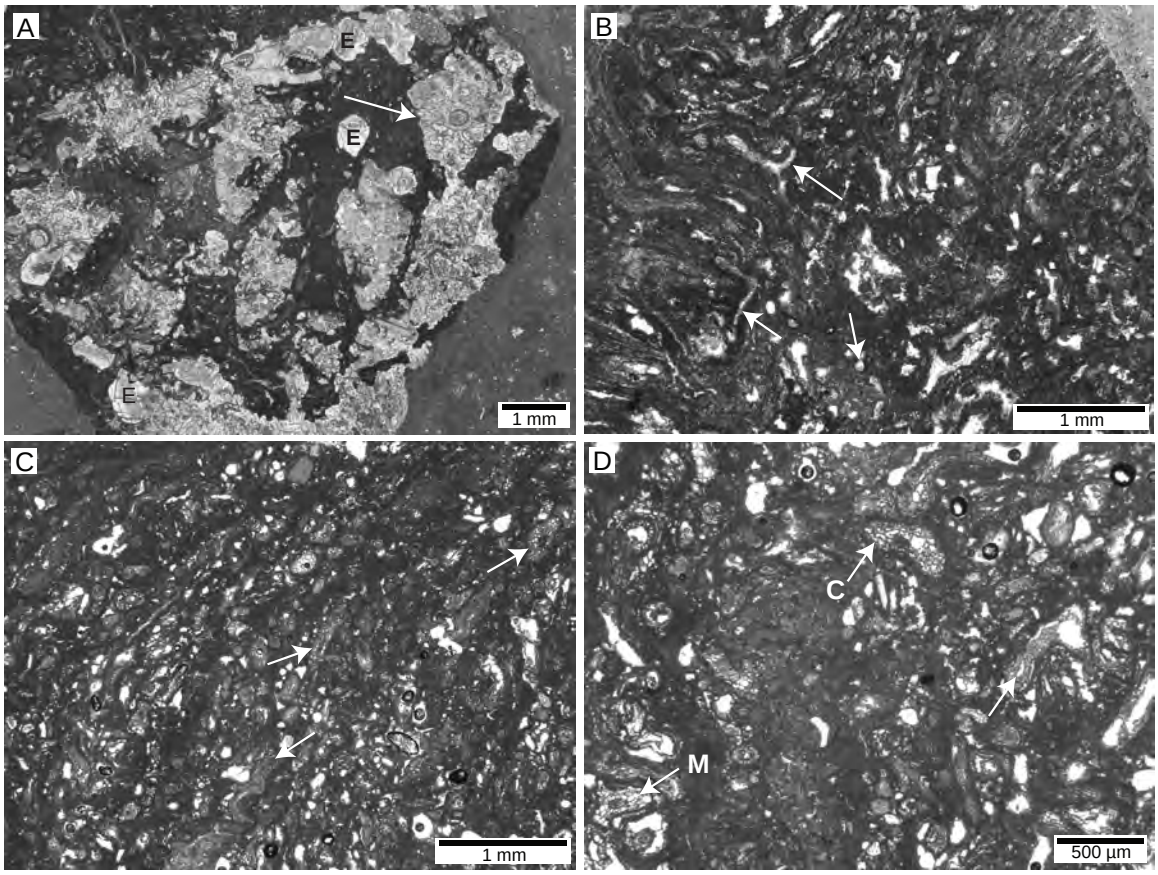


**Figure 4.5.** Micritic Laminae A) Photomicrograph of a blackened clast with small fragments of Nullarbor Limestone incorporated in the dense micrite composition typical of blackened clast microstructures. The edges of some fragments show smooth dissolution boundaries (arrow) with echinoderm fossils (E) preferentially preserved; Eucla Quarry. B) Photomicrograph of a blackened clast microstructure dominated by root mat laminae. The laminae have double micrite walled tubules with hollow central pores (arrows), which are shown in different orientations (either spheres or long tubules); Cape Spencer. C) Photomicrograph of calcified roots and their cellular structures in a Cape Spencer blackened clast. Tubules have internal micrite walls that create isodiametric and elongated compartments corresponding to the different sections of roots, medulla and cortex respectively (arrows). D) Higher magnification photomicrograph of previous calcified root fabrics in C. Root cellular structures are exceptionally well preserved and show a distinct subdivision between the medulla (M) and cortex (C). Some root structures have only the cortex preserved with a hollow central vascular cylinder (arrow).

*Calcareous Filaments*

Black clasts also contain calcareous filaments that are 0.1 – 0.2 μm wide and 1 – 5 μm long. Such filaments have smooth outer surfaces and are typically interwoven with the calcareous coatings described above, implying that they formed concurrently. The filaments are embedded in the microcrystalline calcite and appear to follow an underlying micro-topography that creates undulations in the filament along its length (Fig. 4.7A). Filaments are generally separate, although they locally entwine with neighbouring filaments to create rope-like amalgamations that bridge across small pores (< 3 μm). Calcareous coating material obscures the ends of most filaments but where visible they have complex bifurcating terminal attachments to the underlying substrate (Fig. 4.7B).

*Microtubules*

Pleistocene to sub-recent blackened clasts at Cape Spencer have a multitude of small, straight, hollow, and uniform microtubules. Such cylinders dominate the micritic microstructure in most of the blackened clast samples. These microtubules do not form laminae; instead they are randomly distributed and commonly intersect one another through the minimicrite and micrite matrix (Fig. 4.8A). Microtubules occur as two different morphologies.

**Hollow microtubules.—**The most common form of microtubule is a hollow cylinder 1.50 – 1.75 μm in diameter and 5 – 75 μm in length (Fig. 4.8B). This diameter is constant, whereas the length is dependant upon the orientation of the tube, again indicating that the tubes are unsystematically orientated. The minimicrite and micrite along the margins of these tubes have extensively etched surfaces. Such etchings are usually in the form of pits and prisms. Disordered clusters of elongate minimicrite crystals occur with these etchings

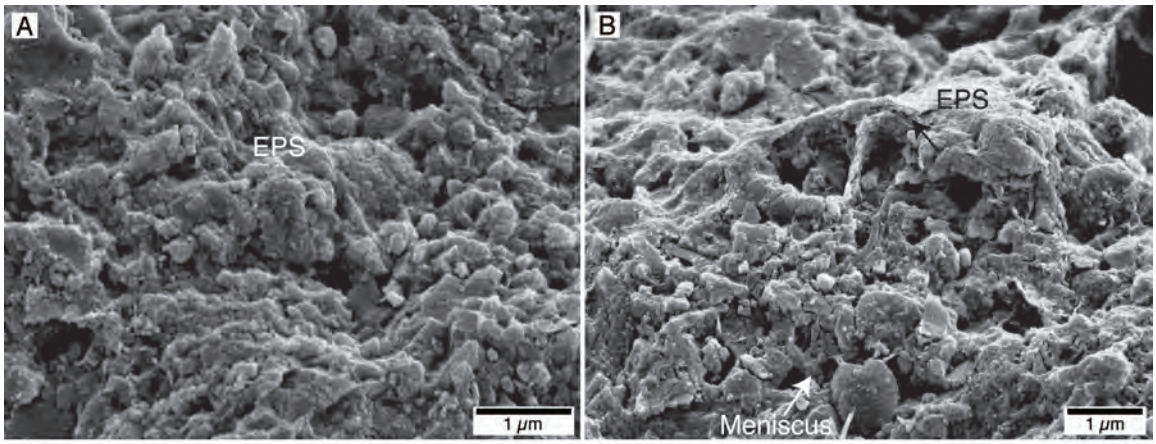


**Figure 4.6.** Calcareous Coatings A) SEM image illustrating the variability in interpreted EPS coatings in blackened clasts microstructures. The mosaics of EPS coatings obscure the underlying micrite and minimicrite and create a cascading facade of undulating calcareous coatings; Forrest. B) SEM image of a fragmented EPS coating showing the thickness (arrow) and distribution over a minimicrite matrix. The EPS coatings commonly have meniscus structures that bridge between individual zones of EPS and larger grains (arrow); Forrest.

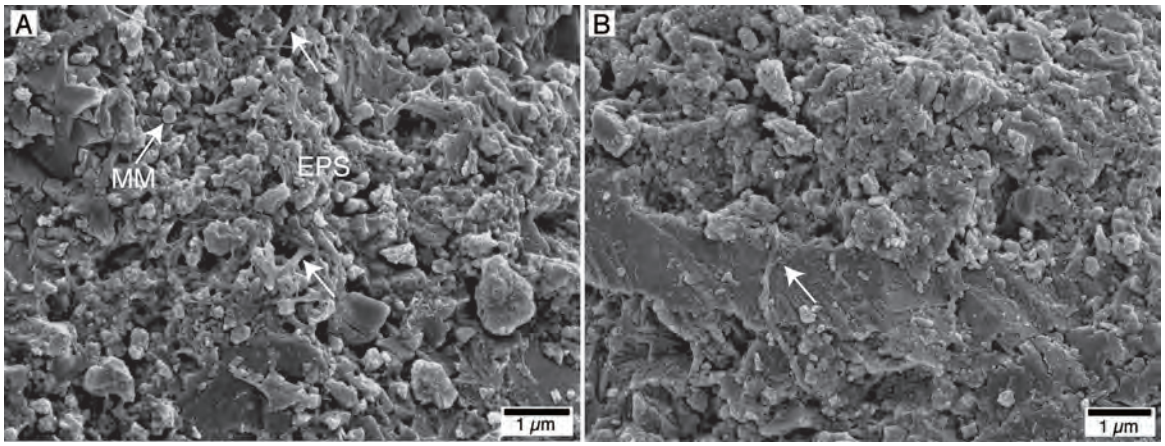


**Figure 4.7.** Calcareous Filaments A) SEM image of minimicrite (MM) and EPS coatings with an abundance of interpreted algal filaments. The filaments commonly are embedded in the EPS coatings and form bridges across small pores with bifurcating terminal attachments (arrow); Forrest. B) SEM image of an individual algal filament embedded in EPS coatings and minimicrite along its lower portion, bifurcating terminal attachment (arrow) and smooth surface, which is characteristic for all filaments in blackened clast microstructures; Forrest.

(Fig. 4.8C). The minimicrite crystals are 75 – 200 nm wide and 300 – 575 nm long, have rounded margins, and are commonly obscured by thin zones of smooth calcareous coatings. These smooth coatings continue into the hollow microtubes where they form thick veneers (Fig. 4.8B).

**Zoned microtubules.—**The second type of microtubule shares all the above characteristics except they have a 2 μm wide cortex of elongate minimicrite crystals (~100 nm in diameter and 2 μm in length) that are oriented radially around the hollow tube (Fig. 4.8C). The bulbous ends of these crystals are covered with calcareous coatings and create a hummocky surface on the inside of the tube.

### *Calcareous Spheres*

Calcareous spheres, 750 nm in diameter, are intimately associated with microtubules and calcareous coatings (Fig. 4.8D). Such entities have a characteristic smooth outer surface, are of consistent size, and occur in small clusters. This characteristic smooth outer surface of spheres are frequently etched or corroded (Fig. 4.8D). The boundaries between individual spheres can be locally diffuse as the spheres amalgamate with one another and/or are covered in calcareous coatings.

### *Insoluble Residue*

XRD analyses of insoluble residue indicate a composition of mostly quartz and illite. SEM analyses of this residue confirm the dominance of 10 – 30 μm diameter quartz grains in a smooth and fine-grained illite matrix. These well-rounded grains have a smooth and frosted outer surface (Fig. 4.9). Rare quartz grains have sharp serrated edges in the form of scalloped surfaces and uneven margins.

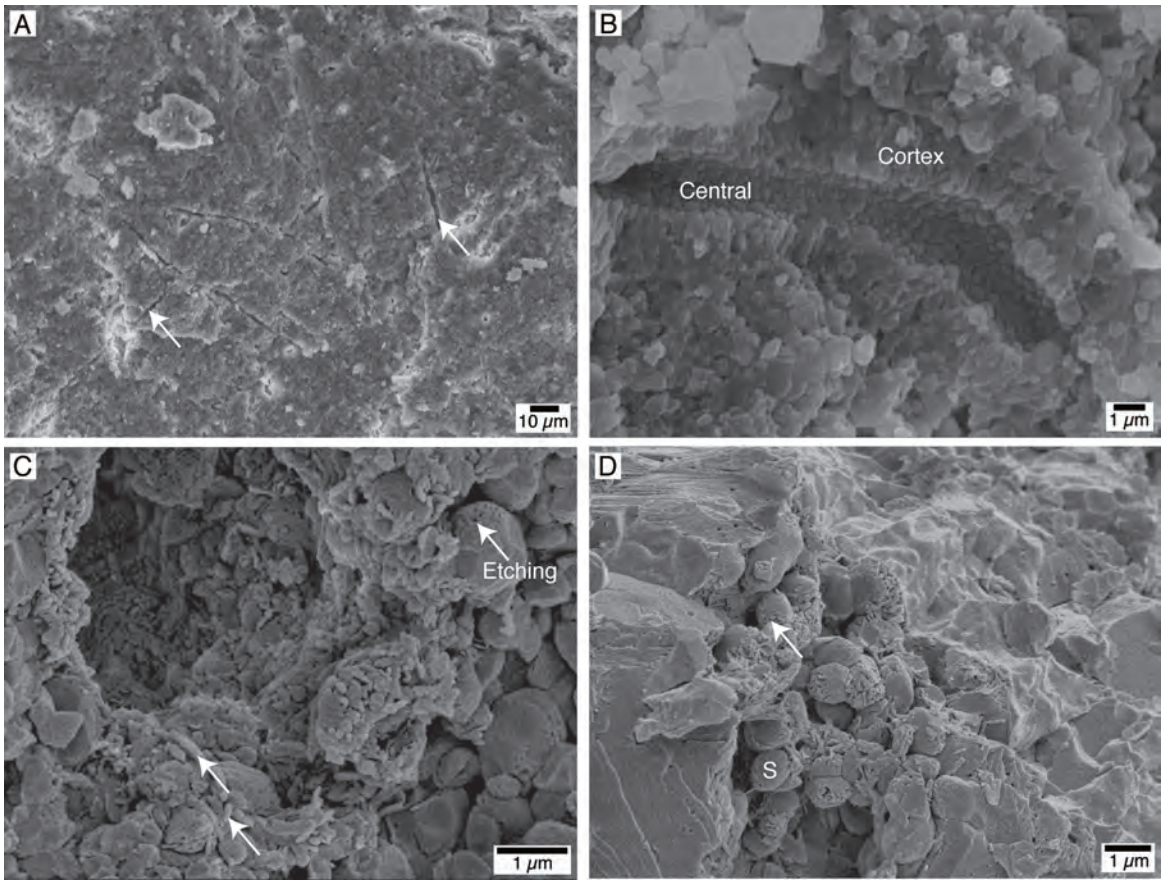


**Figure 4.8.** Microtubules A) SEM image showing microtubules (arrows) in a mosaic of dense minimicrite and micrite. The microtubules cross each other and have no preferred orientation or alignment; Cape Spencer. B) SEM image at higher magnification of an individual tubule that shows a two-part structure. The inner portion (central) is hollow and has a surface of small smooth undulating domes, whereas the outer zone (cortex) is composed of elongated and orientated micrite crystals; Cape Spencer. C) High magnification SEM image of an end on view of a microtubule showing the complex arrangement of microstructures along its periphery. The features are dominated by small elongate and smooth minimicrite crystals (arrow), interpreted to be bacterial in origin, and numerous etched surfaces (arrow) on preexisting minimicrite and micrite crystals in the surrounding matrix; Cape Spencer. D) High magnification SEM image of small calcareous spheres interpreted to be bacterial spores (S) embedded in larger micrite and calcite crystals, most have etched surfaces (arrow) and are covered in varying amounts of EPS; Cape Spencer.

*Stable Isotopes*

Stable carbon and oxygen isotopic analyses of the calcium carbonate and insoluble residue illustrate a distinct trend in carbon fractionation. Isotopic values obtained from the $CO_2$ released during calcium carbonate dissolution show highly negative $\delta^{13}C$ and $\delta^{18}O$ values (Table 4.1). The $\delta^{13}C$ values from five completely to moderately blackened limestone clasts have a minor range in values (-10.4 to -6.5 ‰ PDB). $\delta^{18}O$ values also have only small variations, ranging from -4.8 to -2.5 ‰ PDB. There is however no discernible correlation between degree of blackening and isotopic ratios.

Stable carbon isotope data obtained from combustion of eighteen insoluble residue samples in the elemental analyzer have a consistent highly negative $\delta^{13}C$ values (Table 2). All insoluble residue samples, regardless of location, have a $\delta^{13}C$ value of approximately -26 to -22 ‰ PDB. These values reflect organic carbon components of the residue since all calcium carbonate material was removed in the dissolution process.

*Organic Carbon Content*

Most black pebbles have a significant percentage of carbon in their insoluble residue, although quantitatively these values vary widely (Table 4.2). Total weight percent carbon values range from 1.0 to 34.9 with most samples containing < 10 %. This indicates that carbon from organic matter is found in all samples that show degrees of black coloration, whereas in non-blackened samples there is no organic carbon or insoluble residue. Carbon-oxygen bond peak intensities obtained through SWIR analyses allow the weight percent carbon values to be quantitatively related to the degree of black coloration in the clasts (Fig. 4.10). These data show that there is a direct exponential correlation between the weight percent carbon and the degree of black coloration.

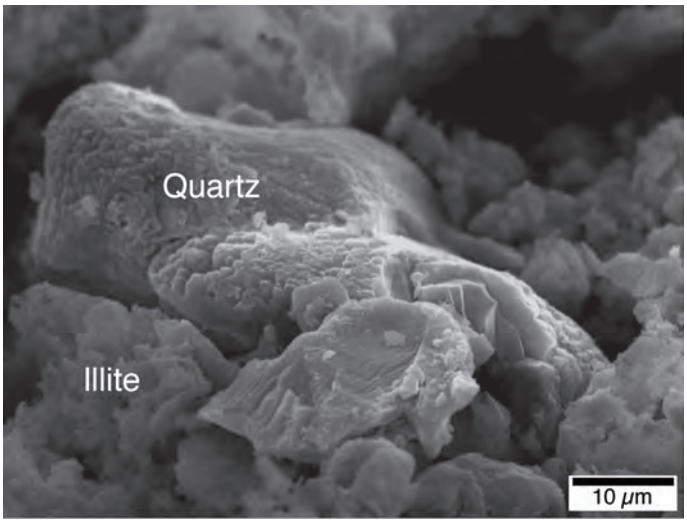


**Figure 4.9.** SEM image of a quartz grain embedded in a matrix of illite clay. The quartz grain has rounded margins and a frosted surface that implies an aeolian origin.

**Table 4.1**
Whole rock stable C inorganic and O isotope data for blackened pebbles
Error/precision of analyses is 0.1 ‰

| Location | Description | $\delta C^{13}$ (‰ PDB) | $\delta O^{18}$ (‰ PDB) |
|---|---|---|---|
| Eucla Quarry | completely blackened clast | -10.4 | -3.1 |
| Eucla Quarry | breecia matrix dark gray colour | -7.8 | -3.7 |
| Cook Quarry | completely blackened clast | -9.8 | -4.8 |
| Cook Quarry | breecia matrix reddish brown colour | -9.9 | -4.6 |
| Rawlinna Quarry | moderately blackened clast | -6.5 | -2.5 |

# INTERPRETATION

Universal morphological and geochemical characteristics of blackened clasts located across the Nullarbor Plain and Cape Spencer demonstrate that they have similar modes of formation. The mechanisms involved are interpreted through these shared morphological traits and are shown to occur only in a specific subsoil environment. Roots derived from overlying plants are thought to be responsible for most of the fabrics occurring in blackened clasts and also the source of the organic C that produces the black color.

## *Rhizogenic Origin of Micritic Laminae*

The most common attribute of the blackened clasts is the abundance of porous micritic tubules and laminae. These features are similar in appearance to calcified root structures in subaerial calcareous paleosols elsewhere and are interpreted as such (Klappa 1978; Klappa 1980; Wright et al. 1988; Alonso Zarza et al. 1998; Alonso Zarza 1999; Kosir 2004). Dense arrangements of these calcified root structures form crudely laminated root mats within the blackened clasts. Such rhizogenic fabrics are relatively minor constituents in partially blackened pebbles, whereas they form the whole microstructure of completely blackened clasts.

Preservation of root structures is not only the function of favourable physiochemical processes in soils that lead to permineralization but also the precipitation of calcite in the living cells of specific plant roots (Klappa 1979; Klappa 1980; Retallack 2001; Kosir 2004; Alonso-Zarza and Wright 2010). Two dominant styles of calcification produce a variety of microstructures that are present in the partitioned and hollow tubules of this study. The products are dependent on whether calcification occurs inside or outside the rhizosphere

**Table 4.2**
Insoluble residue C organic isotope and amount percent organic C data for blackened pebbles
Error/precision of isotope analyses is 0.1 ‰

| Location | Degree of black colouration | $\delta C^{13}$ (‰ PDB) | Amt. % Carbon |
|---|---|---|---|
| Cocklebiddy Cave | completely black | -22.1 | 19.6 |
| Cocklebiddy Cave | slightly black | -21.5 | 3.8 |
| Forrest | completely black | -21.5 | 24.7 |
| Rawlinna Quarry | completely black | -21.9 | 19.2 |
| Cape Spencer | moderately black | -21.3 | 5.5 |
| Madura Pass | completely black | -23.0 | 21.0 |
| Eucla Quarry | slightly black | -24.2 | 1.8 |
| Cook Quarry | completely black | -21.4 | 9.8 |
| Cape Spencer | moderately black | -21.6 | 9.3 |
| Cape Spencer | moderately black | -22.3 | 6.6 |
| Rawlinna Quarry | completely black | -21.9 | 34.9 |
| Rawlinna Quarry | moderately black | -21.4 | 7.2 |
| Forrest | slightly black | -20.8 | 2.7 |
| Eucla Quarry | completely black | -23.3 | 12.6 |
| Cape Spencer | completely black | -21.6 | 23.8 |
| Cape Spencer | completely black | -21.6 | 19.5 |
| Cape Spencer | slightly black | -22.0 | 3.7 |
| Cape Spencer | moderately black | -21.5 | 8.5 |

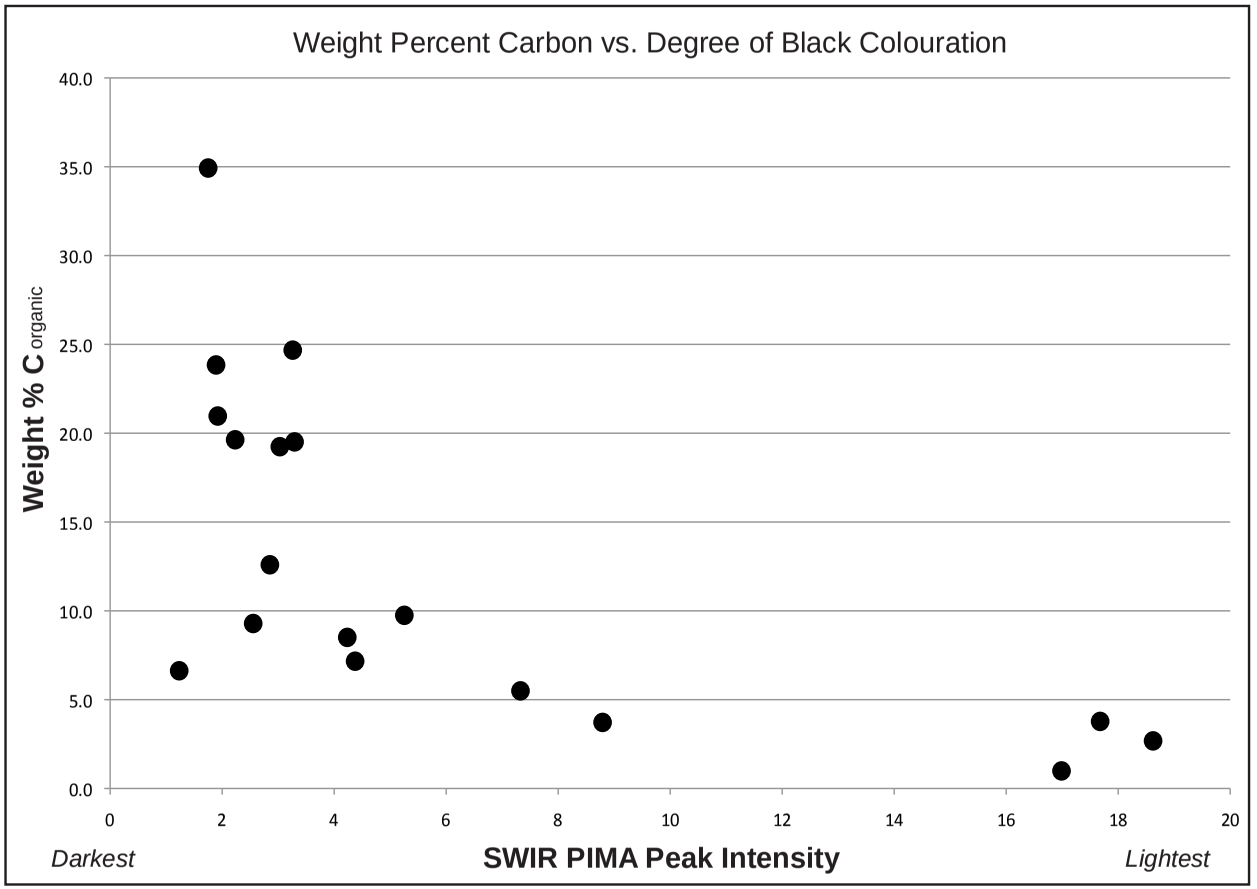


**Figure 4.10.** Graphical representation of weight percent organic carbon of blackened clast insoluble residue compared to the clast's degree of black colouration. The horizontal axis is the SWIR PIMA peak intensity for the carbon-oxygen bond at approximately 1340 nm wavelength. The area contained within the C-O peak represents this peak intensity value. The smaller peak intensities correlate to blacker samples since their black colouration adsorbs most incoming wavelength spectra, whereas lighter samples have larger peak intensities and hence larger values. The data shows that organic carbon increases exponentially with regards to degree of blackness. The inflection point for the change from partially blackened to completely is at approximately 7.5 % organic C.

before the organic components decay (Jaillard et al. 1991; Wright et al. 1995; Alonso Zarza 1999; Kosir 2004). The first, rhizosphere calcification, is an accumulation of $CaCO_3$ around the periphery of plant roots caused by the activities of microbial communities in the soil that produce micritic tubules with hollow centers (Jaillard and Callot 1987; Jones 1994; Kosir 2004). The second, intracellular calcification, occurs within the rhizosphere and preserves the cellular structure of the root (Fig. 4.11). The partitioned tubules and associated laminae in this study are formed by isodiametric mosaics of chambers separated by thin micrite partitions that are interpreted to be calcified portions of the medulla (parenchymatic cells or xylem vessels). The outermost zones of the tubules have a much more elongate morphology and are subsequently interpreted to represent the root cortex (cf. Alonso Zarza et al. 1998; Alonso Zarza 1999).

**Calcification Controls and Soil Conditions.—**The location of calcification in roots not only depends upon the type of surface vegetation but also on local climate, soil hydration states, and chemical composition of pore fluids. Recent calcified roots are almost exclusively found in nutrient-poor calcareous soils under semi-arid climates with seasonal rainfall (Jaillard et al. 1991; Kosir 2004).

Preserved cellular root structures are particularly evident in plants that grow on calcareous alkaline soils that have high acid-neutralizing capabilities (Jaillard and Callot 1987; Hinsinger 1998; Kosir 2004). Calcification of roots enhances production of protons via the exchange of $Ca^{2+}$ and $2H^{+}$ ions and causes acidification in the rhizosphere. This process enhances the ability of plants to acquire mineral nutrients while at the same time causing corrosion of the surrounding limestone bedrock (Jaillard and Callot 1987; McConnaughey and Whelan 1997; Hinsinger 1998; McConnaughey 1998; Kosir 2004). Plants also use $Ca^{2+}$ to stabilize their cell walls by the simple accumulation of $CaCO_3$ in

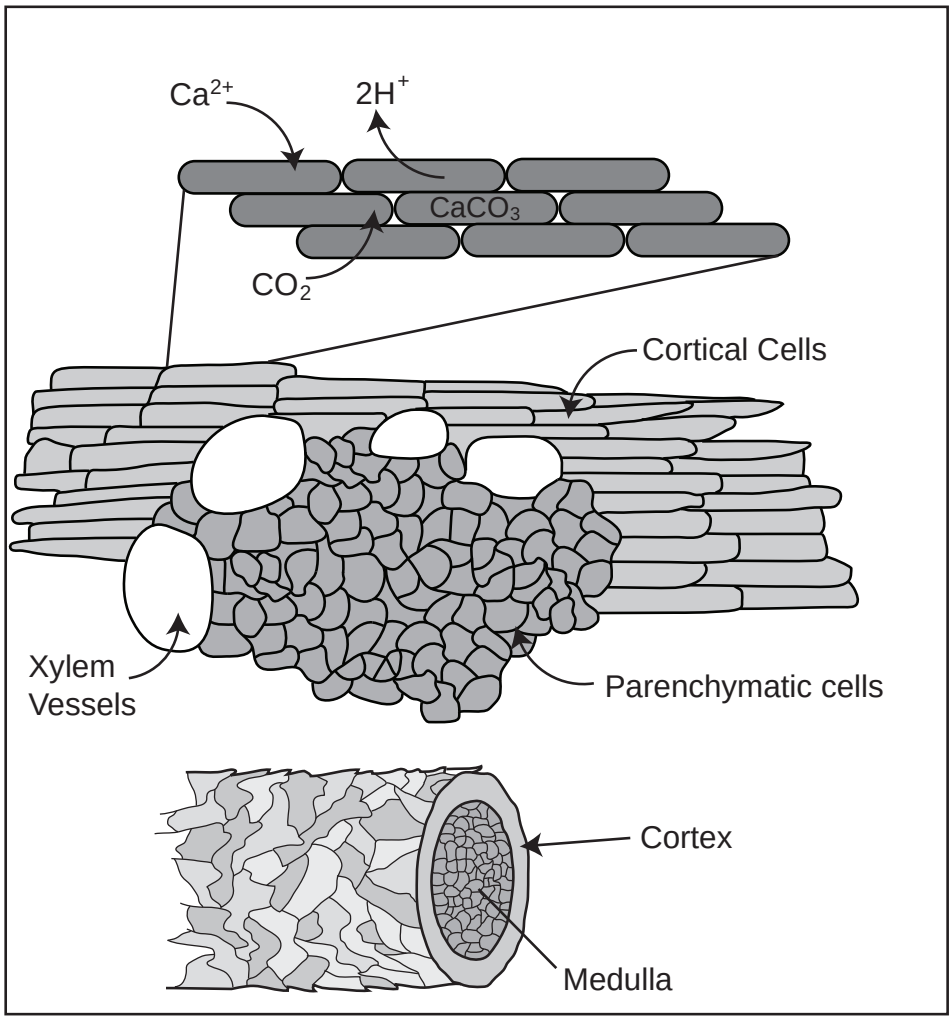


**Figure 4.11.** Diagrammatic illustration showing the commonly preserved arrangements of cells in root mats. Magnification increases from bottom to top with the bottommost illustration showing a root cross-section and the top showing cellular make up and the exchange of ions in the calcification process. Cellular structures within the medulla are characteristically isodiametric in shape and size, whereas the cortical cells have a more elongate morphology (as pointed out with arrows in illustration). Dark microcrystalline walls define the cellular structures with clear sparry calcite cements filling the intervening portions. The topmost diagram illustrates the ion exchange mechanism in the uptake of $Ca^{2+}$ and expulsion of $H^{+}$ by root cells in the calcification process.

root tissue that protects the root from excessive calcium bicarbonate concentrations in the soil fluids (Clarkson 1984; Marschner 1995; Kosir 2004).

**Microbial Communities.—**Calcareous coatings, filaments, and spheres in the microstructure of blackened pebbles are thought to represent preserved microbes or substances created by microbial processes. Calcareous coating mosaics throughout blackened clast are interpreted to be calcified forms of exopolysaccharides or extra-cellular polymers (EPS) (Folk and Chafetz 2000; Jones 2010; Jones 2011). Calcified filaments and small spheres associated with microtubules are thought to be algal filaments, and bacterial spores respectively. These common microbial features indicate that a *Mycorrhizae* type symbiotic relationship between the roots and bacteria/fungi was active during calcification. Fungal hypae and bacteria would have encompassed the external portions of the root fabric and coated them, which is why these microbial fabrics are found preserved along the peripheries of microtubules. EPS and other microbial products are today efficient at binding ions from solution and serving as nucleation sites that lead to favourable conditions for calcite precipitation (Fortin et al. 1997; Leveille et al. 2000).

### *Blackening Agent*

The substance causing the black coloration in limestone clasts at subaerial unconformities has long puzzled carbonate researchers. Black pebbles from the surface and in shallow subsurface hollows across the three locations in this study (Nullarbor Plain, Rawlinna Quarry, Cape Spencer) are shown to be black because of small quantities of organic carbon derived from the decay of terrestrial vegetation in their microcrystalline structure. Organic carbon impregnation of the limestone sediment/rock has been previously proposed as a possible agent in the blackening of carbonates (Ward et al. 1970; Strasser and

Davaud 1983; Strasser 1984).

The amounts of organic carbon within individual blackened clasts change relative to the degree of black coloration. This direct correlation between the amount of carbon in the insoluble residue and color can be graphically expressed to show how much carbon is needed to achieve the blackening process (Fig. 4.10). The carbon content increases exponentially as the sample color becomes progressively darker. This graphical representation shows that a threshold of approximately 7.5 weight % organic carbon needs to be achieved before the limestone fragments become black in color, lose all original fabric and are dominated by calcified root mats. Such a strong correlation between amount of organic carbon and degree of blackness supports the interpretation that organic carbon is the agent responsible for blackening.

Isotopic compositions of the insoluble residue obtained during elemental analyses gives valuable insights into the source of the oxidized organic matter. Uniform $\delta^{13}C$ values of -22 to -26 ‰ PDB are interpreted to indicate that the organic carbon was derived from partially decayed terrestrial plant debris (Cerling 1984; Hoefs 2004). This plant material was likely sourced from C3 vegetation that is typically from higher order plants in humid to temperate climates, whereas C4 (grasses and drier climate plants) flora have higher $\delta^{13}C$ values (Cerling 1984; Paulsen et al. 2003; Hoefs 2004). There is no evidence to suggest that the vegetation was burned before it was incorporated into the limestone; more likely it was derived from decayed organic matter in humic soils.

### *Diagenetic and Depositional Environments*

**Nullarbor Plain.—**The subsoil hollows, because of their uniform nature and distribution across the Nullarbor Plain, have been interpreted to represent dissolution of the Nullarbor

Limestone through stem flow drainage (Miller et al. 2012). This process allows the canopy to collect rainfall that increases the volume of water to the base of the tree trunk by 20x, subsequently focusing water to the bedrock under the soil (Vanstone 1998; Miller et al. 2012). The locations of subsoil hollows are geographically scattered, likely representing the last stages of large vegetation (with canopies large enough to permit stem flow drainage) on the Nullarbor Plain. This situation would have been characteristic of the temperate to semi-arid climate during the late Pliocene, one that immediately followed a humid climate interlude (Miller et al. 2012). Blackened limestone clast formation is thought to have taken place within these subsoil hollows because the particles are restricted to these depressions. The extensive fragmented and angular nature of the clasts was likely initiated by later root excavation and extraction of deep roots when the trees toppled over. This interpretation would help explain the angular nature and why blackened clasts are solely located in these hollows. The presence of pulmonate gastropods also is compatible with this interpretation since the depression created by the blown over tree would have provided conditions favourable for standing fresh water and gastropod inhabitation.

**Rawlinna Quarry.—**The uniform bedding of black limestone pebbles at Rawlinna is unique not only to the Nullarbor Plain but also to other documented examples of black clast deposits, many of which are found in karst depressions. The surfaces on which these beds were deposited have extensive evidence of short-term subaerial exposure and meteoric alteration. Blackened limestone clasts themselves are interpreted to be subaerial in nature (Ward et al. 1970; Esteban and Klappa 1983; Strasser 1984; Vera and Jimenez de Cisneros 1993; Flügel 2004) although at Rawlinna they are found in a matrix of coarse-grained marine sediments that are deficient in fine-grained components. This intermixed nature of marine and terrestrial sediments is interpreted as a short-term subaerial exposure

event followed by subsequent marine transgression. Blackened pebbles would have been formed during an exposure event and then reworked upon marine transgression (where open marine sediments were deposited with them in a high energy setting). This explains why there are small karst depressions filled with both fragmented angular black clasts and marine bioclasts as they represent a transgressive lag deposit. In total there were three small-scale subaerial exposure events before the whole carbonate platform was uplifted and exposed where it remains today.

**Cape Spencer.—**Black clasts occur in paleosols and calcretes throughout the Bridgewater Formation at Cape Spencer. These paleoexposure horizons developed during lowstands in sea level. Clasts are present as angular granule to pebble-size fragments in the reddish brown, clay-rich, terra rossa soils of the Lower Bridgewater. In most cases they increase in number and abundance upward in each paleosol. Clasts in the Upper Bridgewater occur in calcrete horizons and across the modern surface at and near the aeolianites dune crests near the top of the Cape. They are also found in abundance with limestone and calcrete clasts in interdune corridors. The terra rossa paleosols are interpreted to have formed in somewhat more humid climatic conditions than the calcretes (James and Choquette 1990; Wright 1994). It is particularly instructive that the modern exposure surface at the top of the Cape has numerous shallow karst hollows identical to those across the much older surface of the Nullarbor Plain. Blackened clast plates forming at the base of these hollows were likely generated by root mat processes described above and later fragmented by the brecciation processes associated with calcrete formation.

# DISCUSSION

## *Blackening Process*

The correlation of increasing carbon material with intensity of black coloration is a clear indication that the incorporation of organic material in calcite is the main cause of limestone blackening. Impregnation of organic material inside a calcite crystal lattice is difficult (Krumbein and Garrels 1952; Flügel 2004; Jones 2010). Organic compounds can, however, be adsorbed onto calcite crystal surfaces to form monomolecular layers with adsorbed organic carbon increasing with finer crystal size (Suess 1970). This adsorption typically occurs under slightly alkaline and anoxic conditions and involves finely particulate, colloidal, or dissolved organic matter (Krumbein and Garrels 1952; Suess 1970; Strasser 1984). Ward et al. (1970), Strasser and Davaud (1983), and Strasser (1984) postulate that these mechanisms and conditions are the main cause of blackening in Holocene samples (Swiss and French Jura, Florida Keys, Bahamas, and Tunisia). Such an adsorption method would have to take place under specific chemical conditions since organic coatings otherwise inhibit calcite crystal growth, as they cover suitable nucleation sites for subsequent calcite crystallization. Furthermore, organic-rich settings commonly have active microbial communities that metabolize organic components producing $CO_2$ and locally creating highly acidic conditions that would promote calcite dissolution, rather than precipitation (Krumbein and Garrels 1952; Jones 1994; Ström et al. 1994; Hinsinger 1998; Kosir 2004).

The universal morphologic traits and geochemical signatures in this study indicate that adsorption of organic compounds into the calcite crystal lattice is not the main process of blackening. Calcified root cells and associated microbial features are prevalent in the

microstructure of all blackened limestone clasts and are subsequently thought to have initiated the blackening process. Incorporation of partially decayed organic matter occurred during the processes of root tissue calcification as organics were trapped in the cellular structures and voids between roots. This process allowed for substantial organic carbon to become incorporated with the recently precipitated calcite leading to black coloration. This interpretation would explain why root mat fabrics dominate the blackest samples whereas the uncolored or partially blackened clasts lack both high amounts of organic carbon and numerous root textures. Trapping of organic matter in cellular structures of roots is a viable method of incorporating an adequate volume of organic carbon to produce the black coloration, whereas adsorption of organics on crystal faces does not provide enough organic material to cause the degree of black coloration documented. This latter process likely caused only partial blackening and explains why there is a lack of root fabrics in partially blackened clasts.

Calcified roots are almost invariably located in laminated calcareous soils in semi-arid climates that have a pronounced seasonal moisture regime (Jaillard et al. 1991; Alonso Zarza et al. 1998; Alonso Zarza 1999; Kosir 2004). These types of soils do not contain large quantities of organics and hence the calcified roots in them do not produce blackened clasts. The soils where blackened clasts are formed must have been stratified with a zone of high calcium bicarbonate concentration. The abundance of calcified root cells, as opposed to extracellular calcite precipitates, suggests that the soil was moist for extended periods of blackened clast formation (Wright et al. 1988; Wright 1994; Kosir 2004). These conditions would have been characteristic of a thin humic soil overlying a flat lying and regionally extensive carbonate substrate. The mostly organic-rich soil profile would have not created conditions where plant roots had the necessity to calcify

their rhizosphere for nutrient extraction or protect themselves from $CaCO_3$-rich pore fluids. The calcification of root mats and eventual formation of blackened clasts were instead hosted at the base of a stratified humic soil profile where plant roots had direct contact with the underlying limestone bedrock. This B – C soil horizon was the only location of high calcium bicarbonate concentrations in the soil profile and the location of blackened clast formation (Fig. 4.12A).

Roots derived from higher order plants on the surface penetrate through organic rich soils and often encounter lithified limestone substrates where they cluster to form dense root mats. Such a high density of roots along a carbonate substrate creates conditions where acid (amino and acetic) secretion by the root into the rhizosphere causes a slow kinetic process dissolving the underlying carbonate substrate (Fig. 4.12B) (Ström et al. 1994). Roots within this B – C horizon would have not only chemically dissolved the substrate but also physically eroded the underlying limestones (Fig. 4.12C). This process explains why most blackened clasts contain small corroded fragments of the underlying limestone (Fig. 4.5A). The chemical dissolution process would have created a local abundance of calcium bicarbonate ions in the pore fluids sourced from the underlying carbonate lithologies. This situation would have created a localized alkaline and possibly anoxic microenvironment at the B-C soil horizon. Such alkaline conditions are interpreted to have caused dissolution of silica that is evident in the etching on the surface of quartz grains. This $SiO_2$ would have been incorporated into the blackened clast microstructure and may explain why the clasts are so resistant to weathering. Water in the soils pore system did not flow along this horizon, causing the fluids to become supersaturated with respect to $CaCO_3$.

Environments at the B-C soil horizon where root mats developed would provide conditions favourable for rhizogenic calcification in the roots of certain plants. The

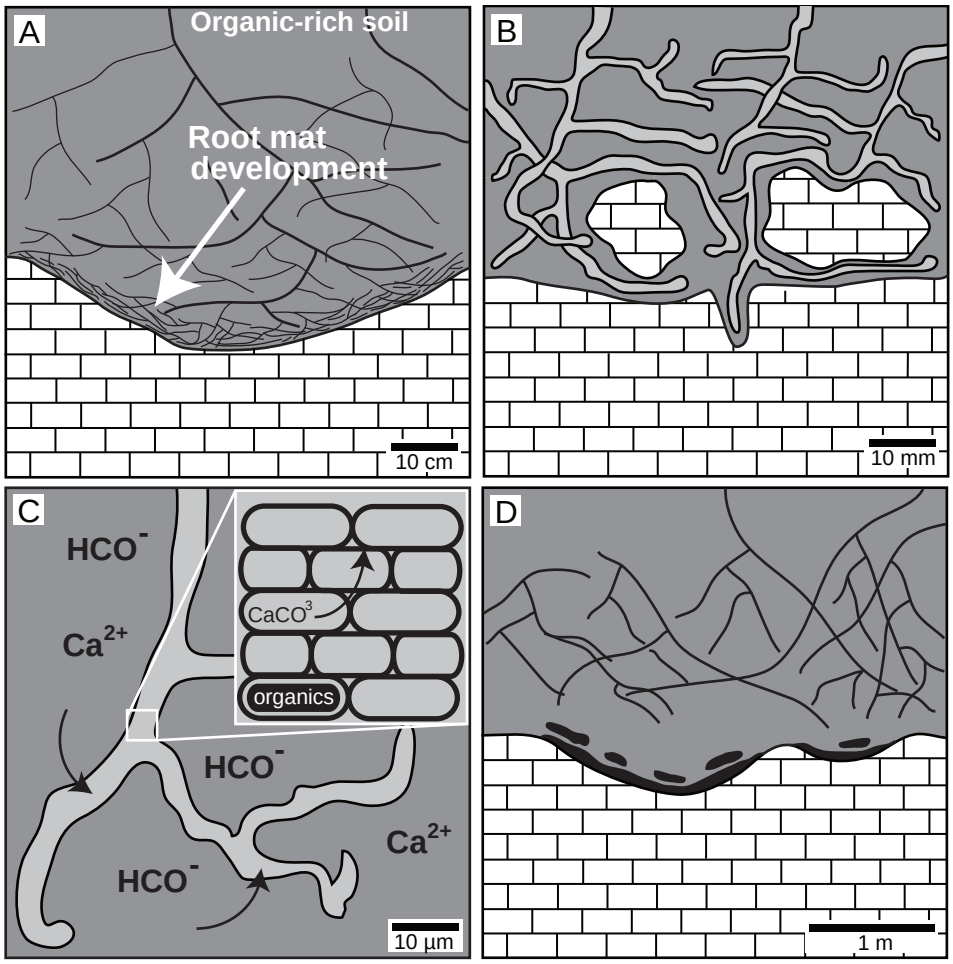


**Figure 4.12.** Illustration showing the mechanism invoked for the blackening of limestone at the base of soil profiles through different spatial scales. A) Roots from overlying vegetation penetrate though the soil and encounter an underlying limestone substrate. The roots cluster at this impervious boundary and create dense mats composed of plant roots and root hairs. B) The root mats both physically erode and fragment the underlying substrate and excrete amino and acetic acids that chemically dissolve the limestone. This process both introduces calcium bicarbonate ions into the pore fluids and mechanically excavates small corroded fragments of the underlying limestone. C) The newly introduced calcium bicarbonate ions are used by roots to calcify their cellular structures in order to protect them from this alkaline microenvironment. During the processes of cell calcification partially degraded organics are trapped in the cellular structures and incorporated into the newly lithified root mats. D) The process of root cell calcification and incorporation of organics occurs along this narrow alkaline environment, interpreted to be < 5 cm wide, creates lithified plates of blackened limestone along the soil and limestone substrate boundary. These plates are fragmented by further root activity, trees toppling over, marine transgression, or other physical soil processes.

thickness of such a zone would have been <5 cm because most blackened clasts have a thin platy morphology. The thin roots within this zone would have calcified from calcium bicarbonate saturated fluids that were derived from the underlying carbonate lithologies. This root calcification would have created new lithified limestone layers at the base of soils that were ultimately formed at the expense of underlying carbonates. Particulates of partially decayed organic carbon were both trapped in the cellular structures of roots or between roots throughout the calcification process and became incorporated into their calcified remains. This allowed for substantial organic material to be incorporated into the microporosity of the roots cellular structure and directly caused the blackening of the newly formed limestone fragments (Fig. 4.12D). The organic matter was entombed in the calcified cell and spared from further degradation and oxidization that destroyed all other organics in the soil.

## CONCLUSIONS

Researchers have long debated the formation of blackened limestone clasts at subaerial exposure surfaces. New evidence from samples located on the southern margin of Australia give a new interpretation as to how these enigmatic clasts form. They occur regionally at subaerial exposure surfaces and most commonly in shallow subsoil hollows sculpted into the underlying limestone bedrock. The black coloration of these pebbles is due to the incorporation of varying amounts of organic carbon, derived ultimately from decayed C3 terrestrial vegetation. The amount of organic matter incorporated into the limestone clasts is shown to determine what degree of black coloration the clast will have. Based on the observations herein organic matter must be approximately 7% of the insoluble

residue to cause complete blackening in limestone.

Formation of blackened limestone clasts is interpreted to have began at the B-C soil horizon where a high density of roots were in contact with underlying limestone bedrock or sediment. Acid secretion from the roots created a corrosive microenvironment and caused dissolution of the underlying limestone. This newly liberated calcium bicarbonate in the pore fluids caused the roots within this narrow zone to calcify in order to protect themselves from these $CaCO_3$ saturated fluids. Calcification of root cells and tissues caused soil derived organic matter to become trapped within the cellular structures of the roots as they were undergoing calcification. Such a mechanism for causing black coloration in limestones at subaerial exposure surfaces could be used to explain the origins of worldwide occurrences, help identify exposure events, and perhaps most importantly define narrow climatic conditions for their formation that can be further used for paleoclimate reconstruction.

## ACKNOWLEDGEMENTS

The Natural Sciences and Engineering Research Council of Canada (NSERC) Discovery Grant to NPJ and the Geological Survey of Western Australia (GSWA) funded this research. We thank the helpful staff at GSWA (R. Hocking and the Carlislie staff), L. O'Connell, and Y. Bone for field assistance. This study would not have been possible without the guidance of Paul Wright. The authors also wish to thank B. Jones, G. Braybrook, and D. Rollings for their help with SEM analyzes, A. Grant for XRD analyzes, S. Beyer for SWIR analyses, and A. Vuletich and K. Klassen for elemental and stable isotope analyses.

## REFERENCES


Alonso Zarza, A.M., 1999, Initial stages of laminar calcrete formation by roots; examples from the Neogene of central Spain: Sedimentary Geology, v. 126, p. 177-191.

Alonso Zarza, A.M., Sanz, M.E., Calvo, J.P., and Estevez, P., 1998, Calcified root cells in Miocene pedogenic carbonates of the Madrid Basin; evidence for the origin of Microcodium b: Sedimentary Geology, v. 119, p. 181.

Alonso-Zarza, A.M., 2003, Palaeoenvironmental significance of palustrine carbonates and calcretes in the geological record: Earth-Science Reviews, v. 60, p. 261-298.

Alonso-Zarza, A.M., and Wright, V.P., 2010, Calcretes, *in* Alonso-Zarza, A.M., and Tanner, L.H., eds., Carbonates in Continental Settings: Facies, Environments and Processes: Developments in Sedimentology: Oxford, Elsevier, p. 225-267.

Australian Water Resources Council, 1976, Review of Australia's water resources: Canberra, Australian Government Publishing Service, p. 170.

Belperio, A.P., Murray-Wallace, C.V., and Cann, J.H., 1995, The last interglacial shoreline in southern Australia: Morphostratigraphic variations in a temperate carbonate setting: Quaternary International, v. 26, p. 7-19.

Cerling, T.E., 1984, The stable isotopic composition of modern soil carbonate and its relationship to climate: Earth and Planetary Science Letters, v. 71, p. 229-240.

Clarkson, D.T., 1984, Calcium transport between tissues and its distribution in the plant: Plant, Cell & Environment, v. 7, p. 449-456.

Crawford, A.R., and Ludbrook, N.H., 1965, The Geology of Yorke Peninsula: Adelaide, W.L. Hawes 96 p.

Esteban, M., and Klappa, C.F., 1983, Subaerial exposure environment, *in* Scholle, P.A.,

Bebout, D.G., and Moore, C.H., eds., Carbonate Depositional Environments: Tulsa, American Association of Petroleum Geologists, p. 1-54.

Feary, D.A., and James, N.P., 1998, Seismic stratigraphy and geological evolution of the Cenozoic, cool-water Eucla Platform, Great Australian Bight: AAPG Bulletin, v. 82, p. 792-816.

Flügel, E., 2004, Microfacies of carbonate rocks: analysis, interpretation and application: Berlin, Springer-Verlag, 976 p.

Folk, R.L., and Chafetz, H.S., 2000, Bacterially induced microscale and nanoscale carbonate precipitates, *in* Riding, R.E., and Awramik, S.M., eds., Microbial sediments: Berlin, Springer, p. 40-49.

Folk, R.L., Roberts, H.H., and Moore, C.H., 1973, Black Phytokarst from Hell, Cayman Islands, British West Indies: Geological Society of America Bulletin, v. 84, p. 2351-2360.

Fortin, D., Ferris, F.G., and Beveridge, T.J., 1997, Surface-mediated mineral development by bacteria: Reviews in Mineralogy, v. 35, p. 161-180.

Goede, A., Harmon, R.S., Atkinson, T.C., and Rowe, P.J., 1990, Pleistocene climatic change in southern Australia and its effect on speleothem deposition in some Nullarbor caves: Journal of Quaternary Science, v. 5, p. 29-38.

Hardy, R., and Tucker, M., 1988, X-ray powder diffraction of sediments, *in* Tucker, M., ed., Techniques in sedimentology: Oxford, Blackwell Sci. Publ., p. 191-228.

Hinsinger, P., 1998, How Do Plant Roots Acquire Mineral Nutrients? Chemical Processes Involved in the rhizosphere: Advances in Agronomy, v. 64, p. 225-265.

Hocking, R.M., 1990, Eucla Basin: Geological Survey of Western Australia, v. Memoir 3, p. 548-561.

Hoefs, J., 2004, Stable isotope geochemistry: Berlin, Springer-Verlag 244 p.

Hou, B., Frakes, L.A., Sandiford, M., Worrall, L., Keeling, J., and Alley, N.F., 2008, Cenozoic Eucla Basin and associated palaeovalleys, southern Australia; climatic and tectonic influences on landscape evolution, sedimentation and heavy mineral accumulation: Sedimentary Geology, v. 203, p. 112-130.

Jaillard, B., and Callot, G., 1987, Mineralogical segregation of soil mineral constituents under the action of roots: Proceedings of the International Working Meeting on Soil Micromorphology, v. 7, p. 371-375.

Jaillard, B., Guyon, A., and Maurin, A.F., 1991, Structure and composition of calcified roots, and their identification in Calcareous soils: Geoderma, v. 50, p. 197-210.

James, N.P., and Bone, Y., 1991, Origin of a cool-water, Oligo-Miocene deep shelf limestone, Eucla Platform, southern Australia: Sedimentology, v. 38, p. 323-341.

James, N.P., and Choquette, P.W., 1990, Limestones - The meteoric diagenetic environment, *in* McIlreath, I.A., and Morrow, D.W., eds., Diagenesis: Ottawa, Geological Association of Canada, p. 35-74.

Jones, B., 1994, Diagenetic processes associated with plant roots and microorganisms in karst terrains of the Cayman Islands, British West Indies: Developments in Sedimentology, v. 51, p. 425-475.

Jones, B., 2010, Microbes in caves; agents of calcite corrosion and precipitation: Geological Society Special Publications, v. 336, p. 7-30.

Jones, B., 2011, Biogenicity of terrestrial oncoids formed in soil pockets, Cayman Brac, British West Indies: Sedimentary Geology, v. 236, p. 95-108.

Klappa, C.F., 1978, Biolithogenesis of Microcodium; elucidation: Sedimentology, v. 25, p. 489-519.

Klappa, C.F., 1979, Calcified filaments in Quaternary calcretes; organo-mineral interactions in the subaerial vadose environment: Journal of Sedimentary Petrology, v. 49, p. 955-968.

Klappa, C.F., 1980, Rhizoliths in terrestrial carbonates: classification, recognition, genesis and significance: Sedimentology, v. 27, p. 613-629.

Kosir, A., 2004, Microcodium revisited: root calcification products of terrestrial plants on carbonate-rich substrates: Journal of Sedimentary Research, v. 74, p. 845-857.

Krumbein, W.C., and Garrels, R.M., 1952, Origin and classification of chemical sediments in terms of pH and oxidation-reduction potentials: Geology, v. 60, p. 1-33.

Kyser, T.K., 1987, Stable isotope geochemistry of low temperature processes: Short Course Handbook, v. 13: Toronto, Mineralogical Association of Canada, 452 p.

Lang, R.A., and Tucci, P., 1997, A preliminary study of the causes of the blackening of pebbles in the Cenomanian "breccia with black pebbles" of Camporosello (Lepini Mountains, Italy): Geologica Romana, v. 33, p. 89-97.

Leinfelder, R.R., 1987, Formation and significance of black pebbles from the Ota Limestone (Upper Jurassic, Portugal): Facies, v. 17, p. 159-170.

Leveille, R.J., Fyfe, W.S., and Longstaffe, F.J., 2000, Geomicrobiology of carbonate-silicate microbialites from Hawaiian basaltic sea caves: Chemical Geology, v. 169, p. 339-355.

Lintern, M.J., Sheard, M.J., and Chivas, A.R., 2006, The source of pedogenic carbonate associated with gold-calcrete anomalies in the western Gawler Craton, South Australia: Chemical Geology, v. 235, p. 299-324.

Lintern, M.J., Sheard, M.J., and Gouthas, G., 2004, Key findings from the South Australian regolith project: Regolith 2004; proceedings of the CRC LEME regional regolith

symposia 2004, p. 220-224.

Lowry, D.C., 1970, Geology of the Western Australian part of the Eucla Basin: Bulletin - Geological Survey of Western Australia, v. 122: Perth, Geological Survey of Western Australia, 199 p.

Lowry, D.C., and Jennings, J.N., 1974, The Nullarbor karst Australia: Zeitschrift fuer Geomorphologie, v. 18, p. 35-81.

Marschner, H., 1995, Mineral nutrition in higher plants: Amsterdam, Acadmenic Press, 889 p.

McConnaughey, T., 1998, Acid secretion, calcification, and photosynthetic carbon concentrating mechanisms: Canadian Journal of Botany, v. 76, p. 1119-1126.

McConnaughey, T.A., and Whelan, J.F., 1997, Calcification generates protons for nutrient and bicarbonate uptake: Earth-Science Reviews, v. 42, p. 95-117.

Miller, C.R., James, N.P., and Bone, Y., 2012, Prolonged carbonate diagenesis under an evolving late Cenozoic climate; Nullarbor Plain, southern Australia: Sedimentary Geology, v. 261-262, p. 33-49.

O'Connell, L.G., James, N.P., and Bone, Y., 2012, The Miocene Nullarbor Limestone, southern Australia; deposition on a vast subtropical epeiric platform: Sedimentary Geology, v. 253-254, p. 1-16.

Paulsen, D.E., Li, H.-C., and Ku, T.-L., 2003, Climate variability in central China over the last 1270 years revealed by high-resolution stalagmite records: Quaternary Science Reviews, v. 22, p. 691-701.

Retallack, G.J., 2001, Soils of the past. An introduction to paleopedology: Oxford, Blackwell Science, 404 p.

Sandiford, M., 2007, The tilting continent; a new constraint on the dynamic topographic

field from Australia: Earth and Planetary Science Letters, v. 261, p. 152-163.

Sandiford, M., Quigley, M., de Broekert, P., and Jakia, S., 2009, Tectonic framework for the Cenozoic cratonic basins of Australia: Australian Journal of Earth Sciences, v. 56, p. 5-18.

Shinn, E.A., and Lidz, B.H., 1988, Blackened limestone pebbles; fire at subaerial unconformities, *in* James, N.P., and Choquette, P.W., eds., Paleokarst: New York, Springer-Verlag, p. 117-131.

Strasser, A., 1984, Black-pebble occurrence and genesis in Holocene carbonate sediments (Florida Keys, Bahamas, and Tunisia): Journal of Sedimentary Petrology, v. 54, p. 1097-1109.

Strasser, A., and Davaud, E., 1983, Black pebbles of the Purbeckian (Swiss and French Jura); lithology, geochemistry and origin: Eclogae Geologicae Helvetiae, v. 76, p. 551-580.

Ström, L., Olsson, T., and Tyler, G., 1994, Differences between calcifuge and acidifuge plants in root exudation of low-molecular organic acids: Plant and Soil, v. 167, p. 239-245.

Suess, E., 1970, Interaction of organic compounds with calcium carbonate,ÄîI. Association phenomena and geochemical implications: Geochimica et Cosmochimica Acta, v. 34, p. 157-168.

Tucker, M.E., 1973, Ferromanganese nodules from the Devonian of the Montagne Noire (S. France) and West Germany: Geologische Rundschau, v. 62, p. 137-153.

Vanstone, S.D., 1998, Late Dinantian palaeokarst of England and Wales; implications for exposure surface development: Sedimentology, v. 45, p. 19-37.

Vera, J.A., and Jimenez de Cisneros, C., 1993, Palaeogeographic significance of black

pebbles (Lower Cretaceous, Prebetic, southern Spain): Palaeogeography, Palaeoclimatology, Palaeoecology, v. 102, p. 89-102.

WARD, W.C., FOLK, R.L., and WILSON, J.L., 1970, Blackening of eolianite and caliche adjacent to saline lakes, Isla Mujeres, Quintana Roo, Mexico: Journal of Sedimentary Petrology, v. 40, p. 548-555.

WHITE, M.E., 1994, After the greening: The browning of Australia: Kenthurst, Kangaroo Press Pty Ltd., 288 p.

WRIGHT, V.P., 1994, Paleosols in shallow marine carbonate sequences: Earth-Science Reviews, v. 35, p. 367-395.

WRIGHT, V.P., PLATT, N.H., MARRIOTT, S.B., and BECK, V.H., 1995, A classification of rhizogenic (root-formed) calcretes, with examples from the Upper Jurassic-Lower Cretaceous of Spain and Upper Cretaceous of southern France: Sedimentary Geology, v. 100, p. 143-158.

WRIGHT, V.P., PLATT, N.H., and WIMBLEDON, W.A., 1988, Biogenic laminar calcretes: evidence of calcified root-mat horizons in paleosols: Sedimentology, v. 35, p. 603-620.

# CHAPTER 5

# CONCLUSIONS

The Cenozoic limestones on and beneath the Nullarbor Plain have been shown to host an ~ 14 m.y. record of superimposed meteoric diagenesis under an evolving humid to semi-arid climate. Such changes can now be resolved into eight discrete stages of alteration during three broad climate phases. This paragenetic framework now permits a detailed interpretation of the Neogene climate history of the Plain for the first time. Integrated petrographic, geochemical, and biological analyses of palustrine ooids and blackened limestone clasts have resulted in new explanations for these diagenetic entities that were previously scientific enigmas.

The initial diagenesis of the limestones (Phase 1) occurred under a humid to temperate climate. Following uplift, the recently deposited sub-tropical marine sediment composed of aragonitic and Mg-calcite bioclasts underwent mineralogical equilibration with meteoric waters. This interaction led to extensive dissolution and formation of mouldic porosity, low-Mg sparry calcite cement precipitation, and recrystallization of high-Mg components to low-Mg calcite. Extensive microkarstic cavity networks developed shortly after this lithification. These cavities were then filled with muddy carbonate sediment and fresh water bioclasts that filtered down from overlying lacustrine depositional systems. These sediments were in turn later pedogenically modified by palustrine processes to create copious micritic ooids.

Palustrine ooids formed within Phase 1 have an appearance similar to their marine counterparts precipitated in highly agitated marine waters. These palustrine ooids, however,

are micritic and formed via a complex interaction with microbes, physical soil processes, and changing hydration states. This study has proposed a subaerial mechanism by which spherically coated grains are formed in place within the soil, without the necessity of constant grain movement to achieve sphericity. Such a process is interpreted to involve sediment aggradation by a combination of microbial and root activities. Mucus films derived from surrounding microbial communities then coat the peloids, creating a thin uniform layer that encompasses the entire nucleus during the wet season when soil moisture levels are high. Seasonal changes to more arid conditions caused this mucus layer, which has a dominantly Mg, Ca, Si, and Al ion composition gained from surrounding pore fluids, to dehydrate. As the mucus layers dehydrated water was lost and clay minerals precipitated within the mucus coating that mimic the shape of the underlying mucus structure and subsequently preserve its fabric. This seasonal alternation resulted in relatively thick and spherical cortical coatings while the grain was in place and not moving.

Phase 2 spanned approximately 8 m.y. and was highlighted by massive dissolution and the formation of spectacular deep and shallow cave systems under a temperate to humid climate. Such cave networks reflect not only the wet climate of the time, but the depths of the deep and shallow cave systems illustrate a strong correlation with widely variable late Miocene to early Pliocene eustasy. Deep caves are interpreted to have originated under a temperate climate in the form of small karst cavities along pre-existing fault lineations. Dissolution occurred at a depressed water table related to the late Miocene global low sea level. A humid Pliocene climate interlude coinciding with a rise in sea level created a second and more regional network of small shallow caves. Deep cave passages were further developed during this time as phreatic dissolution sculpted them into the long and sizeable passages that are preserved today.

The last regional phase of diagenesis, Phase 3, has taken place since the middle Pliocene when the humid climate rapidly shifted towards increasing aridity. This change is marked by the final segment of karsting on the surface of the Plain in the form of small subsoil hollows, created by stem flow drainage processes under the last remaining large trees. These hollows are filled with a distinctive breecia dominated by angular black limestone clasts. This event was followed by an extended period of doline formation resulting in roof collapse of earlier formed shallow and deep caves. Deep cave collapse created the large dolines that dot the Plain today and give access to the long underground cave passages. Shallow cave collapse dolines are filled with red brown calcium carbonate colluvium and gypsum. This period marked the transition into a truly arid climate system where vegetation was limited due to low regional rainfall and high evaporation rates. Accretionary pedogenic calcrete now forms much of the surface of the Plain and is a testament to this arid climate, which fully developed over about the last 500 ky.

Blackened limestone clasts, like those from Phase 3, are present globally at many post-Carboniferous exposure surfaces, however, their origins are still poorly understood. This study has focused not only on the blackened clasts found on the Nullarbor Plain but also from Rawlinna Quarry and the Cape Spencer to determine how these problematic pebbles formed. Clasts have their characteristic black colouration because each particle contains varying amounts of organic carbon, although > 7.5 weight % carbon is needed to achieve complete blackening. Blackened clast microstructure is dominated by micritic laminae interpreted to represent the calcified cellular structures of roots derived from the overlying vegetation. Genesis of these clasts is thought to have taken place at the base of the soil near the B – C boundary where roots come into contact with a lithified limestone substrate and cluster to created dense root mats. These mats secrete acids that slowly dissolve

the surrounding limestone making a microenvironment where fluids are high in calcium bicarbonate. This oversaturation causes the roots to uptake $Ca^{2+}$ and causes their cells to calcify and create lithified plates of limestone. Partially decayed organics are trapped within the cellular structures as this calcification process proceeds and this organic carbon is the cause of their black colouration.

The documentation and interpretation of diagenetic properties within the Nullarbor Plain illustrates the complexities associated with subaerial alteration under a changing climate. The complete record of subaerial alteration in this low lying carbonate plain provides important insights into the effects of climate, tectonics, groundwater movement, sea level, and topography on the style and formation of a variety of meteoric diagenetic fabrics. These findings have direct application to other prolonged post-Carboniferous unconformities globally. Newly proposed mechanisms for the formation of palustrine ooids herein provide insight into how coated grains form in soils and have direct application to other calcareous soil settings where these grains are found, namely calcretes. Finally, blackened clasts have been shown to form not via heat from forest fires but rather from a complex interaction between roots and the underlying carbonate substrate. These aspects will increase our understanding of the depositional and diagenetic processes operating at subaerial unconformities and how these processes are preserved in carbonate rocks throughout geologic history.

# APPENDIX A

Location of Sample Codes

**Appendix A** – Geographic Location of Sample Codes

| Sample Code | Geographic Location |
|---|---|
| NC1 | Cocklebiddy Cave |
| NC2 | Come By Chance Quarry |
| NC3 | Madura Pass |
| NC4 | Mundrabilla Quarry |
| NC5 | Wilson Bluff Type Section |
| NC6 | Eucla Quarry |
| NC7 | Abrakurrie Cave |
| NC9 | Abrakurrie Cave |
| NC10 | Weebubbie Cave |
| NC11 | Watson Quarry |
| NC12 | Cook Quarry |
| NC13 | Mullamullang Cave |
| NC14 | Madura Quarry |
| NC15 | Narina Cave |
| NC16 | Madura Cave |
| NC17 | Caiguna Quarry |
| NC18 | Haig Cave |
| NC19 | Old Homestead Cave |
| NC20 | Forresst Tipp |
| NC21 | Balladonia Quarry |
| NC22 | Rawlinna Quarry |

# APPENDIX B

Stable Isotopes

**Appendix B** – Stable Carbon (Cinorganic) and Oxygen Isotope Data

Error/precision of analyses is 0.1 ‰

| Location | Diagenetic Phase | δ 13C/12C | δ 18O/16O | δ 18O/16O PDB |
|---|---|---|---|---|
| NC6.6 | 6 | -10.38 | 27.69 | -3.12 |
| NC6.14 | 8 | -5.26 | 30.89 | -0.01 |
| NC9.6 | 3 | -11.07 | 26.25 | -4.52 |
| NC11.11 | 8 | -4.05 | 29.32 | -1.54 |
| NC11.9 | 5 | -6.98 | 26.78 | -4.01 |
| NC22.7 | 6 | -6.51 | 28.30 | -2.52 |
| NC11.6 | 7 | -8.53 | 26.78 | -4.01 |
| NC14.2 | 8 | -1.75 | 32.56 | 1.61 |
| NC11.10 | 3 | -9.58 | 26.79 | -3.99 |
| NC11.10 | 3 | -9.61 | 26.76 | -4.03 |
| NC9.4 | 7 | -11.74 | 25.47 | -5.28 |
| NC19.6 | 3 | -9.59 | 26.66 | -4.12 |
| NC12.5 | 3 | -8.87 | 26.44 | -4.33 |
| NC22.8 | 5 | -9.43 | 25.79 | -4.96 |
| NC2.9 | 8 | -9.33 | 28.94 | -1.91 |
| NC2.9 | 8 | -9.27 | 28.96 | -1.89 |
| NC1.4 | 3 | -10.52 | 27.33 | -3.47 |
| NC12.4 | 5 | -8.66 | 25.89 | -4.87 |
| NC12.21 | 6 | -9.75 | 25.98 | -4.78 |
| NC12.1 | 1 | -6.91 | 27.67 | -3.14 |
| NC22.4 | 1 | -6.56 | 27.59 | -3.21 |
| NC3.10 | 7 | -10.73 | 25.33 | -5.41 |
| NC12.21M | 6-matrix | -9.85 | 26.13 | -4.63 |
| NC3.14 | 5 | -11.66 | 25.28 | -5.45 |
| NC3.3 | 8 | -5.54 | 29.33 | -1.53 |
| NC6.6M | 6 | -7.95 | 27.08 | -3.71 |
| NC6.7 | 5 | -9.43 | 24.75 | -5.97 |
| Star 29 | Standard | -2.49 | 9.90 | -20.37 |
| Star 23 | Standard | 0.59 | 19.67 | -10.90 |
| Star 49e | Standard | -1.58 | 17.98 | -12.54 |
| TSLST | Standard | 1.93 | 28.70 | -2.14 |
| TSLST | Standard | 2.05 | 28.76 | -2.08 |
| DOL2 | Standard | 1.01 | 22.63 | -8.03 |
| DOL2 | Standard | 0.95 | 22.61 | -8.04 |
| TSLST | Standard | 1.90 | 28.72 | -2.12 |
| TSLST | Standard | 1.98 | 28.80 | -2.05 |

# APPENDIX C

ICP MS Data

**Appendix C** - ICP MS Data Majors

| Sample | Diagenetic Phase | Ca (wt.%) | Mg (ppm) | Na (ppm) | P (ppm) | S (ppm) | Sr (ppm) |
|---|---|---|---|---|---|---|---|
| NC1.1A | 6 | 35.75 | 5084.46 | 325.26 | DL | 306.85 | 1015.67 |
| NC1.1B | 6 | 35.62 | 4464.43 | DL | DL | DL | 758.11 |
| NC1.1C | 6 | 27.45 | 4915.42 | DL | DL | 315.57 | 508.62 |
| NC1.4 | 3 | 36.37 | 8053.06 | 1175.34 | DL | 724.45 | 817.63 |
| NC3.8 | 6 | 33.00 | 3906.43 | 330.27 | DL | 588.29 | DL |
| NC6.6 | 6 | 30.30 | 21010.70 | 637.91 | DL | 883.00 | 1060.94 |
| NC6.7 | 1 | 38.30 | 2901.32 | DL | DL | DL | 236.77 |
| NC6.14 | 8 | 26.95 | 7269.60 | 1986.31 | DL | 1016.62 | 416.03 |
| NC11.6 | 7 | 22.75 | 7726.76 | 2970.31 | DL | 337.38 | 277.85 |
| NC11.11 | 8 | 21.22 | 5504.16 | 1051.00 | DL | 725.16 | 306.67 |
| NC12.11 | 8 | 23.88 | 21633.13 | 250.66 | DL | 19102.08 | 290.40 |
| NC12.21 | 6 | 37.92 | 3801.04 | DL | DL | 373.57 | 1123.81 |
| NC14.2A | 8 | 34.24 | 10031.64 | 2173.91 | DL | 1107.47 | 949.26 |
| NC20.1A | 6 | 35.18 | 3615.24 | DL | DL | 288.72 | 740.62 |
| NC20.1B | 6 | 36.91 | 6843.29 | DL | DL | 393.44 | 1135.17 |
| NC20.1C | 6 | 33.97 | 5031.98 | 736.14 | DL | 610.09 | 771.44 |
| NC22.1 | 1 | 37.33 | 5415.95 | 266.13 | DL | 428.58 | 629.04 |
| NC22.5A | 6 | 37.99 | 4916.14 | 294.83 | DL | 452.53 | 946.20 |
| NC22.5B | 6 | 36.15 | 3650.37 | 400.26 | DL | 393.86 | 650.02 |
| NC22.8 | 5 | 37.64 | 5666.19 | DL | DL | 206.84 | 562.89 |
| NC-EN1 | Standard | 34.12 | DL | 5028.90 | DL | DL | 1249.87 |
| NC-STOG1 | Standard | 39.85 | 1264.44 | DL | DL | DL | 174.76 |
| NC-PB1 | Standard | 0.00 | DL | DL | DL | DL | DL |

**Appendix C** - ICP MS Data Minors (ppm)

| Sample | Diagenetic Phase | Ba138 | Pb208 | U238 | Al27 | Si28 | Ti47 | Cr52 | Mn55 | P31 | K39 |
|---|---|---|---|---|---|---|---|---|---|---|---|
| NC1.1A | 6 | 13 | 1 | 101 | 850 | 66 | 5 | 15 | 27 | 19 | 767 |
| NC1.1B | 6 | 0 | 0 | 0 | 11 | 5 | 1 | 1 | 1 | 4 | 150 |
| NC1.1C | 6 | 57 | 14 | 92 | 23804 | 125 | 113 | 105 | 63 | 17 | 46671 |
| NC1.4 | 3 | 12 | 1 | 2 | 3097 | 23 | 11 | 10 | 9 | 10 | 584 |
| NC3.8 | 6 | 23 | 2 | 2 | 720 | 51 | 4 | 1656 | 117 | 18 | 392 |
| NC6.6 | 6 | 19 | 2 | 1 | 6204 | 2 | 48 | 18 | 31 | 19 | 508 |
| NC6.7 | 1 | 2 | 0 | 1 | 188 | 39 | 1 | 13 | 5 | 12 | 473 |
| NC6.14 | 8 | 56 | 3 | 0 | 9565 | 15 | 44 | 12 | 59 | 161 | 395 |
| NC11.6 | 7 | 45 | 6 | 1 | 32056 | 45 | 111 | 38 | 67 | 52 | 60278 |
| NC11.11 | 8 | 96 | 6 | 2 | 21265 | 35 | 141 | 422 | 125 | 435 | 45698 |
| NC12.11 | 8 | 57 | 2 | 2 | 10228 | 89 | 89 | 12 | 35 | 53 | 252 |
| NC12.21 | 6 | 13 | 2 | 0 | 1152 | 0 | 6 | 4 | 39 | 91 | 431 |
| NC14.2A | 8 | 42 | 3 | 2 | 3082 | 89 | 25 | 39 | 55 | 49 | 688 |
| NC20.1A | 6 | 82 | 0 | 1 | 903 | 0 | 3 | 4 | 15 | 16 | 344 |
| NC20.1B | 6 | 23 | 1 | 1 | 993 | 755 | 7 | 39 | 23 | 25 | 589 |
| NC20.1C | 6 | 218 | 17 | 43 | 10268 | 46 | 48 | 178 | 78 | 42 | 222 |
| NC22.1 | 1 | 8 | 1 | 2 | 1930 | 89 | 4 | 44 | 17 | 6 | 4862 |
| NC22.5A | 6 | 13 | 1 | 10 | 534 | 0 | 1 | 18 | 21 | 11 | 329 |
| NC22.5B | 6 | 11 | 1 | 12 | 305 | 0 | 2 | 8 | 18 | 8 | 370 |
| NC22.8 | 5 | 9 | 0 | 3 | 13 | 0 | 0 | 0 | 0 | 19 | 0 |
| NC-EN1 | Standard | 1 | 0 | 0 | 0 | 0 | 0 | 0 | 0 | 1 | 268 |
| NC-STOG1 | Standard | 1 | 0 | 1 | 1 | 0 | 0 | 1 | 389 | 2 | 221 |

# APPENDIX D

Elemental Analyses

**Appendix D** – Elemental Analyzer Data - Organic Carbon content and Corganic Isotope Compositions.

Error/precision of isotope analyses is 0.1 ‰

| Sample # | Description | Amt % C | δ 13C/12C |
|---|---|---|---|
| NC1.1A | Black clast in hollow | 19.63 | -22.05 |
| NC1.1B | Partially black clast hollow | 3.78 | -21.45 |
| NC20.1A | Black clast in hollow | 24.68 | -21.48 |
| NC20.1A | Black clast in hollow *wgt (0.018mg) | 57.29 | -20.17 |
| NC22.5A | Black clast bedded horizon | 16.58 | -21.61 |
| NC22.5A | Black clast bedded horizon | 19.24 | -21.88 |
| BP-2W | Partially black clast on modern surface | 5.50 | -21.31 |
| NC3.8A | Black clast in hollow | 20.97 | -23.04 |
| BP2-W | Partially black clast on modern surface | 3.72 | -22.06 |
| NC6.6B | Black clast in hollow | 1.83 | -24.24 |
| BP-1B | Partially black clast on modern surface | 8.51 | -21.48 |
| NC12.21 | Black clast in hollow | 9.75 | -21.39 |
| NC3.8B | Partially black clast hollow | 0.99 | -17.82 |
| BP-1C | Partially black clast on modern surface | 9.29 | -21.62 |
| BP-1 | Black clast on modern surface | 6.63 | -22.34 |
| NC22.7B | Black clast bedded horizon | 34.93 | -21.85 |
| NC22.2 | Partially black clast bedded horizon | 7.17 | -21.42 |
| NC20.1C | Partially black clast hollow | 2.68 | -20.82 |
| NC6.6A | Black clast in hollow | 12.59 | -23.31 |
| BP-1A | Partially black clast on modern surface | 23.84 | -21.61 |
| BP2-E | Partially black clast on modern surface | 19.51 | -21.65 |

| STANDARDS | | | |
|---|---|---|---|
| UC-1 | Standard | 111.17 | -25.45 |
| sulfan | Standard | 41.84 | -27.68 |
| sulfan | Standard | 40.23 | -27.68 |
| UC-1 | Standard | 95.47 | -26.26 |
| UC-1 | Standard | 114.23 | -26.11 |

## APPENDIX E

Glossary of Terms

**Alveolar Fabric -** Common structure in pedogenic carbonates occurring within tubular cavities where thin threads of micrite form septa that cross the cavities and create a chambered fabric.

**Charophyte -** A member of a group of complex, fresh to brackish water green algae of the phylum Charophyta. The egg-containing structure of these algae is commonly fossilized and termed a *gyrogonite*.

**Doline -** A basin or funnel shaped hollow in limestone, ranging in width from meters to kilometers and in depth from a few meters to several hunderds of meters. A distinction can be made between dolines formed mainly as a result of limestone dissolution (solution dolines) or by the collapse of the surface into underlying cavities (collapse dolines).

**Exopolysaccharides -** These are high-molecular-weight polymers that are composed of sugar residues and are secreted by a microorganism into the surrounding environment. Microorganisms synthesize a wide spectrum of multifunctional polysaccharides including intracellular polysaccharides, structural polysaccharides and extracellular polysaccharides or exopolysaccharides **(EPS)**.

**Lacustrine -** Pertaining to, produced by, or formed in a lake or lakes.

**Micrite -** Semiopaque crystalline matrix of limestones consisting of carbonate mud with crystals less than 4 microns; microcrystalline calcite.

**Minimicrite -** Micrite that has crystal sizes less than 1 micron in size.

**Paleokarst -** An ancient karst landscape that is no longer actively undergoing dissolution.

**Phreatic -** The zone below the water table and in the saturated zone.

**Pulmonate Gastropod -** Any terrestrial or freshwater gastropod belonging to the subclass Pulmonata.

**Subsoil Hollows -** Shallow karst depressions into carbonate substrate at the base of soils, or had developed at the bases of soils, typically underlying large canopy trees.

**Vadose -** The zone above the water table and in the zone of perculation or unsaturated zone.

The Nullarbor Plain in southern Australia is an uplifted succession of Cenozoic marine carbonates whose surface has been exposed for ~14 m.y. The limestones, particularly the Miocene Nullarbor Limestone, show a complex record of meteoric diagenesis involving dramatic regional climate change. Initial alteration was in a humid middle Miocene climate with widespread microkarst, regional lacustrine sedimentation and later palustrine modification. Low sea levels during the late Miocene created extensive deep cave formation under the influence of a moderate climate. This was followed by shallow cave formation caused by a Pliocene sea level highstand and corresponding humid climate interlude. The late Pliocene saw the onset of modern semi-arid climatic conditions, and the creation of subsoil hollows filled with blackened limestone lithoclasts, deep and shallow dolines, and indurated pedogenic calcrete that now forms much of the surface of the Nullarbor Plain. The importance of this comprehensive diagenetic history is its applicability to the understanding of ancient subaerial exposure surfaces.

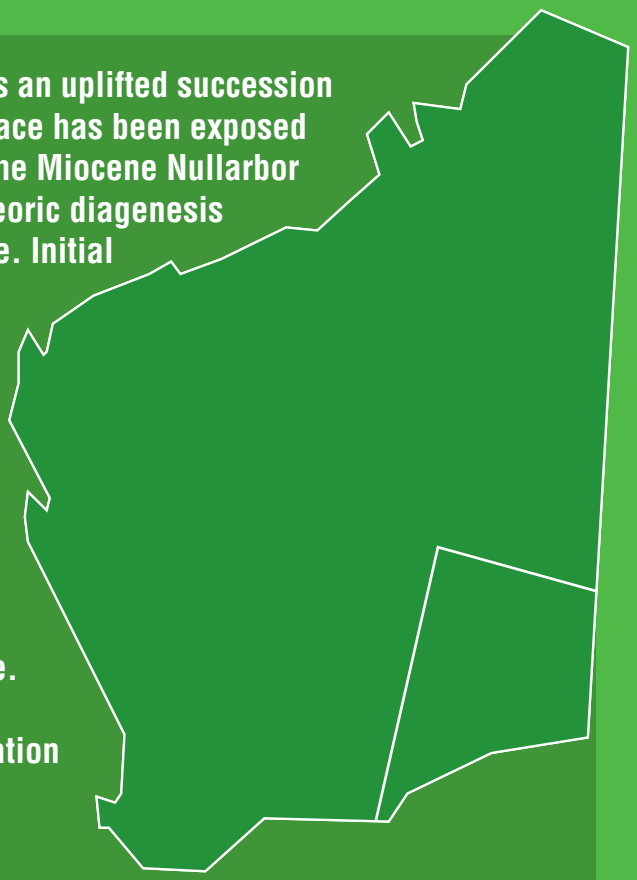

Further details of geological products and maps produced by the Geological Survey of Western Australia are available from:

Information Centre
Department of Mines and Petroleum
100 Plain Street
EAST PERTH WA 6004
Phone: (08) 9222 3459 Fax: (08) 9222 3444

http://www.dmp.wa.gov.au/GSWApublications